Fillers
Synthesis, Characterization and Industrial Application

Edited by Amar Patnaik

Fillers - Synthesis, Characterization and Industrial Application

Edited by Amar Patnaik

IntechOpen

Supporting open minds since 2005

Contributors

Ertugrul Altuntas, Eyyup Karaogul, Tufan Salan, M. Hakki Alma, Vladimir Shmalko, David Olubiyi Obada, David Dodoo-Arhin, Yongdan Hou, Muyideen Balogun, Mahmud Muhammad, Shih-Ying Chang, Lung-Chuan Tsao, Yan-Hua Huang, Qi Wang, Kenxin Chen, Wenbin Cao

Notice
Statements and opinions expressed in the chapters are these of the individual contributors and not necessarily those of the editors or publisher. No responsibility is accepted for the accuracy of information contained in the published chapters. The publisher assumes no responsibility for any damage or injury to persons or property arising out of the use of any materials, instructions, methods or ideas contained in the book.

We are IntechOpen,
the world's leading publisher of Open Access books
Built by scientists, for scientists

4,100+
Open access books available

116,000+
International authors and editors

120M+
Downloads

151
Countries delivered to

Our authors are among the
Top 1%
most cited scientists

12.2%
Contributors from top 500 universities

Interested in publishing with us?
Contact book.department@intechopen.com

Numbers displayed above are based on latest data collected.
For more information visit www.intechopen.com

Meet the editor

Amar Patnaik is an Associate Professor of the Mechanical Engineering Department at MNIT Jaipur, India. Previously, he served as an Assistant Professor at NIT Hamirpur, India. He earned his PhD in the field of Composite Materials (2009) at NIT Rourkela, India. He has more than 10 years of teaching experience and has taught a broad spectrum of courses related to mechanical engineering. He has published more than 180 SCI indexed journal articles in the field of polymers, metals and ceramic composites, biomaterials, and coatings with 7 Indian patents. He has also published about 10 book chapters in the area of advanced materials and has presented at least 70 talks at national and international meetings. Dr. Patnaik is a life member of various technical societies.

Contents

Preface

Over the last few decades, incorporation of fillers in composites has acquired an important place in commercial applications. Initially, these fillers were generally composed of cheap, easily available diluents and were entitled as fillers. However, their ability to tailor the properties of final material has burgeoned and that's why these filler-based composites find different applications in today's fast-growing world. Various organic and inorganic fillers are utilized in composites to enhance the properties and simultaneously reduce the cost of materials. Particulate fillers are responsible for delivering many advantages, namely cost reduction, improved processing, density control, thermal properties, electrical properties, flame retardancy, enhanced mechanical properties, and wear resistance.

This book embraces all the chapters that are concerned with the effect of incorporating different fillers or particulates on fabricated composites. It delivers a comprehensive study associated with the sections of material science, polymer technology, anisotropic elasticity phenomena, fracture mechanics, applied mechanics, material synthesis, mechanical and thermomechanical characteristics, tribological behavior, etc.

Significant research efforts all around the world are continuing to explore the properties of composite materials. Researchers are collectively focusing their efforts on the use of particulate fillers in composites for miscellaneous applications. To ensure a sustainable future, the use of fillers is the best solution to improve the properties and reduce the ultimate cost of materials. This book is solely focused on fillers, and some of the important topics include but are not limited to synthesis, characterization, and application of organic and inorganic particulate-filled composites.

Several critical issues and suggestions for future work are comprehensively discussed in this book with the hope that it will provide a deep insight into the state of the art of fillers. I would like to thank the publisher and Ms. Maja Bozicevic for invaluable help in the organization of the editing process. Next, a special thanks go to those who invested their time and effort in the compilation of the material that became this book. Many authors who contributed their expertise and perspectives are clearly the backbone of this work and they deserve the lion's share of the commendations.

Dr. Amar Patnaik
Malaviya National Institute of Technology,
Jaipur, India

Chapter 1

The Effects of Novel Additives Used in PVA/Starch Biohybrid Films

Eyyup Karaogul, Ertugrul Altuntas, Tufan Salan and Mehmet Hakki Alma

Abstract

The main aim of this chapter is to indicate the importance of additives and modifications used for PVA/starch biohybrid films. The additives and modifications used to improve the mechanical, thermal, and morphological properties of films are plasticizers, cross-linkers, fillers, physical and chemical treatment, and natural materials as well as thermoplastic starch. Plasticizers are preferred for higher molecular dynamism because of flexibility of functional groups in PVA and starch. Their flexibility is considerably affected by carboxyl and hydroxyl groups of plasticizers. The use of cofunctional groups increases the plasticity, flexibility, and physicochemical and mechanical properties of films. Moreover, cross-linking modifications are also effective to enhance the properties of biofilms. These modifications improve the tensile strength, modulus of elasticity, water resistance, thermal resistance, swelling behavior, and antibacterial activity of films. Fillers are also used to enhance the properties of PVA/starch films. In this way, the properties such as gas barrier, mechanical stiffness, transparency and thermal stability of the filler-added films are improved. The chemical and physical modifications provide stronger hydrogen bonds in films due to increasing carboxyl groups. Thus, the physical, biological, and chemical properties of films are improved because of the changing molecular structure via esterification, etherification, hydrogen bonding, and oxidation.

Keywords: PVA/starch biobased films, modifications, formation methods, physicochemical properties

1. Introduction

Petrochemical-based plastics are being replaced by biobased materials because of being widely eco-friendly. In the last decades, the biobased films have been investigated due to their biodegradability and for being suitable , generally obtainable, and less expensive materials in the industry. The plastics produced from petrochemical sources (e.g., polyesters and polyolefins) have been commonly used in the packaging industry due to their potential features. They are obtainable in large quantities and at low cost, displaying advantageous properties (i.e., good tensile strength, enriched barrier properties, and heat sealing) and applicability in the industry [1, 2]. However, these plastics are totally nonbiodegradable and

expose a serious ecological problem due to hydrophobic properties and very low water vapor transmission rate [2, 3]. The growing public interest on the environment is induced by a growing research on biohybrid films (i.e., biobased films) as alternatives to traditional nondegradable plastics due to the harmful effect of petroleum-based plastic packaging [4]. The eco-friendly polymeric resources can be categorized into three main groups depending on the raw material used: renewable natural, biodegradable synthetic polymers, and microbially produced biopolymers. The renewable natural polymers can be obtained from several sources such as starch, cellulose, chitosan, etc. [5], while biodegradable synthetic polymers such as polyvinyl alcohol, polycaprolactone, polylactic acid, polybutylene succinate, and copolymers are produced by using natural or petroleum-based monomers. On the other hand, microbially produced biobased polymers (e.g., polyhydroxybutyrate and valerate copolymer) are manufactured via various microorganisms.

Starch among all natural biopolymers has been believed to be one of the most suitable biopolymer resources due to its biodegradable, regularly available, and inexpensive features. There are two major polymers of starch: amylose and amylopectin. Amylose is a linear molecule with a spiral structure unlike a branched structure of amylopectin. Moreover, the molecular weight of amylose is commonly a smaller molecule (1–1.5 million), while amylopectin is a large molecule (50–500 million) [6]. Various starches have been used in the biohybrid films because of changing amylose/amylopectin ratio. And these are classified by amylopectin content [7]. In most studies, biobased films have been manufactured from starch of corn, wheat, rice, potato, tapioca, and cassava [8]. Various starch types have been also used to the biobased films because of changing amylose and amylopectin ratio [7–10].

However, the biobased films obtained from starch have demonstrated some disadvantages such as brittleness, low processability, high water sensitivity (i.e., low moisture resistance and hydrophilic character), and poor mechanical properties compared to petroleum-based conventional polymers [37]. Moreover, the starches are not thermoplastic biopolymers due to the intra- and intermolecular hydrogen bonds, because the degradation temperature of starch exceeds the melting temperature [11]. These make them inadequate for some packaging purposes limiting their widespread industrial applications [12–14]. Therefore, physicochemical and biological properties of the starch should be improved. Several modification techniques are needed to improve the mechanical and physical properties to overcome the inadequate features of the starch-based biobased films [15]. Thus, several efforts have been made to improve thermal properties of starch by blending with a plasticizer for its stability, elasticity, and edibility. Despite the above-mentioned modifications and applications, the biodegradable films produced from starch are still limited due to poor mechanical and hydrophilic properties along with susceptibility to the biological attacks. Accordingly, polyvinyl alcohol (PVA) known as synthetic biodegradable polymer and thermoplastic starch was utilized together to obtain excellent compatibility [16]. In several studies, starch was used with polyvinyl alcohol (PVA). As an example, various starches such as corn, potato, rice, and tapioca have been studied in combination with PVA polymers [9, 10].

PVA is an important polymer having superior gas barrier properties along with higher strength, tear, and flexibility than those of natural biobased polymers. Nevertheless, it has weak dimensional stability owing to high water uptake. Furthermore, PVA has relatively high manufacturing cost in comparison with the other commercial polymers in the market. Thus, if PVA is blended with renewable and abundant natural sources like starch, the manufacturing costs can be reduced. This method also resulted in improved moisture resistance and rapid biodegradation [17, 18].

Over the last 10 years, hundreds of studies about PVA/starch biobased films have been carried out on the topic using various production techniques. The researchers

used the PVA and starch together for the purpose of exposing their superior properties and eliminating the poor properties. The main aim of this chapter was to investigate the effects of additives and modifications on the several properties of various novel additives on the PVA/starch-based biodegradable hybrid films. Moreover, the review of the studies was explained in a molecular chemistry point of view in the specific subheadings. So, the results obtained from the literature have been evaluated based on the effect of different novel additives on the several properties of PVA/starch-based biodegradable films.

2. Formation of PVA/starch films

PVA/starch-based biodegradable formulations are produced from polyvinyl alcohol (PVA) and starch known as main compositions with different additives such as plasticizer, cross-linkers, and filing materials. Until now, PVA/starch blend biobased films have been prepared using casting (sol-gel or mixing) and thermal (extruder or extrusion) methods by many researchers in the literature.

In casting method, PVA is dissolved in hot water with the gelatinized starch in order to form intermolecular interaction. The obtained mixture is then stirred in a mechanical high-speed mixer for homogenization [19] over 1000 rpm/min and at 85–95°C temperature, and then some of the additives are added into the mixture under continuous stirring. After removing the bubbles formed during the preparation of biobased films by an aspirator, it is dried at room temperature [20]. The hybrid films are generally heated in an oven at 80–95°C for 1 h to induce the cross-linking reactions [21]. Another approach for the fabrication of PVA/starch blend biobased films is using a single or twin screw extruders. Primarily, the plasticizing starch is mechanically mixed with PVA, and then, PVA/starch blend granules are obtained following the extrusion process under the optimum conditions at various temperature and screw speeds. After that, the biobased films are obtained from the prepared granules by using the blown film extrusion or hot-press molding [4, 22].

In casting method, considerable amounts of water are evaporated from aqueous solutions or suspensions with a high energy-consuming process to obtain PVA/starch hybrid films [23]. The PVA/starch blends are generally produced via solution casting method. Nevertheless, this method has several deficiencies such as low solution density, low manufacturing yield, high energy consumption, etc., which limit its industrial practices [19]. On the other hand, the extrusion films have a great importance due to energy-efficiency process, high productivity, and continuous industrial production possibilities. However, the solution casting method has gained much more attention compared to extrusion process for the production of PVA/starch blend films in scientific publications due to its easy applicability in laboratories [4, 23, 24].

3. Use of additives and modifications in PVA/starch biobased formulations

Various additives such as plasticizers (e.g., glycerol and sorbitol), cross-linkers (e.g., glutaraldehyde and epichlorohydrin), fillers (e.g., silicium dioxide and calcium carbonate), and natural raw materials (e.g., cellulose and chitosan) as well as thermoplastic starch have been used to improve the mechanical, thermal, and morphological properties of PVA/starch-based biodegradable hybrid films. Furthermore, a variety of methods including esterification, oxidation, and etherification were applied in order to modify the starch [25]. These novel additives and the

modifications have been discussed under the following subheadings as plasticizers, cross-linkers, fillers, and chemical and physical modifications.

3.1 Plasticizers

Plasticizers are additives that increase the elasticity. These are the ingredients for nonthermoplastic starch, which are added in order to alter their physical properties. Plasticization takes place in the amorphous zone, which has a higher molecular dynamism. The type and the amount of plasticizer have an important influence on the ability to hinder hydrogen bonding along the polymer chains. The major gain obtained from utilization of plasticizers is that the tensile strength (TS) is decreased, while the elongation at break (E%) increases as well as they become more flexible [26]. One of the most important properties of an efficient plasticizer is to be compatible with the polymer matrix. The plasticizers such as glycerol, polyethylene glycol, urea, ascorbic acid, sorbitol, citric acid, and tartaric acid are usually used [19]. However, the plasticizers in the biobased films cause an increase in permeability to moisture, oxygen, and aromatic compounds [27]. **Table 1** presents the various plasticizers and used methods along with the effects of plasticization on some properties of PVA/starch films.

Water is accepted as a basic plasticizer for PVA/starch biofilms. Physicochemical properties of films could differ based on the changing water content. At the same time, the water is also compatible with other plasticizers. When the plasticizers are added into biofilm formulations, the physical properties are affected due to the increasing relative moisture because of compatibility with water. Possibly, water is absorbed because of polarity compliance to the solubility of other plasticizers added as additives. The plasticizer effect of water could usually be effective when it is used also together or not with an above-mentioned plasticizer. Furthermore, glycerol, sorbitol, and citric acid are generally favored as an efficient plasticizer for PVA/starch films. According to previous studies, the E% increased while TS decreased because of increasing glycerol, sorbitol, and citric acid ratio from 10 to 50% in the biobased films. It was also reported that E% and TS of sorbitol or citric acid–added films were higher than those of the glycerol-added films. However, the water absorption property of the biobased film decreased with the increasing glycerol ratio due to its hydrophobicity [29]. Moreover, the swelling behavior of the film containing glycerol was the lowest compared to the sorbitol- and citric acid-added films due to weaker hydrogen bonding capabilities, unlike the solubility value due to weaker hydrogen bonding capable [8].

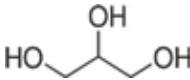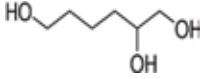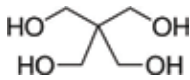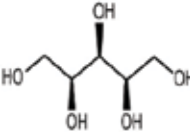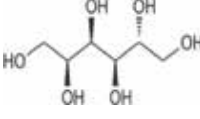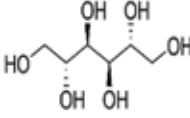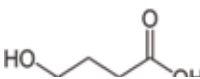| Plasticizers added	Characteristics of PVA/starch film and obtained improvement	Processing method	Reference
Water	A large decrease in tensile strength in all the tested films was recorded when the storage relative humidity increased from 15% to 33%.	Casting	[8]
Glycerol	E% increased while TS decreased. TS, E%, swelling behavior, and degree of the compatibility with PVA and starch were lower compared to sorbitol and citric acid. However, solubility was higher.	Casting	[8]
Urea	It had a good interaction, homogeneity, and sensitivity to the water with PVA and starch in comparison with glycerol and sorbitol.	Casting	[28]
Formamide	It was not a good plasticizer and could not improve the compatibility and flexibility of the blend. It exhibited synergistic effects and the compatibility, especially E%, with simultaneously added urea in the blend.	Casting	[19]

Table 1.
Effect of plasticization on some characteristics of PVA/starch films along with obtained improvements.

The homogeneity of PVA/starch biobased films could also be enhanced with the addition of urea, like glycerol. However, urea as a plasticizer showed stronger interactions with starch and PVA in biofilms than those of glycerol and sorbitol [11, 28]. Consequently, urea was considered a better plasticizer to improve the flexibility of PVA/starch films [19]. Furthermore, the crystallinity of biobased films was also decreased by the addition of urea and formamide. These agents could penetrate into the crystallization zone of PVA/starch biobased films during the process forming new hydrogen bonds with starch and PVA molecules, which damage the crystal region of PVA in the biobased films. However, formamide is not a good plasticizer and could not develop the compatibility and flexibility of the biobased films, while the compatibility was improved when it combined with urea. When the additives containing both urea and formamide are simultaneously used, their synergistic effects and the compatibility could occur in the blend. Besides, while TS and young modulus of biobased films were significantly decreased, the E% was substantially improved. With the increasing amount of urea in the biobased films, the sensitivity to water increased, while the melting point of blends decreased. It was likely due to the facilitation of molecular ability of both urea and formamide as a plasticizer [19].

3.2 Effects of functional group type and number of plasticizers on the properties of biobased films

Physicochemical properties of blend films are substantially affected by the functional groups of plasticizers used in PVA/starch biobased films. The total number of both carboxyl and hydroxyl groups in plasticizers were given in **Table 2** along with their behaviors in films. For instance, as regards the hydroxyl and carboxyl groups of glycerol (H.3, C.0) and succinic acid (H.0, C.2), the E% of the glycerol-added film has shown a high enhancement than that of the films containing succinic acid, contrarily to the TS behavior. However, when malic acid (H.1, C.2) in the same carboxyl number with succinic acid (H.0, C.2) was added to the film, the TS and E% were improved compared to glycerol (H.3, C.0) and sorbitol (H.6, C.0) because of the presence of two functional groups. Depending on the increasing functional groups of plasticizer, TS and E% of tartaric acid (H.2, C.2) added biobased films with two same functional groups were greater than those of malic acid, glycerol, and sorbitol [6, 30]. Furthermore, the biobased films containing citric acid (H.1, C.3) were stronger and more flexible than that of containing glycerol [7, 30] and xylitol (H.5, C.0) [31]. On the other hand, when the glycerol and xylitol added films were compared, it was found that xylitol-added biobased films had a higher strength and more elasticity than glycerol-added biobased films due to its 5 hydroxyl groups [31]. Even a few xylitol molecules can play an extra role in plasticizer than others [32]. Similarly, the comparison of glycerol- and sorbitol-added films showed that TS and E% of sorbitol-added film were greater than glycerol [7, 30]. Consequently, E% value increases while TS decreases with an increase in the total functional groups and the amount of these plasticizers in blend films.

The concept of plasticization could be understood with the analysis of different properties such as elongation at break (mentioned above) or glass transition point (Tg). For instance, Aydin et al. reported that the addition of plasticizers reduced the Tg point clearly and the change of plasticizing performances could be observed by increasing Tg point. Apart from the above-mentioned plasticizers, 1,4-Butanediol (H.2, C.0), 1,2,6-Hexanetriol (H.3, C.0), pentaerythritol (H.4, C.0), xylitol (H.5, C.0), and mannitol (H.6, C.0) from 2 to 6 hydroxyl groups have also been investigated based on the changes in Tg point. Among the investigated plasticizers, 1,4-butanediol demonstrated the maximum plasticizing effect for starch and PVA due to small molecular size and geometry [32]. **Table 2** shows the effects of the various plasticizers with different functional groups and number on the properties of PVA/starch films.

Plasticizer added	PVA/starch film characteristics and obtained improvement	Funct. groups		Formula	Reference
		H[1]	C[2]		
		Numbers			
1,4-Butanediol	Among the investigated plasticizers with 2 and 6 hydroxyl groups, it showed the highest plasticizing effect for starch and PVA due to small molecular size and geometry.	2	—		[32]
Glycerol	The E% of the glycerol-added film was higher than that of succinic acid on the contrary TS.	3	—		[6]
1,2,6-Hexanetriol	Further penetration into the chain fragment of starch and PVA was prevented because of their larger molecular geometry.	3	—		[32]
Pentaerythritol	Due to molecular size and geometry, its plasticizer efficiency was generally lower than 1,4-butanediol, 1,2,6-Hexanetriol, xylitol, and mannitol.	4	—		[32]
Xylitol	Compared to the glycerol, its TS and E% had more potential[1]. However, after its continuous addition, penetration capability into molecular chains tended to be lower[2].	5	—		1[31], 2[32]
Sorbitol	Mechanical properties of sorbitol-added films were higher than those of glycerol-added films.	6	—		[30]
Mannitol	It can enhance the thermal stability.	6	—		[32]
Succinic acid	It is too fragile to be used in applications	—	2		[6]
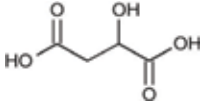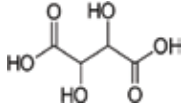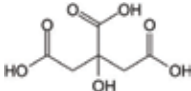
Plasticizer added	PVA/starch film characteristics and obtained improvement	Funct. groups		Formula	Reference
		H[1]	C[2]		
		Numbers			
Malic acid	It has a good effect on the TS and E% than those of glycerol, sorbitol, and succinic acid due to both hydroxyl and carboxyl groups.	1	2		[6, 30]
Tartaric acid	Compared to malic acid, glycerol, and sorbitol, it had a higher TS and E%.	2	2		
Citric acid	Due to hydroxyl and carboxyl groups, its TS and E% were stronger than those of glycerol and xylitol.	1	3		[31]

Table 2.
Effect of functional group type and number on the plasticization in PVA/starch films.

The different plasticizing effect of xylitol and mannitol was attributed to lower penetration capability. Due to larger molecular geometry and size of 1,2,6-Hexanetriol and pentaerythritol, further penetration into the chain fragment of starch and PVA was prevented. Moreover, the plasticizer efficiency of pentaerythritol was generally lower than that of 1,4-butanediol, 1,2,6-Hexanetriol, xylitol, and mannitol. Consequently, the increase in hydroxyl groups and molecular size of the plasticizers such as mannitol caused an improvement in the thermomechanical stability on the contrary of xylitol. For example, the maximum amount of mannitol (due to more hydroxyl number) in the films tends to interact more with the blend, on the contrary, with lower hydroxyl number plasticizers [32]. Based on the literature data obtained, it could be expressed that the molecular structure and geometry of plasticizers could inhibit or support their penetration into the molecular chain segments and reduce or increase inter- and intramolecular interactions, although the number of hydroxyl groups of plasticizers is hydrogen bonding quarters for starch and PVA.

The presence of two type of functional groups could also significantly influence other properties of biobased films. For instance, the citric acid could improve the water stability and inhibit degradation of starch molecules [15]. Due to the very strong interaction of water with glycerol and sorbitol, the solubility values were higher than the plasticizer with carboxyl groups. While the solubility of tartaric and citric acids was easy in water, their solubility value was lower than that of glycerol and sorbitol [7]. Eventually, the degree of swelling and mechanical properties of biofilms could decrease or increase slightly with the increasing content of plasticizer depending on functional groups [30]. However, the degree of swelling of the films without plasticizer was higher than that of films containing additives, while the solubility of films without plasticizer was lower [7].

3.3 Effect of plasticizers added simultaneously into biobased films

When the plasticizers having both hydroxyl and carboxyl groups were simultaneously added into the biobased films, their physicomechanical properties were better than those of plasticizers with only hydroxyl group-containing agents. Yoon et al. reported that as the additives containing both hydroxyl and carboxyl groups were simultaneously added into the formulation, the TS and %E were enhanced compared to the glycerol, having only hydroxyl groups. For instance, %E of the glycerol-succinic acid–added films increased, while only succinic acid–added film showed inadequate potential. The usage of the plasticizer composed of both hydroxyl and carboxyl groups could enhance the flexibility and strength. Moreover, the degree of swelling and solubility values of the comalic acid-/tartaric acid-added films were higher than those of coglycerol-/succinic acid-added films. [6]. This was because the hydroxyl (-OH) group number of malic acid-tartaric acid (7 hydroxyl number) was higher (i.e., having a more hydrophilic character) than glycerol-succinic acid mixture (5 hydroxyl number). %E of the glycerol or sorbitol-succinic acid–added films increased, while %E of succinic acid–added film decreased with increasing amount of additives. Nevertheless, TS of glycerol or sorbitol-succinic acid–added films decreased, while TS of succinic acid–added film diminished with increasing content of additive. The results of TS and %E mentioned above showed that using cohydroxyl/carboxyl group as a functional group increased physicochemical and mechanical properties of films [30]. Eventually, when the plasticizers having both hydroxyl and carboxyl groups were used simultaneously, TS and %E of the films were found to be better than the films containing plasticizer having only the hydroxyl group [7].

3.4 Cross-linkers

Cross-linking modification method is an effective and frequently applied approach to enhance the physicochemical and mechanical properties of PVA and starch [33]. Cross-linking can be carried out via treatment of granular starch using functional or multifunctional materials, which generated stable ether (R-O-R) or ester (R-CO-OR) linkages with the hydroxyl groups (-OH) in starch [9, 34]. Some of these multifunctional compounds are monosodium phosphate, sodium trimetaphosphate, sodium tripolyphosphate, epichlorohydrin, phosphoryl chloride, a mixture of adipic and acetic anhydrides, and a mixture of succinic anhydride and vinyl acetate. Cross-linker starch showed better compatibility and interaction with PVA than those of unmodified starch; such as, water absorption and TS of starch cross-linked films with sodium trimetaphosphate were higher than those of uncross-linked starch films, unlike E%. Moreover, weight loss in the soil of uncross-linked starch films was higher than that of the cross-linked starch films. Since the weight loss of starch under the soil is related to the amount of moisture, the use of cross-linked starch improves the water resistance of the biobased films [9].

When epichlorohydrin was used for cross-linking, the TS and %E of starch/PVA blend films increased. Thermal degradation of biofilms has been diminished by the cross-linker epichlorohydrin [35]. If sodium carbonate and sodium hexametaphosphate as the other cross-linkers are used, the equilibrium moisture content of the biofilms is significantly reduced by lowering their hydrophilic characteristic. Furthermore, these modifications increase the TS and modulus of elasticity of biofilms, unlike elongation at break [33].

In a study, the usage of sodium trimetaphosphate and sodium tripolyphosphate as the cross-linker enhanced the physicochemical properties such as swelling behavior compared to the uncross-linked starch [8]. Likewise, the swelling of the

biofilms was intensely reduced after utilization of cross-linker epoxidized natural rubber owing to the interaction between the mixtures. Thus, the hydrophilicity of the blend film decreases due to the reduction of the number of free hydroxyl groups in PVA and starch molecule. And, %E of film improves with the addition of cross-linker in blend polymer [36]. Singha and Kapoor have reported that the TS of PVA/starch cross-linked with glutaraldehyde has shown improvement. Moreover, modification with glutaraldehyde also improved the thermal stability of films. Moreover, their antibacterial activities against Gram-positive bacteria compared to Gram-negative bacteria indicated good resistance [15]. Additionally, borax can also be used as a cross-linker for starch and PVA. The enthalpy and crystallinity slightly decreased with increasing concentration of borax due to increasing cross-linking. Also, it improved the TS and %E of biobased films compared to the biobased films without cross-linker. Citric acid as another cross-linker can also be preferred for biobased films. This cross-linker decreases the water absorption of biobased films. So, citric acid also acts not only as a plasticizer but also as a cross-linker [29].

3.5 Fillers used in PVA/starch biobased films

Filled PVA/starch biobased films are the high-potential class of hybrid materials composed of filler incorporated into a biobased matrix [37]. With the aim to attain synergic effects, such a collaboration between environmental biopolymers and fillers is one of the most impressive ways to improve the features of this bioblends [38]. Because of the nature and the geometry of the filler, the properties of biobased films such as gas barrier, mechanical stiffness, transparency, and thermal stability have been enhanced [37, 39].

In a study, the use of silica as a filler has increased the TS of biobased films [40]. With the increase of silica amounts in blend film, the water absorption and water vapor transmission of starch have been decreased. This was due to the complex structure designed by links between silica and hydroxyl groups of starch and PVA. This phenomenon prevented the water molecules from dissolving and developed the water resistance of the biofilm. Furthermore, silica has also improved the compatibility between PVA and starch and formed a rigid structure. Even, according to SEM results, the low amount of silica has provided excellent diffusion and interaction between starch and PVA. On the other hand, filler silica has shown less effect on the biodegradability of the films because of decreasing microorganism penetration rate [9].

Nano-calcitine was preferred as a filler for PVA/starch film because of its positive effects on the physicochemical properties of blend films. As an example, the addition of nano-calcitine into blend film reduced the crystallinity, water solubility, biodegradability, and oxygen permeability. At the same time, it increased TS, limiting oxygen index, decomposition temperature, and water absorption [41]. Simultaneously, addition of nano-SiO_2/TiO_2/$CaCO_3$ into PVA/starch blends increased the TS of biofilms enhancing the interfacial adhesion through inter- and intramolecular interactions. With nano-TiO_2, an increase in clearness of biofilm was noticeably observed. However, water vapor permeability of biofilms containing nano-SiO_2 was lower than that of biofilms containing nano-TiO_2/$CaCO_3$ [4, 42]. Therewithal, TS and Young's modulus of biobased films were also increased with filler TiO_2 unlike E% [43].

Zirconium phosphate as another filling material had an attractive effect in the biobased films because of composing new hydrogen links. The addition of zirconium phosphate decreased the moisture uptake, while the degradation temperatures of biobased films increased [44]. The filler clay had an important effect on biobased films due to its hydrophilicity. The use of clay in biofilm increased TS and

heat resistance, enhanced the barrier properties to water vapor, and lowered glass transition temperature [24].

In PVA/starch biohybrid film, natural raw materials were also added as fillers such as cellulose nanofibers, chitosan, and feather keratin. In investigations, cellulose nanofibers blocked the recrystallization of starch by decreasing the mobility of polymer chains. Hence, the physicomechanical properties and crystal structure of blend film were significantly enhanced. In relation to this, storage conditions of biobased films improved. Cellulose nanofibers significantly enriched also the stiffness and strength of blend films by the storage conditions [34]. Similarly, the storage conditions of biobased films in natural weathering could be also enhanced by added graphene into PVA and starch [45]. Moreover, when the chitosan known as a natural filler was added to biofilms, their physicochemical properties such as TS, E%, water vapor permeability, and oxygen transmission rate improved. Also, water vapor and oxygen permeability, water uptake, and hydrophobic character of the chitosan-added bioblend film were better than biofilm without chitosan due to its incorporation [46]. As different inorganic salts are used in the biobased films, their crystalline [47], thermal, water vapor barrier, and mechanical properties can be significantly affected via strong hydrogen bonds. For this reason, Jiang et al. have reported that LiCl, $MgCl_2,6H_2O$, $CaCl_2$, and $AlCl_3,6H_2O$ salts have provided a good compatibility with PVA and starch [48, 49]. Moreover, the ZnO added biobased films have shown good dispersion, homogeneity, mechanical properties, and water resistance [49]. Another filler salt, $AlCl_3,6H_2O$, can show compatibility with PVA and starch. Hence, these salts have presented great destroying effect on the crystalline and good mechanical properties [50].

3.6 Chemical modifications

The chemical modifications applied to the biohybrid films produced from PVA and starch have improved their physical-biological-chemical properties because of the changing molecular structure of blend. For instance, the carboxyl group of PVA and starch has occurred in bioblend films after oxidation of starch with H_2SO_4 and $KMnO_4$. After the increase of polar carboxyl groups by oxidation, the hydrogen bonds in blend molecules were stronger than those of nonmodified ones. At the same time, their TS and E% have improved [44]. After modification, hydroxypropyl distarch phosphate converted from starch has shown highest TS and capability of retarding evaporation of water due to being compatible with fillers [4]. In another modification, PVA and starch blend grafted with methylmethacrylate had a higher E% and water desorption. For this reason, polysaccharide chain of starch and OH- groups of PVA are mostly occupied with monomers [51]. However, Yoon et al. depicted that TS increased on the contrary E% after using to blend film modified methylmethacrylate with acrylamide [31].

The plasma and irradiation treatment known as novel modification were also applied to PVA and starch blend films. These treatments can influence physicochemical properties of biohybrid films. Therefore, the treatment can cause a chemical bonding or graft functional groups on the PVA and starch backbone without any additives [52, 53]. Hence, the carbonyl groups of biofilms are improved with plasma treatment by using rotary argon plasma equipment. In addition, while E% of blend films can tolerate, its TS could also be lower. The plasma or irradiating pretreated with PVA and starch exhibited better thermal, processing, and mechanical (tensile) properties and toughness due to the induction of the cross-linking reaction [53]. With irradiated or plasma modifications, biofilms could prolong the storage conditions up to 15 days [54].

3.7 Physical modifications

Physical modification of PVA and starch could be safely used in biohybrid films. In generally, gelatinized, ungelatinized, fast and slow drying, varying amylose contents of raw material starch, changing of PVA and starch ratio, and impregnation of antioxidants were preferred in blend films for this modification. Applying physical modifications to biobased films affects significantly their physicomechanical properties. For example, gelatinized starch-polyvinyl alcohol blend films illustrate their uniformity of morphologies than the ungelatinized films, which corresponds well with the intensity of newly formed hydrogen bonds between starch, polyvinyl alcohol, and plasticizer. After the starch was gelatinized, the melting point of blend film decreased because of forming stronger hydrogen bonding interactions at an elevated preparation temperature [11]. At the same time, the gelatinized procedure is believed as a useful way to eliminate the crystalline structure [55]. In the fast (at 50°C) and slow (at 5°C) drying modification of the blend films, solubility, TS, E%, and degree of swelling values of the biobased films are preferable at slow drying than those of fast drying owing to the hydrogen bonding interaction forming at low temperature [56].

With increasing amylopectin contents of starch in blend film, the %E and Tg increased while TS decreased. The linear structure of amylose improved the tensile property of films (especially, the amount of elongation) and the degree of crystallinity. However, because of the amorphous structure of amylopectin, %E of blend film was lower. Increasing amylose ratio in blend film significantly increased %E values as it plays an important role in cross-linking [7]. Moreover, changing rates of PVA and starch illustrated important role in blend films. The TS of the film decreased with increasing starch content in PVA compared to pure PVA film [5]. At the same time, the crystallinity of PVA in blend film decreased importantly compared to pure PVA film. On the other hand, the water absorption of blend film increased with the increasing starch ratio, because the water absorption of PVA is weaker than that of starch [29].

The impregnation of antioxidants into the biofilm is another physical modification technique bringing antioxidative effect in biofilms. For instance, PVA/starch biofilms impregnated with catechin showed antioxidant and antimicrobial properties, while TS and %E of films decreased. Moreover, the biofilm containing catechin hinders lipid oxidation and microbial growth on raw meat during storage condition without substantial change in redness compared with commercial polyethylene pack [57].

4. Conclusion

PVA/starch biohybrid films are widely becoming an eco-friendly alternative to petrochemical-based plastics due to their biodegradability and for being suitable , generally obtainable, and less expensive materials. These biohybrid films have been obtained by using casting (sol-gel or mixing) and thermal processing (extruder or extrusion) methods. A great number of components in PVA/starch biobased films have been added to the matrix in order to improve physicochemical and mechanical properties. Moreover, various additives such as plasticizers, cross-linkers, fillers, and natural raw materials as well as thermoplastic starch have been used to improve the mechanical, thermal, and morphological properties of PVA/starch-based biodegradable hybrid films.

Plasticization in starch and PVA involves place in the amorphous area for higher molecular dynamism as well as their flexibility. Elasticity and other properties of biobased films are significantly affected by the functional groups (carboxyl and hydroxyl groups) of plasticizers. The using of cohydroxyl/carboxyl group as

a functional group increases the flexibility and physicochemical and mechanical properties of films. Cross-linking modifications in biobased films increase amorphous zone in molecular structure. This formation is effective to enhance the physicochemical and mechanical properties. These modifications improve the TS [2], modulus of elasticity [33], water resistance [49], thermal resistance [16], swelling behavior [8], and antibacterial activity of biofilms [15], unlike %E [2]. The filler in PVA/starch biobased films has a high potential class. Nature and the geometry of the filler-added biobased films have enhanced their properties such as gas barrier, mechanical stiffness, transparency, and thermal stability. The chemical modifications occur in the carboxyl group in molecular structure of PVA and starch because of oxidation. With increasing of carboxyl groups, the hydrogen bonds in biobased films were stronger than those of nonmodified ones. This stronger hydrogen bonding has improved physical-biological-chemical properties of biobased films because of the changing molecular structure of blend. Moreover, applied physical modifications to biobased films also significantly affect their physicomechanical properties. Consequently, these modifications applied to starch and PVA cause the esterification, etherification, hydrogen bonding, and oxidation in their molecular structure.

Author details

Eyyup Karaogul[1*], Ertugrul Altuntas[2], Tufan Salan[3] and Mehmet Hakki Alma[2]

1 Department of Food Engineering, Harran University, Sanliurfa, Turkey

2 Department of Forest Industry Engineering, Kahramanmaras Sutcu Imam University, Kahramanmaras, Turkey

3 Department of Materials Science and Engineering, Kahramanmaras Sutcu Imam University, Kahramanmaras, Turkey

*Address all correspondence to: eyyupkaraogul@gmail.com

IntechOpen

References

[1] Tharanathan RN. Biodegradable films and composite coatings: Past, present and future. Trends in Food Science and Technology. 2003;**14**(3):71-78. DOI: 10.1016/S0924-2244(02)00280-7

[2] Ismail H, Zaaba NF. Effect of additives on properties of polyvinyl alcohol (PVA)/tapioca starch biodegradable films. Polymer-Plastics Technology and Engineering. 2011;**50**(12):1214-1219. DOI: 10.1080/03602559.2011.566241

[3] Klingbeil M. Working Document of Biodegradable Waste Management. Brussels: European Commission; 2000

[4] Wang W, Zhang H, Dai Y, Hou H, Dong H. Effects of various nanomaterials on the properties of starch/poly(vinyl alcohol) composite films formed by blow extrusion process. Iranian Polymer Journal. 2015;**24**(8):687-696. DOI: 10.1007/s13726-015-0359-7

[5] Azahari NA, Othman N, Ismail H. Biodegradation studies of polyvinyl alcohol/corn starch blend films in solid and solution media. Journal of Physical Science. 2011;**22**(2):15-31

[6] Yoon SD, Chough SH, Park HR. Effects of additives with different functional groups on the physical properties of starch/PVA blend film. Journal of Applied Polymer Science. 2006;**100**(5):3733-3740. DOI: 10.1002/app.23303

[7] Yun YH, Yoon SD. Effect of amylose contents of starches on physical properties and biodegradability of starch/PVA-blended films. Polymer Bulletin. 2010;**64**(6):553-568. DOI: 10.1007/s00289-009-0158-4

[8] Lee WJ, Youn YN, Yun YH, Yoon SD. Physical properties of chemically

modified starch(RS4)/PVA blend films-Part 1. Journal of Polymers and the Environment. 2007;**15**(1):35-42. DOI: 10.1007/s10924-006-0040-5

[9] Ismail H, Zaaba NF. Effect of unmodified and modified sago starch on properties of (sago starch)/silica/PVA plastic films. Journal of Vinyl and Additive Technology. 2014;**20**(3):185-192. DOI: 10.1002/vnl.21344

[10] Ooi ZX, Ismail H, Abu Bakar A, Aziz NA. Effects of jackfruit waste flour on the properties of poly(vinyl alcohol) film. Journal of Vinyl and Additive Technology. 2011;**17**(3):198-208. DOI: 10.1002/vnl.20269

[11] Luo XG, Li JW, Lin XY. Effect of gelatinization and additives on morphology and thermal behavior of corn starch/PVA blend films. Carbohydrate Polymers. 2012;**90**(4):1595-1600. DOI: 10.1016/j.carbpol.2012.07.036

[12] John MJ, Thomas S. Biofibres and biocomposites. Carbohydrate Polymers. 2008;**71**(3):343-364

[13] Alves V, Costa N, Hilliou L, Larotonda F, Goncalves MP, Sereno A, et al. Design of biodegradable composite films for food packaging. Desalination. 2006;**199**(1-3):331-333

[14] Bastos DC, Santos AEF, da Silva MLJ, Simao RA. Hydrophobic corn starch thermoplastic films produced by plasma treatment. Ultramicroscopy. 2009;**109**(8):1089-1093

[15] Singha AS, Kapoor H. Effects of plasticizer/cross-linker on the mechanical and thermal properties of starch/PVA blends. Iranian Polymer Journal. 2014;**23**(8):655-662. DOI: 10.1007/s13726-014-0260-9

[16] Lum YH, Shaaban A, Mitan NMM, Dimin MF, Mohamad N, Hamid N,

et al. Characterization of urea encapsulated by biodegradable starch-PVA-glycerol. Journal of Polymers and the Environment. 2013;**21**(4):1083-1087. DOI: 10.1007/s10924-012-0552-0

[17] Han XZ, Chen S, Hu XG. Controlled-release fertilizer encapsulated by starch/polyvinyl alcohol coating. Desalination. 2009;**240**(1-3):21-26

[18] Russo MAL, O'Sullivan C, Rounsefell B, Halley PJ, Truss R, Clarke WP. The anaerobic degradability of thermoplastic starch: Polyvinyl alcohol blends: Potential biodegradable food packaging materials. Bioresource Technology. 2009;**100**(5):1705-1710

[19] Yan JA, Tian HF, Zhang YH, Xiang AM. Effect of urea and formamide plasticizers on starch/PVA bioblend sheets. Journal of Applied Polymer Science. 2015;**132**(33):1-8. DOI: Artn 4231110.1002/App.42311

[20] Priya B, Gupta VK, Pathania D, Singha AS. Synthesis, characterization and antibacterial activity of biodegradable starch/PVA composite films reinforced with cellulosic fibre. Carbohydrate Polymers. 2014;**109**:171-179

[21] Yao KH, Cai J, Liu M, Yu Y, Xiong HG, Tang SW, et al. Structure and properties of starch/PVA/nano-SiO2 hybrid films. Carbohydrate Polymers. 2011;**86**(4):1784-1789. DOI: 10.1016/j.carbpol.2011.07.008

[22] Julinova M, Dvorackova M, Kupec J, Hubackova J, Kopcilova M, Hoffmann J, et al. Influence of technological process on biodegradation of PVA/waxy starch blends in an aerobic and anaerobic environment. Journal of Polymers and the Environment. 2008;**16**(4):241-249. DOI: 10.1007/s10924-008-0109-4

[23] Thunwall M, Kuthanova V, Boldizar A, Rigdahl M. Film blowing of thermoplastic starch. Carbohydrate Polymers. 2008;**71**(4):583-590. DOI: 10.1016/j.carbpol.2007.07.001

[24] Gao W, Dong H, Hou H, Zhang H. Effects of clays with various hydrophilicities on properties of starch–clay nanocomposites by film blowing. Carbohydrate Polymers. 2012;**88**(1): 321-328. DOI: 10.1016/j.carbpol.2011.12.011

[25] Yun YH, Wee YJ, Byun HS, Yoon SD. Biodegradability of chemically modified starch (RS4)/PVA blend films: Part 2. Journal of Polymers and the Environment. 2008;**16**(1):12-18. DOI: 10.1007/s10924-008-0084-9

[26] Sothornvit R, Krochta JM. Plasticizer effect on mechanical properties of beta-lactoglobulin films. Journal of Food Engineering. 2001;**50**(3):149-155. DOI: Doi 10.1016/S0260-8774(00)00237-5

[27] Jimenez A, Fabra MJ, Talens P, Chiralt A. Edible and biodegradable starch films: A review. Food and Bioprocess Technology. 2012;**5**(6): 2058-2076. DOI: 10.1007/s11947-012-0835-4

[28] Ma XF, Yu JG, He K, Wang N. The effects of different plasticizers on the properties of thermoplastic starch as solid polymer electrolytes. Macromolecular Materials and Engineering. 2007;**292**(4):503-510. DOI: 10.1002/mame.200600445

[29] Zou GX, Ping-Qu J, Liang-Zou X. Extruded starch/PVA composites: Water resistance, thermal properties, and morphology. Journal of Elastomers and Plastics. 2008;**40**(4):303-316. DOI: 10.1177/0095244307085787

[30] Yun YH, Na YH, Yoon SD. Mechanical properties with the functional group of additives for starch/PVA blend film. Journal of Polymers

and the Environment. 2006;**14**(1):71-78. DOI: 10.1007/s10924-005-8709-8

[31] Yoon SD, Park MH, Byun HS. Mechanical and water barrier properties of starch/PVA composite films by adding nano-sized poly(methyl methacrylate-co-acrylamide) particles. Carbohydrate Polymers. 2012;**87**(1):676-686. DOI: 10.1016/j. carbpol.2011.08.046

[32] Aydin AA, Ilberg V. Effect of different polyol-based plasticizers on thermal properties of polyvinyl alcohol: Starch blends. Carbohydrate Polymers. 2016;**136**:441-448. DOI: 10.1016/j. carbpol.2015.08.093

[33] Liu Z, Dong Y, Men H, Jiang M, Tong J, Zhou J. Post-crosslinking modification of thermoplastic starch/ PVA blend films by using sodium hexametaphosphate. Carbohydrate Polymers. 2012;**89**(2):473-477. DOI: 10.1016/j.carbpol.2012.02.076

[34] Panaitescu DM, Frone AN, Ghiurea M, Chiulan I. Influence of storage conditions on starch/PVA films containing cellulose nanofibers. Industrial Crops and Products. 2015;**70**:170-177. DOI: 10.1016/j. indcrop.2015.03.028

[35] Kim DH, Na SK, Park JS, Yoon KJ, Ihm DW. Studies on the preparation of hydrolyzed starch-g-PAN (HSPAN)/ PVA blend films—Effect of the reaction with epichlorohydrin. European Polymer Journal. 2002;**38**(6):1199-1204. DOI: 10.1016/S0014-3057(01)00301-9

[36] Riyajan SA, Sukhlaaied W. Surface modification and swelling behavior of biodegradable polymer blends from PVA, starch and epoxidized natural rubber. KGK, Kautschuk Gummi Kunststoffe. 2012;**65**(9):30-34

[37] Ray SS, Okamoto M. Polymer/ layered silicate nanocomposites: A review from preparation to processing. Progress in Polymer Science. 2003;**28**(11):1539-1641. DOI: 10.1016/j. progpolymsci.2003.08.002

[38] Alexandre M, Dubois P. Polymer-layered silicate nanocomposites: Preparation, properties and uses of a new class of materials. Materials Science and Engineering R. 2000;**28**(1-2):1-63. DOI: Doi 10.1016/ S0927-796x(00)00012-7

[39] Gain O, Espuche E, Pollet E, Alexandre M, Dubois P. Gas barrier properties of poly(epsilon-caprolactone)/clay nanocomposites: Influence of the morphology and polymer/clay interactions. Journal of Polymer Science: Polymer Physics. 2005;**43**(2):205-214. DOI: 10.1002/ polb.20316

[40] Ismail H, Zaaba NF. The mechanical properties, water resistance and degradation behaviour of silica-filled sago starch/PVA plastic films. Journal of Elastomers and Plastics. 2014;**46**(1):96-U19. DOI: 10.1177/0095244312462163

[41] Kisku SK, Sarkar N, Dash S, Swain SK. Preparation of starch/PVA/CaCO3 nanobiocomposite films: Study of fire retardant, thermal resistant, gas barrier and biodegradable properties. Polymer-Plastics Technology and Engineering. 2014;**53**(16):1664-1670. DOI: 10.1080/03602559.2014.919650

[42] Tang S, Zou P, Xiong H, Tang H. Effect of nano-SiO2 on the performance of starch/polyvinyl alcohol blend films. Carbohydrate Polymers. 2008;**72**(3):521-526. DOI: 10.1016/j. carbpol.2007.09.019

[43] Sreekumar P, Al-Harthi MA, De S. Reinforcement of starch/polyvinyl alcohol blend using nano-titanium dioxide. Journal of Composite Materials. 2012;**46**(25):3181-3187. DOI: 10.1177/0021998312436998

[44] Yang YJ, Liu CH, Chang PR, Chen Y, Anderson DP, Stumborg M. Properties and structural characterization of oxidized starch/PVA/alpha-zirconium phosphate composites. Journal of Applied Polymer Science. 2010;**115**(2):1089-1097. DOI: 10.1002/app.31099

[45] Bin-Dahman OA, Jose J, Al-Harthi MA. Effect of natural weather aging on the properties of poly(vinyl alcohol)/starch/graphene nanocomposite. Starch-Starke. 2017;**69**(7-8):1600005

[46] Akter N, Khan RA, Tuhin MO, Haque ME, Nurnabi M, Parvin F, et al. Thermomechanical, barrier, and morphological properties of chitosan-reinforced starch-based biodegradable composite films. Journal of Thermoplastic Composite Materials. 2012;**27**(7):933-948. DOI: 10.1177/0892705712461512

[47] Jiang X, Luo Y, Hou L, Zhao Y. The effect of glycerol on the crystalline, thermal, and tensile properties of CaCl2-doped starch/PVA films. Polymer Composites. 2016;**37**(11):3191-3199. DOI: 10.1002/pc.23517

[48] Jiang X, Li H, Luo Y, Zhao Y, Hou L. Studies of the plasticizing effect of different hydrophilic inorganic salts on starch/poly (vinyl alcohol) films. International Journal of Biological Macromolecules. 2016;**82**:223-230. DOI: 10.1016/j.ijbiomac.2015.11.046

[49] Akhavan A, Khoylou F, Ataeivarjovi E. Preparation and characterization of gamma irradiated starch/PVA/ZnO nanocomposite films. Radiation Physics and Chemistry. 2017;**138**(Supplement C):49-53. DOI: 10.1016/j.radphyschem.2017.02.057

[50] Jiang X, Zhao Y, Hou L. The effect of glycerol on properties of chitosan/poly(vinyl alcohol) films with AlCl3·6H2O aqueous solution as the solvent for chitosan. Carbohydrate Polymers. 2016;**135**(Supplement C):191-198. DOI: 10.1016/j.carbpol.2015.08.094

[51] Parvin F, Rahman MA, Islam JMM, Khan MA, Saadat AHM. Preparation and characterization of starch/PVA blend for biodegradable packaging material. Multi-Functional Materials and Structures III. 2010;**123-125**: 351-354. DOI: 10.4028/www.scientific.net/AMR.123-125.351

[52] Zhai ML, Yoshii F, Kume T, Hashim K. Syntheses of PVA/starch grafted hydrogels by irradiation. Carbohydrate Polymers. 2002;**50**(3):295-303. DOI: 10.1016/S0144-8617(02)00031-0

[53] Yang SY, Huang CY. Plasma treatment for enhancing mechanical and thermal properties of biodegradable PVA/starch blends. Journal of Applied Polymer Science. 2008;**109**(4):2452-2459. DOI: 10.1002/app.28338

[54] Senna MM, El-Shahat HA, El-Naggar AWM. Characterization of gamma irradiated plasticized starch/poly(vinyl alcohol) (PLST/PVA) blends and their application as protected edible materials. Journal of Polymer Research. 2011;**18**(4):763-771. DOI: 10.1007/s10965-010-9473-6

[55] Chen P, Yu L, Simon GP, Liu X, Dean K, Chen L. Internal structures and phase-transitions of starch granules during gelatinization. Carbohydrate Polymers. 2011;**83**(4):1975-1983. DOI: 10.1016/j.carbpol.2010.11.001

[56] Park HR, Chough SH, Yun YH, Yoon SD. Properties of starch/PVA blend films containing citric acid as additive. Journal of Polymers and the Environment. 2005;**13**(4):375-382. DOI: 10.1007/s10924-005-5532-1

[57] Wu JG, Wang PJ, Chen SC. Antioxidant and antimicrobial effectiveness of catechin-impregnated PVA-starch film on red meat. Journal of Food Quality. 2010;**33**(6):780-801. DOI: 10.1111/j.1745-4557.2010.00350.x

Determining the Filler Activity in the Sintering of Pitch Composites

Vladimir Shmalko, Valeriia Karchakova, Oleh Zelenskyi and Fedir Cheshko

Abstract

Evaluation of the activity of fillers for sintering composites can be obtained from the results of testing the mechanical strength, in particular, the shear strength of pitch composites. The dependence of the strength of composites on the content of fillers is described by an extremum curve. At the point of maximum strength of the composites, the optimum ratio of components is realized. At this moment, the whole pitch matrix is in the interfacial layer on the surface of the filler particles. The contact angle of fillers wetting with binders is a necessary but not sufficient condition. The activity of the fillers with respect to the particular binder is characterized by the adhesive strength of the material obtained after carbonization of the "binder-filler" system. The activity of the fillers determines caking and sintering capacity of the pitch binders. It is shown that anthracite is the most active filler for the investigated pitches. Several methods for determining caking and sintering capacity of pitches are given. One of them is the determination of these indicators by the work of destroying the pitch composites. It is shown that fillers have a significant influence on the structure of the pitch matrix in composites.

Keywords: filler, activity, pitch, adhesion, sintering

1. Introduction

The properties of traditional materials, such as metals and their alloys, do not always allow, even with the most modern processing methods, to achieve such characteristics in strength, durability, and reliability, in order to provide the highest operational capabilities for a variety of designs and equipment. In areas such as missile technology, aviation, automotive, chemical industry, and many others, the optimum characteristics of materials have long been achieved through the use of composites [1]. The composites can be defined as materials that consist of two or more chemically and physically different phases separated by a distinct interface [2]. It is known that the structure of the matrix in composites is formed with a significant influence of the filler. The division of fillers into active and inert or active, semi-active, and inactive [3] is overly simplistic, since the activity of the filler is not its specific feature or fundamental property. Nevertheless, the activity of the filler, especially for sintering pitch composites, is a very important characteristic. The activity of the filler determines their behavior during sintering and the final properties of the composite.

The activity of the filler is mainly determined by three factors:

- The ratio between the adhesion energy of the matrix to the filler and the cohesive energy of the matrix [4].

- The amount of filler introduced.

- The degree of dispersion of the filler particles, which determines the area of the contact surface of the matrix with the filler. The particle size of the filler is the most important property that affects the hardening of the composite. For each type of binder and filler, there is an optimum degree of filling [5].

Filler activity refers to certain properties of the filled system. Therefore, the concepts of structural, kinetic, and thermodynamic activity were introduced [6].

The structural activity means the ability of the filler to change the molecular and supramolecular structures of the composites (the degree of crystallinity, the size and shape of the elements of the structure, etc.).

Kinetic activity is the ability of the filler to influence the mobility of certain kinetic units of the polymer, the relaxation processes, and the viscoelastic characteristics during the deformation of the composite.

Thermodynamic activity is the ability of the filler to influence the state of thermodynamic equilibrium, the phase, and thermodynamic parameters of the filled polymer.

The free surface energy of the filler particles has a basic value and determines the adhesion interaction and wettability of the surface. In this connection, the role of functional groups on the surface plays an important role and their reactivity [7].

Unfortunately, until now there is no single approach to measure the degree of activity of fillers. This is due, in particular, to the lack of theoretical developments for sintering composites, in which the adhesive strength varies with the sintering temperature. In the sintering of pitches with fillers, the cohesive strength of the cement matrix increases with carbonization, thereby increasing the adhesive strength of the composite. Since the basis of the activity of fillers is their adhesive interaction with the binder, it seems that the measure of their activity should be the methods of determining the adhesive strength.

The interaction of the filler with the binder is most often evaluated on the basis of wetting, while the quantitative characteristic is the wetting contact angle [8].

Wetting is the result of an adhesive interaction between the surface of the solid (filler) and the contacting liquid (binder). Quantitatively, adhesion is characterized by the work of adhesion, which is expressed by the equation of Dupree:

$$W_a = \gamma_L + \gamma_S + \gamma_{SL}, \tag{1}$$

where γ_L is the surface energy (tension) of the liquid phase, γ_S is the surface energy of the solid phase, γ_{SL} is the interfacial surface tension, and W_a is the work of adhesion. A rise in the interfacial attraction results in an increase in the work of adhesion. Eq. (1) can be rewritten to determine the work of cohesion *(W_c)* when the two phases are identical and no interface is present as shown in Eq. (2) for a solid phase:

$$W_c = 2\gamma_S \tag{2}$$

Adhesive strength—W_s—work of bond failure:

$$W_s = W_a + W_{def} \tag{3}$$

W_{def} can be very large and differs from W_a by n times.

The wetting contact angle (Young's equation) is associated with the work of adhesion W_a:

$$\cos\theta = 2\,W_a/W_c - 1 \qquad (4)$$

where W_a is the work of adhesion of the wetting liquid to the solid body and W_c is the wetting cohesion work.

Systems of pitch-carbon filler are very difficult to describe. The properties of the binders are always more detailed than the properties of the fillers. Usually, as a direct evaluation of the quality of the binder, the contact angle of surface wetting of the filler uses their adhesion interaction during mixing. The pitch filler systems are thermodynamically nonequilibrium, and the equilibrium contact angle in such a system is unattainable [9]. When describing composites, the binder properties are always paid more attention. Evaluation of the filler is more modest. Therefore, for pitch filler compositions, one can speak of an "apparent" contact wetting angle or of a "dynamic edge angle," as it is determined in some works [10].

The pitch matrix is a self-filled system that, when heated, even without an external filler, gives a solid residue (semicoke, coke), which can be considered as a dispersed-hardened system, i.e., as independent composite material with all the features of physicochemical and mechanical properties [5].

The wetting angle for the pitch filler compositions is determined by sessile drop, spreading drop, pendant drop, and other methods [11–13].

In addition to the wetting contact angle, the surface tension and capillary pressure are used as a quantitative evaluation of the filler-binder contact interaction [14].

The softening temperature determines its chemical composition, surface tension, viscosity, the particle size of the coke, its texture, chemical functional groups on the surface and porosity [15]. The final properties of carbonized pitch composites (e.g., electrodes designed for high current densities) are largely determined by the interaction of pitch with the filler surface. Pitch should penetrate into the pores of coke and fill the voids between the coke particles. It is believed that the wettability of coke by pitch is a direct indicator of the degree of their interaction. A good wetting of the filler surface with a pitch is a necessary, but insufficient, condition for a strong adhesion bond and high physical and mechanical properties of the resulting composite material.

Imperfection of existing estimates of binder-filler interaction leads to new attempts to assess the process of wetting fillers with pitch. In Ukraine, the technique [16] is used, according to which the determination of the wetting power of the pitch is carried out in metal or glass tubes into which the filler (coke) and pitch grains are loaded in a ratio of 15:5. The tubes loaded in this manner are placed in a laboratory electric oven, where they are kept for a certain time at a temperature of 200°C, which ensures the flowability of the test pitch, but does not lead to caking of the test coke. Then, the tubes are cooled and the coke is removed, not bound (not impregnated) with a pitch.

The wetting power (m) of pitch is calculated by the following formula:

$$m = m_{coke}/m_{pitch} \qquad (5)$$

where m is the mass of bound coke (the difference between the initial sample of coke (m_{coke}) and the removed part of the latter), g, and m_{pitch} is the initial mass of the pitch buried in the tube, g.

In the apparatus for determining wetting characteristics, according to the procedure of [17], granular coke 0.25–0.5 mm in size is placed in a cylinder on top of which a layer of solid pitch with a grain-size composition of 1–2 mm is applied. This composition is heat treated in a drying chamber with forced air supply at a predetermined temperature and a time of thermal aging.

The prototype of method [16] is the method for determining the sintering ability of coals [18]. Caking coal is used instead of pitch, and anthracite is used instead of coke. It should be noted that in the prototype, the determination temperature reaches 600°C, which has a decisive influence on the physics-chemistry of the processes taking place.

In our opinion, for pitches as caking binders, it is important to evaluate the adhesive strength of their contact with fillers. In this case, the activity of the fillers will be the "sintering strength" and/or the "sintering capacity" of the pitch [19].

By the strength characteristics of the pitch composites, quantitative estimates of the quality of pitch as a binder relative to the selected filler can be obtained, as well as evaluation of the activity of the fillers with respect to the selected pitch. It is assumed that the use of this approach will allow to determine the optimal mass ratios of the binder-filler. In this case, the transition of the pitch to a solid state must be irreversible. Only then will it fully reproduce the physicochemical processes of interaction between the binder and the filler that occur during the production of the composite.

2. Experiment

In our work, we used industrial pitches as binders. Pitch samples were taken in the production conditions of coke plants. The volume of the sample was up to 4 dm^3; the pitches were mixed, quartered, and sieved through a sieve to a laboratory sample with a fraction of 0.5–0.25 mm. **Table 1** presents their characteristics.

Characteristics	Pitch mark	
	V	**B₁**
Softening point, °C	85.0	72.0
Yield of volatiles, %	53.8	59.0
Quinoline insoluble, %	10.5	8.2
Toluene insoluble, %	33.2	28.2
Ash, %	0.11	0.13

Table 1.
Characteristics of the pitches that were used as a binder.

Samples	W^a	V^{daf}	A, %	d$_t$, g/cm^3	Elemental composition, %	
					C	H
Pitch coke (PC)	3.0	0.8	0.3	1.53	96.5	0.45
Shale coke (SC)	2.8	0.9	0.25	1.50	97.2	0.22
Shale coke > heated at 250 C (SC-T)	0.9	0.5	did not determine	2.0	did not determine	
Anthracite (A)	3.0	5.5	4.0	did not determine	94.0	4.1
Strained glass	0	0	did not determine	2.6	did not determine	
Washed sand	0	0		1.51		

Table 2.
Characteristics of the fillers.

We used both carbon and noncarbon fillers. All the fillers were crushed to the size of particles passing through a sieve with a size of 0.5–0.2 mm holes. **Table 2** gives an overview of the filler characteristics. These are pitch coke (PC), shale cokes (SC), and shale coke after heat treatment (SC-T), which we preheated for 2 hours at a temperature of 250°C to remove moisture. For comparison, we took hardened glass, washed bank-run sand, and anthracite.

3. Results and discussion

The photographs of the surface of the filler grains (**Figure 1**) clearly show the difference in their structure. For shale coke (**Figure 1a, b** and **e, f**), there are at least two types of structures: sponge (**Figure 1a**) and layered fibrous structures (**Figure 1b**). The grain sizes with a spongy structure in **Figure 1a** are about 180–450 μm, and the grains of shale coke with a layered structure are 100–300 microns in diameter and 800 μm in length. The thickness of the layers in the grains of the layered structure according to optical microscopy is <2–5 μm. The surface of the pitch coke grains is most rough with numerous pores (**Figure 1c, g** and **i**), which coincides with the data [20]. Lamellar anisotropic structures are visible on the pitch coke (**Figure 1g**). In the case of good wettability, the caking can give a strong adhesive bond and a significant proportion of adhesion due to the capillary penetration of the pitch in the pores of the filler.

The surface of anthracite grains is the smoothest. It is well visible that the surface is sometimes chipped with folded structures. Anthracite grains have a large variation in size from 20 μm to 100–160 μm. Anthracite dust is present on the surface of the grains in the photographs (**Figure 1d**).

Samples of composites for mechanical testing were prepared as follows. Mixtures of pitch and an inert filler (anthracite, sand, glass, pitch coke (PC), shale coke (SC), and shale coke after heat treatment (SC-T) at 250°C) in different proportions (from 1:1 to 15:1) are charged in cells of ceramic cassette (**Figure 1**), preliminarily placed in a special coking chamber (**Figure 2**). One loading of the cassette camera allows to receive 14 samples of char from the pitch composites. The heat input in the coking chamber was carried out from below, since radial heating of the cylindrical sample has a temperature gradient along the radius of the cylindrical charge—the outer layers of the charge in the coking chamber undergo heat treatment for a longer time than in the central part. With one-sided heating (from below), the temperature gradient in the loading of the coke composition is available in the height of the load. Therefore, semicoke samples of the pitch composite for mechanical testing had a gradient of strength in height, but in the fracture region, samples were prepared at the same temperature (500°C).

Isothermal aging at the final treatment temperature is designed to increase the homogeneity of the composite in the radial plane.

Mechanical test samples of solid residue from the pitch composites are carried out according to the procedure described in [4], using a cassette chamber (**Figure 2**).

Each semicoke sample of the pitch composite was placed in the test cell (**Figure 3**), and mechanical strength tests were carried out so that the fracture region of all samples was in the semicoke plane heated to a temperature of 500°C. All the samples in the fracture region had the same final heating temperature, and the strength of the semicoke sample of the pitch composite was determined in an isothermal layer.

We believe that since the strength of the coke (filler) is higher than that of the semicoke matrix, the destruction of the sample during our tests was mainly carried out on the pitch matrix (cohesive failure), and the filler grains were not destroyed.
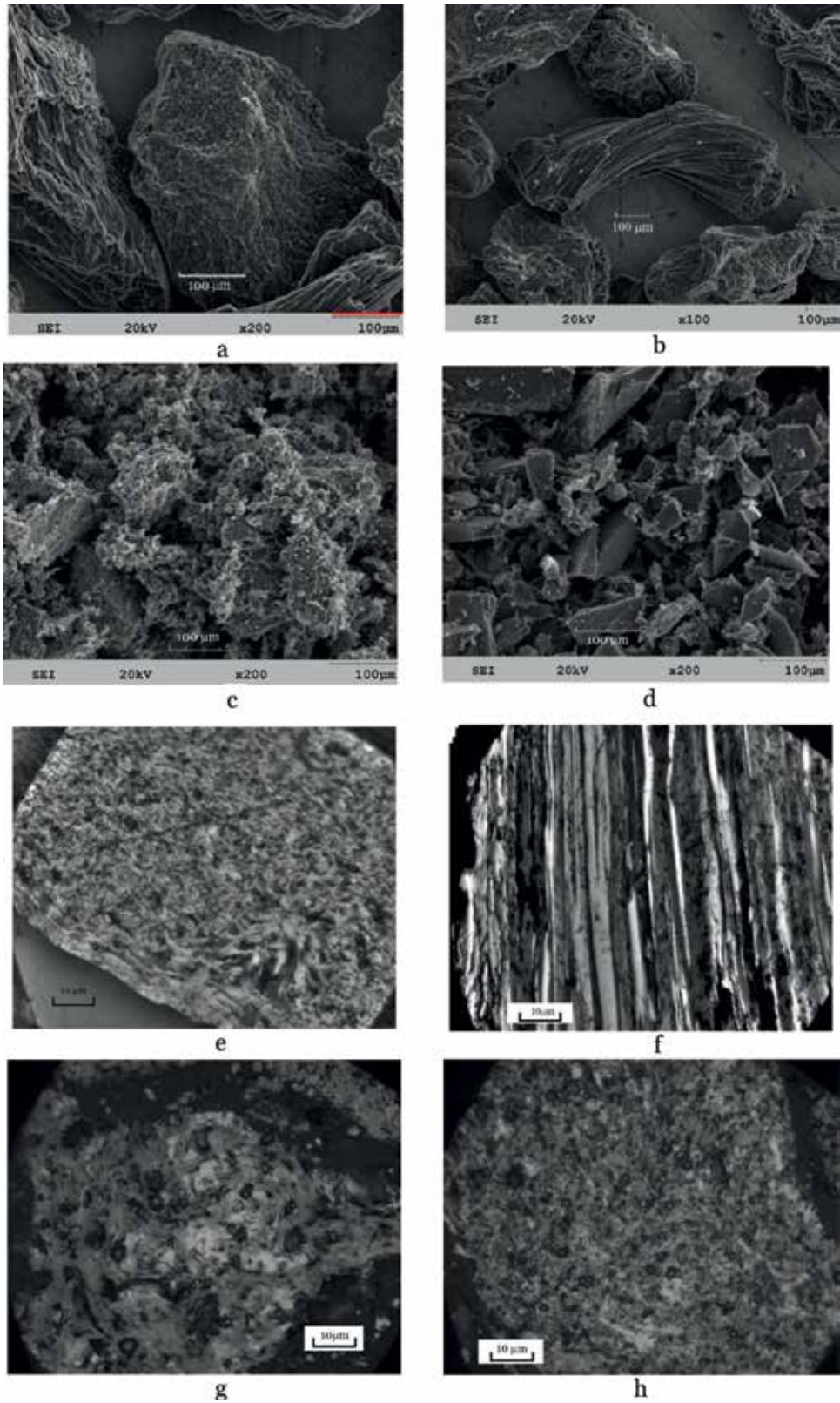
Figure 1.
Structure of filler surface (SEM): a – shale coke (×200); b – shale coke x 100); c – pitch coke (×200); d – anthracite (×200). Optical microscope, polarized light, ×500): e, f – shale coke; g, h – pitch coke.
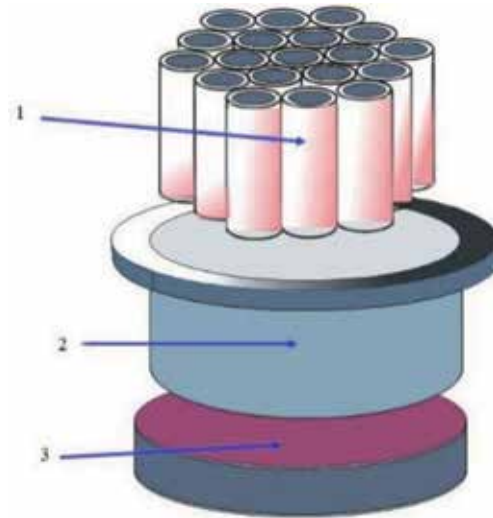
Figure 2.
Coking chamber for samples of pitch composites: 1 – cassette of ceramic cells; 2 – coking chamber; 3 – heater.
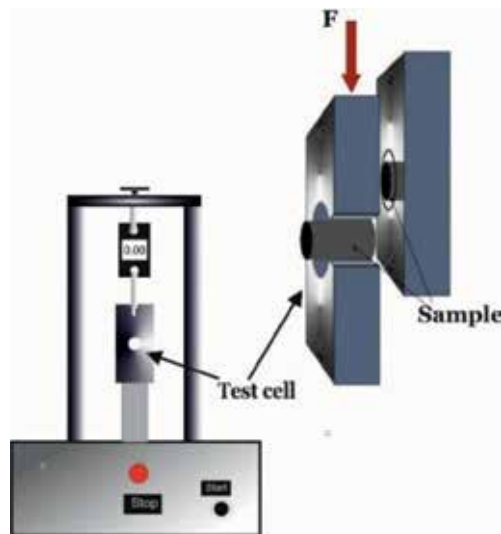
Figure 3.
Test machine and test cell for testing composite for strength.

3.1 Determining the filler activity by the positive root of the parabola equation, which describes the dependence of the pitch composite strength on the filler content

The dependence of the pitch composites of the semicoke's strength on the mass ratio of the pitch and filler is investigated. As a rule, an extreme dependence of the strength on the degree of filling was observed, characterized by the presence of a concentration maximum.

A second-order equation is a reasonable approximation. For all the equations, we calculate the discriminant and determine the roots.

Table 3 shows the equations of the second-order curves describing the dependence of the strength of the semicoke from the pitch composites on the composition

Fillers	Equation	R^2	Roots of equation	
			x_1	x_2
SC-T	$Y = -0.28x^2 + 2.80x + 54.42$	0.92	−9.81	19.81
SC	$Y = -3.69x^2 + 39.2x - 18.8$	0.90	0.5	10.1
PC	$Y = -1.33x^2 - 19.2x + 40.2$	0.76	1.86	16.29
Glass	$Y = -1.3x^2 + 17.9x + 2.02$	0.81	−0.1	13.9
Sand	$Y = -2.77x^2 + 34.1x - 23.6$	0.96	0.74	11.6
Anthracite	$Y = -2.58x^2 + 48.96x + 77.5$	0.96	−1.47	20.45

Table 3.
Strength of pitch composites depending on the filler.

of all the excipients that were tested, the roots of these equations x_1 and x_2, and the determination coefficients (R^2) of the interaction y = f(x).

We do not consider the negative values of the roots x_1 because they do not match the condition of the problem.

The physical meaning of the roots x_2 of the parabola equation is some hypothetical ratio of filler binding, in which the strength of the pitch composite falls to zero. The x_2 indicator can be used as an indicator of the activity of the filler. The higher the value of x_2, the greater the filler activity.

There is some physical meaning of the roots x_2 of the parabola equation. The x_2 indicator can be used as a measure of the activity of the filler or of the sintering ability of the pitch. The higher the value of x_2, the greater the activity of the filler is. That is, the more active the filler, the more its quantity will be agglomerating. By x_2, it is possible to rank the binders for the sintering ability to the fillers. The activity of the filler is the amount of the inverse sintering power of the pitch [21]. In accordance with this indicator, fillers are located (in descending order) in a row:

<p align="center">Anthracite—SC – T—PC—SC – glass—sand</p>

3.2 Determining filler activity by sintering ability

As an example, let us consider the curve for the change in strength of pitch composites with anthracite (**Figure 4**). The strength of the pitch composite increases (the left branch of the curve in **Figure 4**), because the high modulus filler reduces the ability of the entire composition to deform. With an increase in the degree of filling, the individual particles of the filler approach and their boundary (interphase) layers begin to interact with one another, forming a film structure of the matrix between the particles (**Figure 5a**).

We do not take into account here that individual particles in composites are rarely observed [22]. Since binders that solidify are typical nonequilibrium systems, the loss of stability leads to the spontaneous formation of primary clusters—a decrease in surface energy occurs due to a reduction in the interfacial surface and, as a consequence, aggregation of the filler particles. The filler particles on their surface have a layer of a pitch matrix, the so-called interfacial layer (IFL) [23]. There is no clear boundary between IFL and the pitch matrix, but it is established that IFL reduces the concentration of stresses on the surface of the matrix and filler, which affects deformation and fracture in composites [24]. The thickness of the interphase layer

depends on the radius of the filler particles and the fractal dimension of its surface [25]. At low filler concentrations in the matrix, the interphase layers are not an independent phase in the volume of the composite, which does not affect its properties.

Considering the fact that the interfacial layer is an oriented ordered structure, the film has enhanced strength compared to the structure of the remaining volume of the pitch matrix. At the critical point, the complete transition of the pitch matrix to the film structure of the IFL is the main factor of strength increasing of the pitch composites. In addition, the filler-binder ratio at this point is optimal, which corresponds to the maximum on the curve (**Figure 4**).

In the case of a critical binder-filler ratio, the pitch matrix is completely on the surface of the filler particles in a structured (interfacial) layer (**Figure 5a**). The activity of the filler is maximum. With a further increase in the content of the filler in the composite (the right branch of the curve in **Figure 4**), the activity of the filler does not decrease, but the pitch matrix cannot cover the entire surface of the filler grains. The film is not enough to cover the entire surface of the filler grains. The binder film is divided into separate fragments (**Figure 5b**), which is accompanied by a sharp decrease in the strength of the final composite. In this consideration, we do not take into account the effect of agglomeration of filler particles.

Although the amount of the matrix and probably its cohesive strength does not change, the strength of the composite decreases. The strength of the matrix on the surface of the filler particles can be another indicator of the activity of the filler.

In the actual conditions of formation of the contact surface of the filler with a liquid binder, the processes of diffusion of the adhesive into the filler play an important role. A part of the pitch can penetrate into the surface layer of the filler due to capillary phenomena.

The removal of volatile substances from the pitch when carbonized leads to the appearance of shrinkage stresses and defects and, as a result, to rupture the film. That is, a pitch that is carbonized to the semicoke state may not completely cover the filler surface and not create a continuous "carbon skeleton," the ideas of which were previously expressed [26].
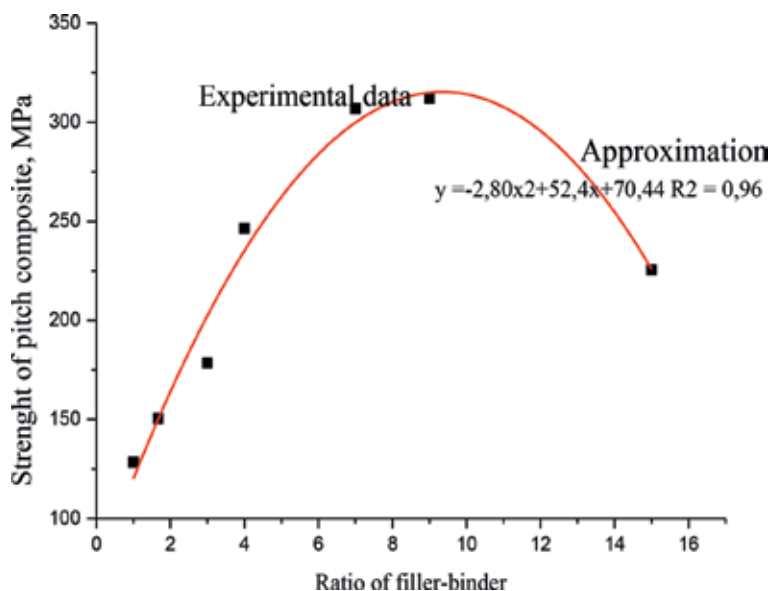

Figure 4.
Experimental points and approximation by the parabola equation for the dependence of the strength of a pitch composite on the amount of filler (anthracite) in it.
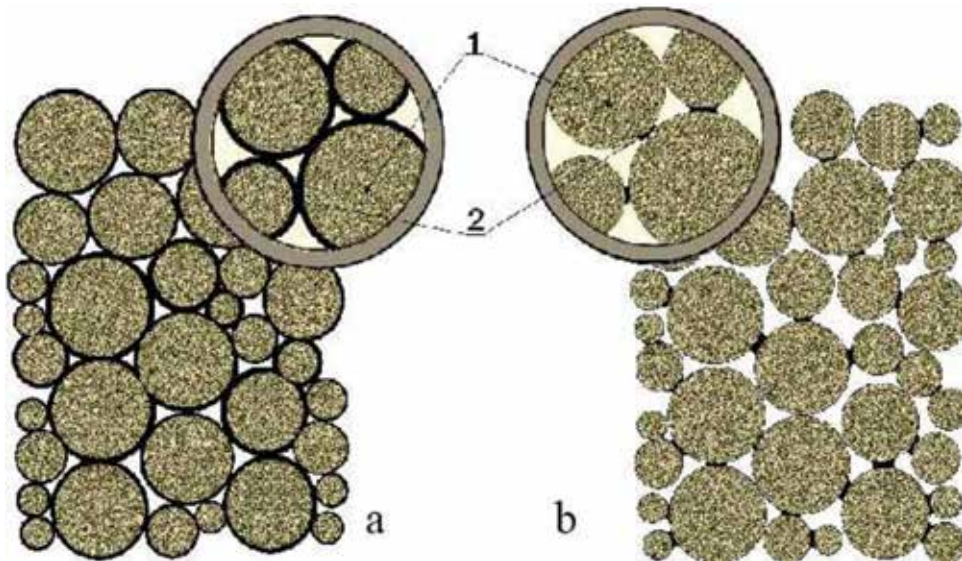
Figure 5.
The microstructure model of the pitch composite: a – a binder in the film on the surface of the filler; b – with pitch deficit: 1 – filler particles, 2 – semi-coke of the matrix.

3.3 Determining filler activity by cohesive strength of the pitch matrix film on the filler surface

Another way to determine the activity of the filler is determining the cohesive strength of the pitch composite in the film state on the filler surface. The more active the filler with respect to the pitch binder, the more IFL is structured on the surface of the filler and, correspondingly, the higher its strength.

We solved the problem of determining the strength of the matrix in the film as follows.

In the filling region, which is characterized by the falling section of the curve of the dependence of the strength of the composite on the degree of its filling (**Figure 4**), the strength of the pitch matrix does not change, despite the reduction in the overall strength of the pitch composite. The loss of strength curve in this descending section is approximated by a straight line:

$$y = b - ax \qquad (6)$$

where y is the strength of the composite and x is the filler content. One can estimate the strength of the "film" pitch matrix by extrapolating this linear dependence on the ordinate axis, which gives the value of the strength of the semicoke of the pitch matrix (film) without the filler (for x = 0). The extrapolation value obtained by extrapolation at zero fill (σ_0) (**Figure 6**) is simultaneously a measure of the activity of the filler and at the same time can serve as a measure of the sinter ability of the pitch.

The sintering thus determined is an indicator of the peculiarity of the pitch to a specific filler. The same pitch with another filler will have a different sintering, because the sintering process depends on the nature of the filler and its physical–chemical interactions with the binder. **Figure 6** shows the variant of approximation of the falling part of the curve of the strength of the pitch composite on the content of coke in it.

In order to compare the pitch with each other, you can enter the parameters of sintering and sinter ability with respect to the filler standard, for example,
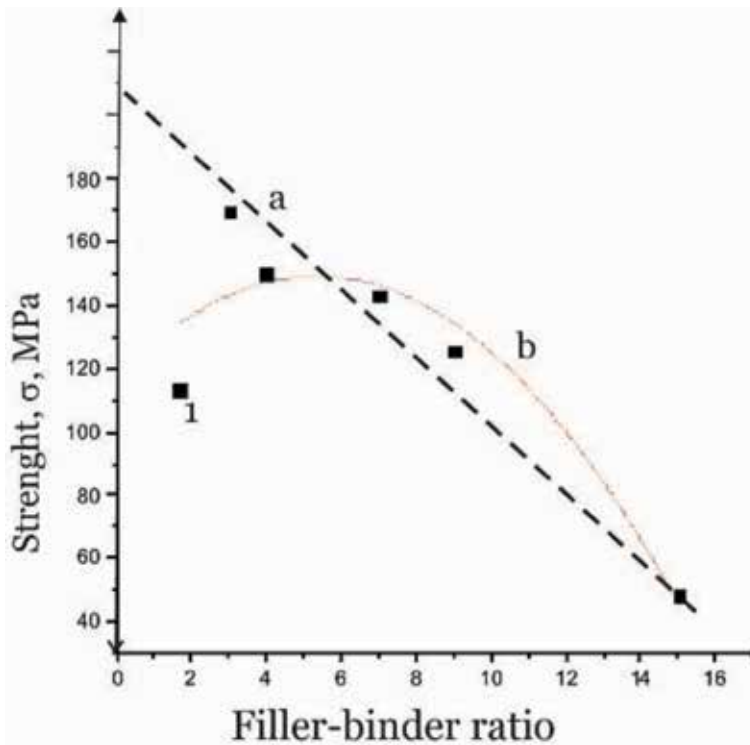
Figure 6.
Approximation of the falling branch of the dependence of the strength of the pitch composite with the coke by a straight line.

anthracite. By the way, anthracite, as a standard, is used to estimate coal by sintering in works [27, 28].

Testing the strength of a semicoke from pitch without filler cannot give an estimate of the pitch sintering. The reason is that when the pitch is heated and sintered during solidification, the solids are formed, which in fact play the role of the filler, which is unevenly distributed in volume. Therefore, such a semicoke is heterogeneous in terms of physical and mechanical properties [29]. In addition, the sintered material contains an uncontrolled amount of pores, which are, in essence, a low modulus filler.

Monitoring of the quality of the B1 (softening point 72°C) and V (softening point 86°C) at the factory (**Tables 4** and **5**) showed that the sinterability (σ_0) of the pitches was significantly higher than the other indicators' quality for these pitches. This means that it is more sensitive than the rest (the error in determining σ_0 is 5%). As a coefficient of measure, free term of the equation (**Table 4** of Eqs. (1)–(6) and **Table 5** of Eqs. (1)–(7)) is adopted. The physical meaning of the free term of these equations is the strength of the semicoke of the pitch film in the absence of the addition of a filler when x = 0.

3.4 Determining filler activity by work of destruction of pitch composite

The area under the dependence curve of the strength of semicoke samples from composites is an integral characteristic—the work of destruction. The term "work of destruction" is used in the physics of polymers [30, 31]. The work of destruction, in fact, is the energy used to overcome the forces of grip (in our case, the sintering) between the pitch matrix and the filler, so this figure can be taken as a measure

№	Softening point °C	V^{daf}, %	Viscosity, $\eta_{140\,Pa*c}$	Wetting power by [16], m	Equation
1	72	58.1	1.51	1.47	y = 78.2–3.4x
2	72	58	1.48	1.43	y = 132.7–5.8x
3	72	58.1	1.37	1.48	y = 146.9–6.9x
4	72	57	1.37	1.37	y = 192.6–10.3x
5	72	57.7	1.42	1.55	y = 83.8–3.8x
6	72	57.5	1.58	1.28	y = 115.8–6.9x

Table 4.
Results of monitoring quality for pitch B₁.

№	Softening point °C	V^{daf}, %	Viscosity, $\eta_{140\,Pa*c}$	Wetting power by [16], m	Equation
1	85	53	2.89	0.8	y = 206.8–11.6x
2	87	53	3.97	0.785	y = 207.8–9.8x
3	86	53	3.96	0.86	y = 263.0–21.7x
4	86	53.8	3.29	0.94	y = 263.0–21.6x
5	86.5	53.7	3.88	0.9	y = 150.3–8.6x
6	86	54.5	3.59	1.0	y = 345.8–31.3x
7	86	54.5	3.42	0.85	y = 275.2–21.3x

Table 5.
Results of monitoring quality for pitch V.

of the sintering ability of the pitch and filler activity. It seems that this definition of the term "sintered ability" has a definite physical content, in contrast to that adopted in coal chemistry: the sintered ability—the property to bake one or another amount of inert material [32].

Since we have a parabolic plot (**Figure 4**), the work of destruction (W, c.u.) will be equal to the area under the parabola:

$$W = \int_{x_1}^{x_2} (ax^2 + bx + c)\,dx \tag{7}$$

Eq. (7), after simple transformations, gives a formula for calculating the work of the destruction of pitch composites:

$$W = {}^a\!/_3\left(x_2^3 - x_1^3\right) + {}^b\!/_2\left(x_2^2 - x_1^2\right) + c\,(x_2 - x_1) \tag{8}$$

The coordinates of the maximum of the parabola with respect to Eq. (8) were constructed using the well-known equations.

The results of calculations of the destruction of pitch composites with different fillers are given in **Table 6**.

As follows from data of **Table 6** and diagrams of **Figure 7**, the greatest sintering ability of the studied pitch is in relation to anthracite, and the smallest—in relation to sand and glass. That is, adhesive interaction is the most potent in a pair of pitch-anthracite. Anthracite is the most active filler. In this regard, anthracite is the reference filler for assessing the sintering ability of coal, as it is customary in the Roga test [33].

Fillers	Coordinates of maximum		The work of destruction, W, cond. Units
	x_0	y_0	
SC-T	5.4	149.4	2417.5
SC	9.0	126.2	1602.3
Glass	8.0	64.0	646.6
Sand	6.3	88.7	498.1
Anthracte	9.4	315.6	4468.6

Table 6.
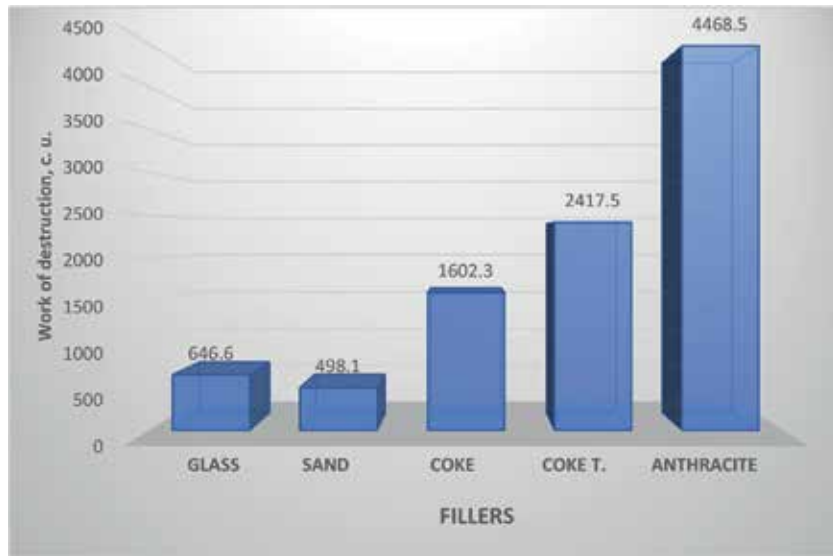*The work of the pitch composite destruction for various fillers.*

Figure 7.
The fillers activity by destruction work of pitch composite.

4. Conclusion

The generally accepted estimate of binders by the contact angle of wetting of the filler surface reflects only the initial stage of the adhesive interaction of the components of the composites. Wetting of fillers with binders is a necessary but not sufficient condition.

The activity of the fillers with respect to the particular binder is characterized by the adhesive strength of the material obtained after the carbonization of the "binder-filler" system. The activity of the fillers determines the sintering ability and sintering capacity of the pitch binders.

The external curve describes the dependence of the strength of composites on the content of fillers in them. Both step V and anthracite in the place of the extreme ratio of the filler-binder are 9:1, and the strength of the composite is 3,10 MPa. At this stage, the pitch matrix is in the interfacial layer on the surface of the filler particles. This optimal ratio is valid only for the given experimental conditions: temperature and grain size of the filler.

We show that anthracite is the most active filler for the resins under study. Some methods use anthracite as a reference filler to determine the sintering of coal and tar. Therefore, it can serve as a standard of activity in evaluating the activity of other fillers.

Acknowledgements

Author details

Vladimir Shmalko*, Valeriia Karchakova, Oleh Zelenskyi and Fedir Cheshko
SE "UKHIN", Ukrainian State Research Institute for Carbochemistry, Kharkiv, Ukraine

*Address all correspondence to: v.shmalko@gmail.com

IntechOpen

References

[1] Klárová. Composite Materials. Ostrava: Coursebook; 2015. 43 p

[2] Jose J, Malhotra S, Thomas S, Joseph K, Goda K, Sreekala M. In: Thomas S et al., editors. Advances in Polymer Composites: Macro- and Microcomposites – State of the Art, New Challenges, and Opportunities Introduction to Polymer Composites. Part One, Polymer Composites. Vol. 1. 1st ed. Wiley-VCH Verlag GmbH&C; 2012. 16 p

[3] Slusarski L, Zaborski M, Donnet JB. Activity of carbon black as a filler in different elastomeric matrices. Die Angewandte Makromolekulare Chemie. 1994;**222**:49-60. DOI: 10.1002/apmc.1994.052220105

[4] Beev AA, Beeva DA, Abaev AM, Kozlov GV, Mikitaev AK. The properties of the interphase layer of the filled polyhydroxyester compositions. Sovremennyie naukoemkie tehnologii. 2006;**3**:60

[5] Karchakova VV, Pokhilko AV, Shmalko VM. Determining the filler activity in the sintering of pitch composites. Coke and Chemistry. 2014;**57**(1):24-29. DOI: 10.3103/S1068364X14010025

[6] Solomko VP. Interstructural filling and its effect on the properties of polymers. Mekhanika Polimerov. 1976;**1**:162-166

[7] Donskoi AA, Baritko NV. The effect of filler surface treatment on properties of low-density heat-shielding materials. In: Handbook of Polymer Research. Chapter 9, V.19. Nova Science Publishers; 2006. pp. 201-232

[8] Bogdanova YG. Adgeziya i ee rol' v obespechenii prochnosti polimernykh kompozitov: Uch. posobie (Adhesion and Its Role in the Strength of Polymer Composites: A Handbook). Moscow: Izd. MGU im. Lomonosova; 2010

[9] Montes Ruiz-Cabello FJ, Rodríguez-Valverde MA, Cabrerizo-Vílchez MA. Equilibrium contact angle or the most-stable contact angle. Advances in Colloid and Interface Science. 2014;**206**:320-327. DOI: 10.1016/j.cis.2013.09.003

[10] Lu Y, Kocaefe D, Kocaefe Y, Bhattacharyay D, Huang X-A, Morais B. Study of the wetting of coke by different pitches. Light Metals. 2016:871-876. DOI: 10.1002/9781119274780.ch147

[11] Sarkar A, Kocaefe D, Kocaefe Y, Bhattacharyay D, Coulombe P. Prediction of contact angle of coke-pitch system from raw material properties using artificial neural network. International Journal of Engineering Inventions. 2017;**6**(4):42-52

[12] Rocha VG, Blanco C, Santamaria R, Diestre EI, Menendez R, Granda M. Pitch/coke wetting behavior. Fuel. 2005;**84**:1550-1556. DOI: 10.1016/j.fuel.2005.02.007

[13] Suriyapraphadilok U. Characterization of coal- and petroleum-derived binder pitches and the interaction of pitch/coke mixtures in pre-baked carbon anodes [thesis]. 2008

[14] Li K, Shen K, Huang Z-H, Shen W, Yang G, Yang J, et al. Wettability of natural microcrystalline graphite filler with pitch in isotropic graphite preparation. Fuel. 2016;**180**:743-748. DOI: 10.1016/j.fuel.2016.04.091

[15] Sarkar A, Kocaefe D, Kocaefe Y, Sarkar D, Bhattacharyay D, Morais B, et al. Coke-pitch interactions during anode preparation. Fuel. 2014;**117**:598-607. DOI: 10.1016/j.fuel.2013.09.015

[16] Rafalskiy PN, Shulga AA, Portyan II, Zharova OV. Otsenka smachivayuschey sposobnosti kamennougolnyih pekov po metodike OAO «UKRGRAFIT». Uglehimicheskiy zhurnal. 2010;**5-6**:31-34

[17] RDC-163 Wetting Characteristics [Internet]. Available from: http://www.lmltd.ru/r-d/equipment/pitch/33-rdc163.html

[18] Shmalko VM, Sklyar MG, Soldatenko EM. Opredelenie spekayuschey sposobnosti ugley (Determination of the sintering ability of coals). Koks i Himiya. 1984;**10**:8-10

[19] Karchakova VV, Solovyov MA, Shmalko VM. Primenenie metoda opredeleniya spekaemosti i spekayuschey sposobnosti ugley dlya harakteristiki kamennougolnyih pekov i uglerodistyih napolniteley (The application of the method for determining the sinterability and sintering ability of coals to characterize coal tar pitch and carbonaceous fillers). Uglehimicheskiy zhurnal. 2013;**3-4**:32-38

[20] Ovchinnikova SA, Cheshko FF, Pityulin IN, Karchakova VV. Microstructure of electrode pitch at OAO Zaporozhkoks. Coke and Chemistry. 2010;**53**(1):31-34. DOI: 10.3103/S1068364X10010072

[21] Karchakova VV, Pokhilko AV, Shmalko VM. DoslIdzhennya spIkannya pekovih kompozitsIy z riznimi napovnyuvachami (Investigation of sintering of pitch compositions with different fillers). In: II International scientific and technical conference "Progress in oil and gas and petrochemical industry; May 2014; Lviv: NU Lviv Polytechnic; 2014. p. 135

[22] Kiseleva OA. Polistrukturnaya teoriya prochnosti kompozitsionnyih materialov (Polystructural theory of strength of composite materials).

Tambov: GBOU VPO Tambov State Technical University; 2013. 22 p

[23] Auguie D, Oberlin M, Oberlin A. Formation of thin mesophase layers at the interface between filler and binder in prebaked anodes. Effect of mixing on mesophase. Carbon. 1981;**19**(4):211-284

[24] Marosi G, Bertalan I, Rusznák P. Role of interfacial layers in the properties of particle-filled polyolefin systems. Colloids and Surfaces. 1989;**23**(3):185-198

[25] Kozlov G, Yanovski Y, Zaikov G. The experimental and theoretical estimation of interfacial layer thickness in elastomeric nanocomposites. Chemistry and chemical technology. 2012;**6**(3):345-348

[26] Pitulin IN. Nauchno-tehnologicheskie osnovyi sozdaniya kamennougolnyih uglerodsoderzhaschih materialov dlya krupnogabaritnyih elektrodov (Scientific and technological foundations for the creation of carbonaceous carbon-containing materials for large-sized electrodes). Kharkov: Kontrast; 2004. 480 p

[27] Shmalko VM, Solovyov MA. Metod viznachennya spIklivostI ta spIklivoYi zdatnostI sirovini dlya koksuvannya. TeoretichnI aspekti. (Method of determination of copolymer and copolymer ability of raw materials for coking. theoretical aspects). Uglehimicheskiy zhurnal. 2007;**6**:7-13

[28] Shmal'ko VM, Solov'ev MA. Developing new methods of determining the clinkering properties of rammed coal. Coke and Chemistry. 2009;**52**(2):45-50. DOI: 10.3103/S1068364X0902001X

[29] Denisov VD, Ibragimov IG, Galiev LG. Neodnorodnost fiziko-mehanicheskih svoystv spetsialnogo

koksa v ob'eme reaktora (Inhomogeneity of physical and mechanical properties of special coke in the reactor volume). In: All-Union conference of young scientists and specialists "Modern achievements in the field of research, production and operation of carbon materials and products"; Chelyabinsk; 1984. p. 15

[30] Korohin RA, Solodilov VI, Gorbatkina YA, Otegov AV. Fiziko-mehanicheskie svoystva dispersno-napolnenyih epoksidov (Physicomechanical properties of dispersed-filled epoxides). Plasticheskie Massy. 2013;**4**:37-41

[31] Volyinskiy AL. Effekt Rebindera v polimerah (The Rebinder effect in polymers). Priroda. 2006;**11**:11-18

[32] Sklyar MG, Nesterenko LL. Ob uporyadochenii terminologii v oblasti spekaniya ugley i koksoobrazovaniya (On the ordering of terminology in the field of sintering of coal and coke formation). Koks i Himiya. 1977;**4**:54-57

[33] ISO 335:1974. Hard coal -- Determination of caking power -- Roga test. Publication date. 1974-10

Chapter 3

Dynamic Mechanical Behaviour of Coir and Coconut Husk Particulate Reinforced Polymer Composites: The Effect of Exposure to Acidic Environment

David O. Obada, Laminu S. Kuburi, David Dodoo-Arhin,
Yongdan Hou, Muyideen B. Balogun and Mahmud Muhammad

Abstract

This chapter describes an experimental investigation into the dynamic mechanical properties of coir and coconut husk particulate reinforced polymer composites which were prepared by the hot press method. The composite was immersed in a strongly acidic environment of pH 2.2 for a period of 14 and 28 days (14P and 28P). Values of storage modulus at different vibrational frequencies recorded for the polymers at low temperatures where the molecules are still tightly compressed and the region of first solid state transitions are: Control sample (CS)—913.18, 984.18 and 979.94 MPa; 14P—505.54, 492.47 and 473.60 MPa and 28P—282.25, 298.70 and 285.36 MPa at 2, 5 and 10 Hz, respectively. While values of loss modulus at different vibrational frequencies are: CS—113.32, 109.43 and 107.62 MPa, 14P—92.92, 92.92 and 101.93 MPa and 28P—46.08, 45.61 and 45.18 MPa at 2, 5 and 10 Hz, respectively. Degradation of the mechanical properties was ascribed to the penetration and absorption that occurred between the acid solution and the composite constituents (matrix, filler, and fiber). It was found that frequency variation influenced the dynamic mechanical properties of the polymer composite at the points of measurement.

Keywords: particulate fillers, mechanical integrity, corrosion

1. Introduction

Recently, polymers have become increasingly important for an array of applications by reason of several attractive properties which includes light weight, the ease of processing and its affordability. Fiber reinforced polymers are also attractive as well, due to their biodegradability, high stiffness and strength, good corrosion resistance and many other properties which are important from the tribological point of view, for instance, low coefficient of friction etc. [1–6]. These natural fibers consist of jute, hemp, sisal, coir, banana among others [7].

Among the natural fibers, it is pertinent to note that coir is essentially utilized in view of its low cost, durability among other advantages [8]. Coir has been accounted for as having the highest extension at break among common natural fibers, which allows it absorb strain more than other fibers [9–11]. Reinforcing polymer, for example, polyethylene with natural fiber/particulates to produce polymer composites has gained significant consideration because of their intrinsic properties [12]. Glass fiber has been an interesting option as reinforcement, however, despite the fact that glass fiber reinforced plastics have high quality, their fields of use are exceptionally restricted on account of its inherent higher cost of production [13]. By reason of this, natural fiber reinforced composites have been suggested for use industrially in the off-shore oil and gas industry, in addition to application as composite pipelines, for storage tanks, fluid handling and chemical processing equipment, etc. Therefore from the economic point of view, natural fiber and lignocelluloses, for example, coir and coconut shell powder has remarkable properties as reinforcement/fillers in plastics. Coconut shell particles have become essential as a reinforcement material because of some natural properties like high strength and high modulus [14]. It is worth noting that increment in coconut shell content improves the mechanical strength and water absorption properties of polymer composites, nonetheless, it lessens the stretching at break [15].

In a variety of industrial applications, composite materials are under the attack of corrosive environments (acidic and alkaline). In this way, it is pertinent to note that the influence of exposure or attack of polymer materials to corrosive environments may be quite difficult to notice. It is possible that the material may seem normal but in actual sense may have become embrittled and the mechanical properties may have deteriorated. These mechanically stressed polymers which are exposed to corrosive environments may have crack initiation on the surfaces which propagates by reason of the inherent stresses or with continued exposure to chemical attack. The degradation pathway could occur when the acid, salt or alkaline solution diffuses through the surface and reaches the laminates of the polymer or a situation where the solution penetrates the laminate through micro cracks or other deficiencies/imperfections which may have resulted during the processing stage of the polymer.

Nonetheless, by reason of the continued usage of fiber reinforced polymers (FRPs) and the ambiguities in environmental conditions, etc., the degradation of FRPs in corrosive environments have not been examined in detail. A lot of studies on the durability of FRP composites have laid much emphasis on glass, aramid and carbon composites [16]. Generally, carbon based FRPs are not affected by most corrosive environments. In line with this, to the best of our knowledge, scanty reports are available for the degradation resistance of natural FRPs. For instance, Sindhu et al. [17] studied the reduction of the mechanical properties of coir/polyester and glass/polyester composites under the action of different solvents and environmental weathering. These properties increased with increased aging, but the mechanical properties of samples aged by water, acid and environmental weathering displayed a decrease in their properties. In another study, the resistance of basalt fibers in alkaline solution was noticed to be better than that of glass fibers while the acid resistance was found to be poorer [18, 19].

According to Gill [20], the versatile high performance applications of natural fiber composites, like coir, can replace glass and carbon fibers. It has also been noticed that a considerable level of research have focused mainly on the performance of glass FRP composites in highly corrosive environments. Amaro et al. [21] subjected glass FRP samples in HCl and sodium hydroxide (NaOH) solutions at room temperature (25 °C) for 12, 14 and 36 days. This was followed by conducting experiments on the degradation of mechanical properties. It was concluded that the flexural and impact

strength of the composites reduced with an increase in exposure time with the effect of exposure to the alkaline solution more pronounced than that noticed for the acidic solution. Stamenović et al. [22] investigated the influence of corrosive environments (acidic and alkaline) on the tensile characteristics of glass FRP pipes. It was shown that increasing the pH value of the alkaline solution further degraded the mechanical integrity of the pipe samples, while the samples subjected to the acidic solution provoked an increase in tensile strength and modulus, and decreasing pH values led to a more significant increase. These results from the study of Stamenović et al. [22] corroborate findings of Sindhu et al. [17], where the effects of various corrosive conditions on the mechanical properties of GFRP were investigated. The tensile strength and modulus increased as residence time in acidic solution increased.

On the other hand, Tripathy [23] studied the mechanical properties and interfacial properties of jute fiber filled epoxy resin. It was observed that the moisture intake by natural fibers, insufficient adhesion between untreated fibers and the polymer matrix, led to fiber pull-out with time [24]. Gilbert and Lee [25] investigated the influence of environmental conditions on the mechanical properties of short fiber reinforced composites. The relationship between moisture, acid, and alkali attacks were determined and the chemical properties were evaluated. Potts et al. [26] investigated the tensile properties of short coir reinforced composites. The tensile characteristics were found not to be dependent of fiber length, although the ultimate tensile strength showed some improvement at 10 mm fiber length.

Despite the volume of fiber reinforced polymer composites under investigation, most of the research efforts have been focused on either the characteristics of these polymers or the basic properties of the different phases that make up the composite [12, 27–29]. In our previous work [12, 30], we identified a coir length which enhanced the mechanical and dynamic mechanical (viscoelastic) properties of our developed coconut husk filled composites. Hence, the present work focused mainly on the evaluation of the dynamic mechanical characteristics of the fabricated composite on exposure to an acidic environment. We have considered dynamic mechanical properties of the samples at low temperatures where polymer molecules are tightly compressed and where the first solid-state transitions occur.

2. Materials and methods

Coir (fiber) which was extracted from coconut husk was cleaned with water to remove contaminants and dried at room temperature for 48 h. The dried fibers were soaked in 5 wt.% NaOH solution at room temperature (27 °C) for 30 min as a fiber treatment procedure. The treated coir was subsequently washed with distilled water to remove retained alkali. Furthermore, washed fibers of 30 mm length were open air dried for a day and afterwards dried at 60 °C in a hot air oven for 8 h. Further composite processing is reported elsewhere [30].

2.1 Exposure conditions

Three test conditions were selected in this study to investigate the short term effect of the exposure of the fabricated coir reinforced polymer composite to an acidic medium. According to Mahmoud and Tantawi [31], who investigated the effects of various aggressive acids including HCl, H_2SO_4, HNO_3, and H_3PO_4 on glass FRP composites, H_2SO_4 had a more pronounced effect than the other acids used in their experiments. Additionally, H_2SO_4 is one of agents which FRP components are generally exposed to. Therefore it was used as the acid solution for this study. The condition is an H_2SO_4 solution with pH 2.2 at room temperature. Exposure periods

of 14 and 28 days (14P and 28P) were considered. The sample not exposed to the acid solution was used as control.

2.2 Dynamic mechanical properties of corroded polymer specimens

Dynamic mechanical analysis (DMA) was used to investigate the viscoelastic properties of the exposed polymer samples as reported in our previous study [30]. The frequencies under which DMA measurements were made in this study are: 2, 5 and 10 Hz. The loss and storage moduli at low temperatures where polymer molecules are tightly compressed and where the first solid-state transitions occur were analyzed.

3. Results and discussion

3.1 Storage modulus (E′)

The results in **Figures 1– 3** for control, 14P and 28P samples, respectively, demonstrated the trademark drop in modulus around the first transition stage from elastic to viscous of the composite which can be ascribed to energy release with gradual increase in temperature [32]. Values of storage modulus recorded for the polymers at the point of interest were: Control Sample (CS)—913.18, 984.18 and 979.94 MPa; 14P—505.54, 492.47 and 473.60 MPa and, 28P—282.25, 298.70 and 285.36 MPa at 2, 5 and 10 Hz, respectively.

The values of E′ for the CS (**Figure 1**) increased with the frequency until 5 Hz and a slight decrease is observed at 10 Hz, while values of E′ for 14P sample (**Figure 2**) decreased with frequency until the highest frequency of 10 Hz. In addition, values of E′ for 28P samples (**Figure 3**) increased with the frequency and a slight decrease is observed at 10 Hz. A possible explanation for these are: for the control sample, the tendency of an increase in E′ under a higher frequency and comparatively lower value of E′ for composite subjected to 10 Hz, can be ascribed to increase in molecular mobility of the polymer chains in the first solid
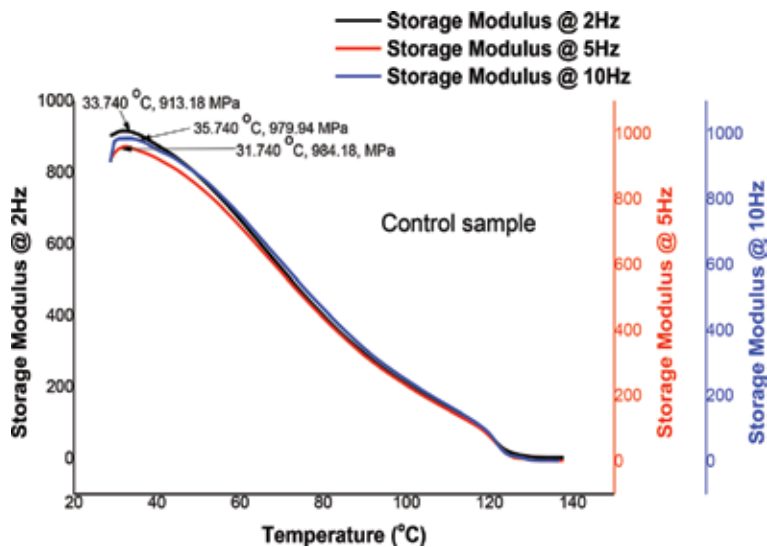

Figure 1.
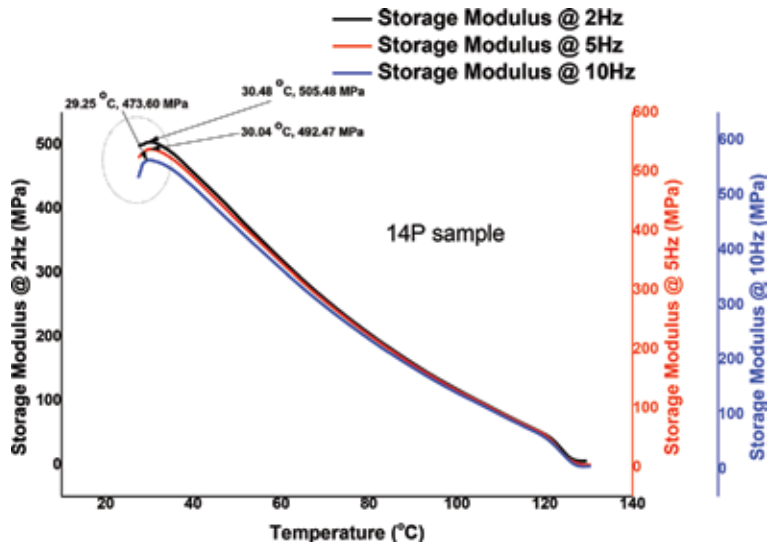*Storage modulus curves of control sample under varying frequencies.*

Figure 2.
Storage modulus curves of 14P sample under varying frequencies.

Figure 3.
Storage modulus curves of 28P sample under varying frequencies.

state transition phase [33]. The continued decrease of storage modulus for the 14P sample can be ascribed to a gradual degradation of the storage modulus due to the influence of exposure to the acidic environment which causes a reduced grip of the tightly bound polymer molecules, allowing them to flow more as compared to polymer molecules in the control sample. It also means at every point of frequency variation, there was an increase in molecular dynamics of the polymer chains because the molecules can move with the force which results in a decline in storage modulus. A similar trend of storage modulus variation at each point of frequency change as observed for the control sample was noticed for the 28P sample. However a decrease in the storage modulus was observed at every corresponding frequency variation, which further explains the effect of exposure to acidic environment

to which the degradation in the fiber/filler/matrix interface can be ascribed, and subsequently allows tightly bound molecules to move with the applied force and cause a decline in the ability of the composite to store energy.

3.2 Loss modulus (E″)

The results in **Figures 4–6** for control, 14P and 28P samples, respectively, show that upon frequency variation, the values of loss modulus (E″) decreased, but an exception was noticed in this trend for the 14P sample. Values of loss modulus recorded for the polymers at low temperatures where the molecules are still

Figure 4.
Loss modulus curves of control sample under varying frequencies.

Figure 5.
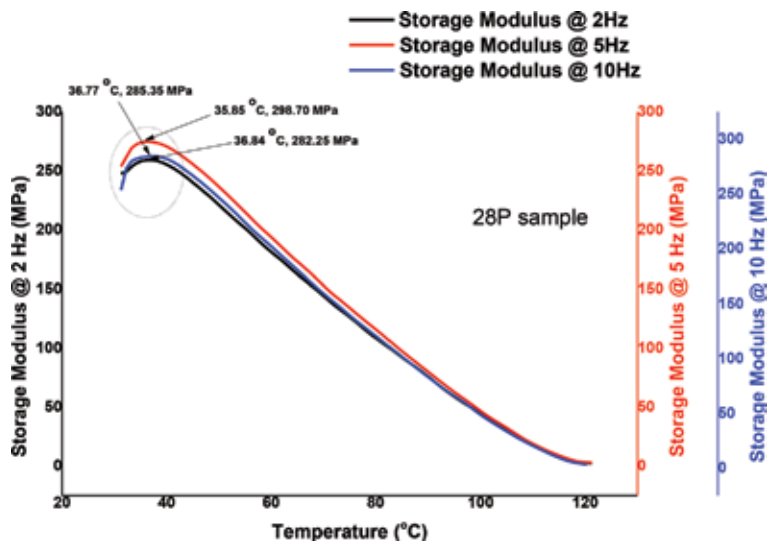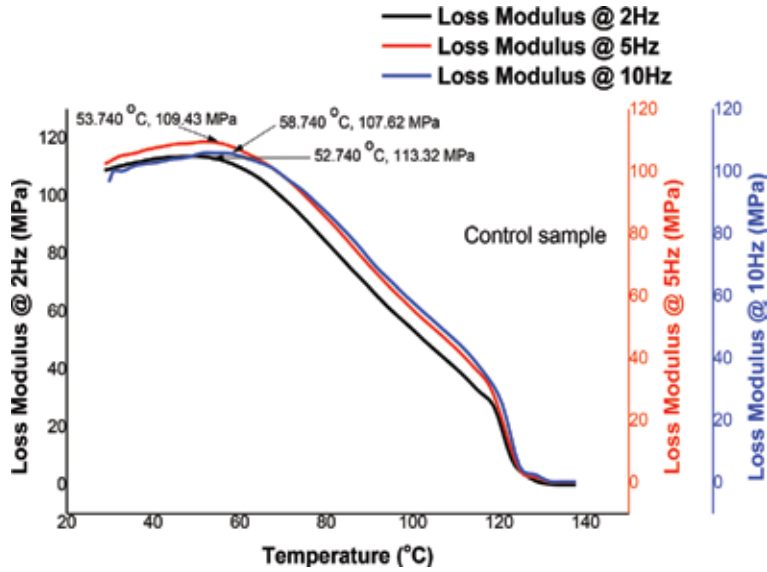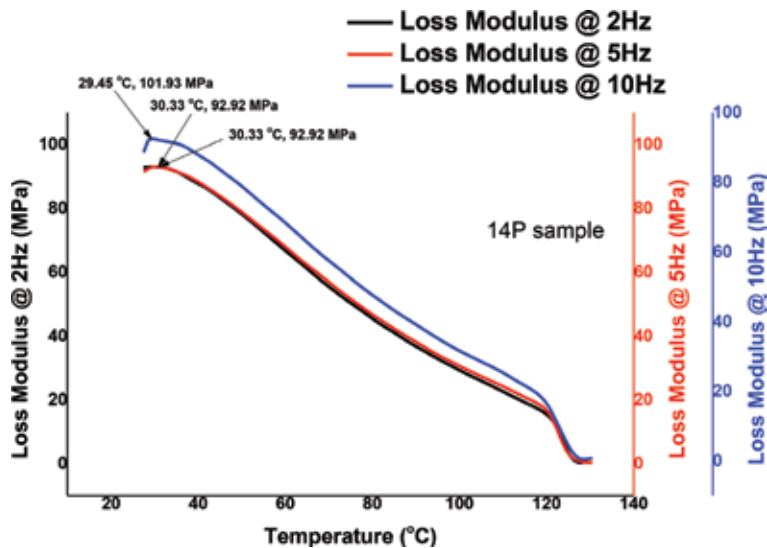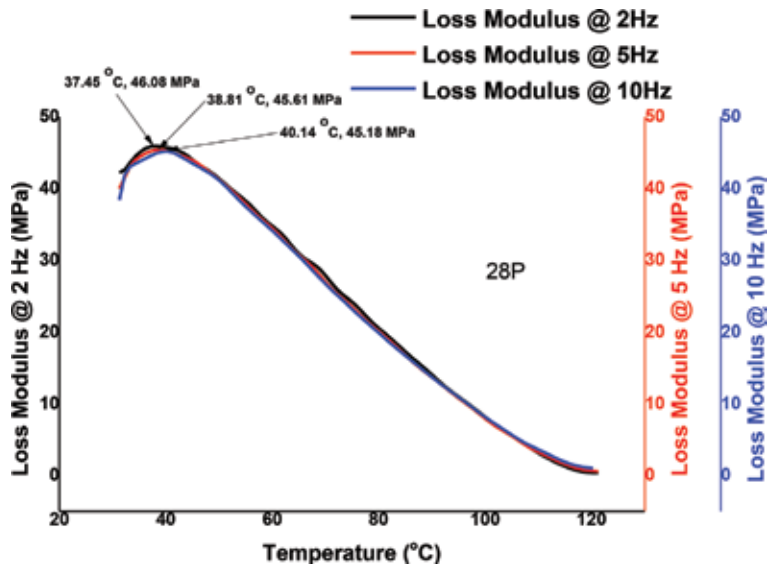*Loss modulus curves of 14P sample under varying frequencies.*

Figure 6.
Storage modulus curves of 28P sample under varying frequencies.

tightly compressed and the region of first solid state transitions were: CS—113.32, 109.43 and 107.62 MPa; 14P—92.92, 92.92 and 101.93 MPa and 28P—46.08, 45.61 and 45.18 MPa at 2, 5 and 10 Hz, respectively. These results indicate that the acid solution provoked degradation in the fiber/filler/matrix interface which may be associated with the occurrence of fractures under stress conditions. These results corroborates findings of Stamenović et al. [22], which suggested that the most significant influence of corrosive solutions was on the fiber-matrix connection and this influence directly reduces the load carrying capacity of composites.

The possible pathways for the reduction in storage and loss moduli after exposure to the acidic environment can be explained or associated with the penetration and absorption that occurred between the acid solution and the composite constituents (matrix, filler and fiber). The solution most likely penetrates through the polymer matrix and has the possibility of separating out in micro-cracks. These assertions have also been buttressed by [31, 34]. Also similar pathways can be attributed to the degradation of the fiber/filler/matrix interface which is caused by the penetration of the acid solution through cracks which may have gained entry through voids in the matrix [17, 22, 35]. According to Hammami and Al-Ghilani [36], the degradation of the mechanical properties of polymers can occur in two stages. Firstly, the polymer is degraded under actions which are as a result of the diffusion of water and the presence of hydrogen ions. Secondly, the fiber itself can be degraded which results to cracks appearing on the surface of the fiber. This to some extent affects the resistance of the composite to stresses. Moreso, according to Stamenović et al. [22], a degradation of the mechanical properties can be associated with the fiber-matrix interface where the acid immersion of the composites promotes the deficiencies of the stress carrying capacity of the polymer composites.

4. Conclusions

The dynamic mechanical properties of coir and coconut husk particulate reinforced composites immersed in an acid solution over periods of 14 and 28 days

were investigated. The dynamic mechanical analysis of the composite not subjected to the corrosive medium was also tested for comparison. The degradation pathway was clarified on the basis of the experimental results. The major conclusions are as follows:

1. The composites exhibited relatively little resistance to corrosion in acid solution by reason of the reduced storage and loss moduli after immersion in the acid solution.

2. In terms of mobility of polymer chains, an increase in frequency or stress loading caused a sharp decline in storage and loss moduli of the immersed samples due to the reduced grip of the tightly bound polymer molecules, allowing them to flow more as compared to polymer molecules in the control sample.

3. Degradation of the mechanical properties can be associated with the penetration and absorption that occurred between the acid solution and the composite constituents (matrix, filler and fiber).

4. It is recommended that the developed composites can be applied in areas where the composites are not exposed to load carrying corrosive environments.

Conflict of interest

The authors declare no conflicts of interest.

Author details

David O. Obada[1]* , Laminu S. Kuburi[1], David Dodoo-Arhin[2,3], Yongdan Hou[4], Muyideen B. Balogun[1] and Mahmud Muhammad[1]

1 Department of Mechanical Engineering, Ahmadu Bello University, Zaria, Nigeria

2 Department of Material Science and Engineering, University of Ghana, Legon, Ghana

3 Institute of Applied Science and Technology, University of Ghana, Legon, Ghana

4 Department of Materials Engineering, Kwame Nkrumah University of Science and Technology, Kumasi, Ghana

*Address all correspondence to: doobada@abu.edu.ng

IntechOpen

References

[1] Thakur VK, Thakur MK, Gupta RK. Raw natural fiber–based polymer composites. International Journal of Polymer Analysis and Characterization. 2014;**19**(3):256-271

[2] Ku H, Wang H, Pattarachaiyakoop N, Trada M. A review on the tensile properties of natural fiber reinforced polymer composites. Composites Part B: Engineering. 2011;**42**(4):856-873

[3] Barari B, Ellingham TK, Ghamhia II, Pillai KM, El-Hajjar R, Turng LS, et al. Mechanical characterization of scalable cellulose nano-fiber based composites made using liquid composite molding process. Composites Part B: Engineering. 2016;**84**:277-284

[4] Unterweger C, Brüggemann O, Fürst C. Synthetic fibers and thermoplastic short-fiber-reinforced polymers: Properties and characterization. Polymer Composites. 2014;**35**(2):227-236

[5] Santos TFA, Vasconcelos GC, de Souza WA, Costa ML, Botelho EC. Suitability of carbon fiber-reinforced polymers as power cable cores: Galvanic corrosion and thermal stability evaluation. Materials & Design (1980-2015). 2015;**65**:780-788

[6] Pei XQ, Bennewitz R, Schlarb AK. Mechanisms of friction and wear reduction by carbon fiber reinforcement of PEEK. Tribology Letters. 2015;**58**(3):42

[7] Li X, Tabil LG, Panigrahi S, Crerar WJ. The influence of fiber content on properties of injection molded flax fiber-HDPE biocomposites. In: 2006 ASAE Annual Meeting. American Society of Agricultural and Biological Engineers; 2006. p. 1

[8] Zaman HU, Beg MD. Preparation, structure, and properties of the coir fiber/polypropylene composites. Journal of Composite Materials. 2014;**48**(26):3293-3301

[9] Satyanarayana KG, Kulkarni AG, Rohatgi PK. Potential of natural fibers as a resource for industrial materials in Kerala. Journal of Scientific & Industrial Research. 1981;**40**(4):222-237

[10] Satyanarayana KG, Sukumaran K, Mukherjee PS, Pavithran C, Pillai SG. Natural fibre-polymer composites. Cement and Concrete composites. 1990;**12**(2):117-136

[11] Munawar SS, Umemura K, Kawai S. Characterization of the morphological, physical, and mechanical properties of seven nonwood plant fiber bundles. Journal of Wood Science. 2007;**53**(2):108-113

[12] Kuburi LS, Dauda M, Obada DO, Umaru S, Dodoo-Arhin D, Iliyasu I, et al. Effects of coir fiber loading on the physio-mechanical and morphological properties of coconut shell powder filled low density polyethylene composites. Procedia Manufacturing. 2017;**7**:138-144

[13] Verma D, Gope PC, Shandilya A, Gupta A, Maheshwari MK. Coir fibre reinforcement and application in polymer composites: A. Environmental Sciences. 2013;**4**(2):263-276

[14] Agunsoye JO, Isaac TS, Samuel SO. Study of mechanical behaviour of coconut shell reinforced polymer matrix composite. Journal of Minerals and Materials Characterization and Engineering. 2012;**11**(8):774-779

[15] Husseinsyah S, Mostapha M. The effect of filler content on properties of coconut shell filled polyester composites. Malaysian Polymer Journal. 2011;**6**(1):87-97

[16] Bank LC, Gentry TR, Thompson BP, Russell JS. A model specification for FRP composites for civil engineering structures. Construction and Building Materials. 2003;**17**(6-7):405-437

[17] Sindhu K, Joseph K, Joseph JM, Mathew TV. Degradation studies of coir fiber/polyester and glass fiber/polyester composites under different conditions. Journal of Reinforced Plastics and Composites. 2007;**26**(15):1571-1585

[18] Ramachandran BE, Velpari V, Balasubramanian N. Chemical durability studies on basalt fibres. Journal of Materials Science. 1981;**16**(12):3393-3397

[19] Nasir V, Karimipour H, Taheri-Behrooz F, Shokrieh MM. Corrosion behaviour and crack formation mechanism of basalt fibre in sulphuric acid. Corrosion Science. 2012;**64**:1-7

[20] Gill RK. Damage in Composite Materials. 1992;**11**:1035

[21] Amaro AM, Reis PN, Neto MA, Louro C. Effects of alkaline and acid solutions on glass/epoxy composites. Polymer Degradation and Stability. 2013;**98**(4):853-862

[22] Stamenović M, Putić S, Rakin M, Medjo B, Čikara D. Effect of alkaline and acidic solutions on the tensile properties of glass–polyester pipes. Materials & Design. 2011;**32**(4):2456-2461

[23] Tripathy A. Degradation studies of coir fiber/polyester and glass fiber/polyester composites under different conditions. Journal of Reinforced Plastics and Composites, Journal of Reinforced Plastics and Composites. 1990;**26**(15):1571-1585

[24] Tsai SW, Hahn HT. Introduction to Composite Materials. Lancaster, PA, USA: Technomic Publishing Co.; 1980

[25] Gilbert P, Lee C. Analytical methods. In: Biotransformation and Fate of Chemicals in the Aquatic Environment: Proceedings of a Workshop Held at the University of Michigan Biological Station; 14-18 August 1979; Pellston, Michigan. American Society for Microbiology; 1980. p. 34

[26] Potts JE, Clendinning RA, Ackart WB. The Proceedings of Degradability of Polymers and Plastic Conference. London: Plastic Institute; 1973. pp. 10-12

[27] Dan-asabe B, Yaro AS, Yawas DS, Aku SY, Samotu IA, Abubakar U, et al. Mechanical, spectroscopic and micro-structural characterization of banana particulate reinforced PVC composite as piping material. Tribology in Industry. 2016;**38**(2):255-267

[28] Samotu IA, Dauda M, Anafi FO, Obada DO. Suitability of recycled polyethylene/palm kernel shell-iron filings composite for automobile application. Tribology in Industry. 2015;**37**(2):142-153

[29] Samotu IA, Bashar DA, Obada DO, Reuben B. A preliminary study on the effect of reinforcing polyesters with Kenaf and sisal fibres on their mechanical properties. West Indian Journal of Engineering. 2015;**38**(1):33-40

[30] Obada DO, Kuburi LS, Dauda M, Umaru S, Dodoo-Arhin D, Balogun MB, et al. Effect of variation in frequencies on the viscoelastic properties of coir and coconut husk powder reinforced composites. Journal of King Saud University-Engineering Sciences. 2018. https://doi.org/10.1016/j.jksues.2018.10.001

[31] Mahmoud MK, Tantawi SH. Effect of strong acids on mechanical properties of glass/polyester GRP pipe at normal and high temperatures. Polymer-Plastics

Technology and Engineering. 2003;**42**(4):677-688

[32] Feng Q-P, Shen X-J, Yang J-P, Fu S-Y, Mai Y-W, Friedrich K. Synthesis of epoxy composites with high carbon nanotube loading and effects of tubular and wavy morphology on composite strength and modulus. Polymer. 2011;**52**(26):6037-6045

[33] Hameed N, Sreekumar PA, Francis B, Yang W, Thomas S. Morphology, dynamic mechanical and thermal studies on poly (styrene-co-acrylonitrile) modified epoxy resin/glass fibre composites. Composites Part A: Applied Science and Manufacturing. 2007;**38**(12):2422-2432

[34] Kawada H, Srivastava VK. The effect of an acidic stress environment on the stress-intensity factor for GRP laminates. Composites Science and Technology. 2001;**61**(8):1109-1114

[35] Stamenović M, Putić S, Drmanić S, Rakin M, Medjo B. The influence of service solutions on the longitudinal and circumferential tensile properties of glass-polyester composite pipes. Materials Science. 2011;**47**(1):61

[36] Hammami A, Al-Ghuilani N. Durability and environmental degradation of glass-vinylester composites. Polymer Composites. 2004;**25**(6):609-616

Active Solders and Active Soldering

Shih-Ying Chang, Yan-Hua Huang and Lung-Chuan Tsao

Abstract

Due to the relatively high stability of ceramic surfaces, ceramics, graphite, and alloys that easily form an oxide passivation layer by natural oxidation, such as aluminum alloys, titanium alloys, and magnesium alloys, are not wetted by common solders and brazing fillers. Moreover, in most applications, the brazing temperature is so high that it causes hot cracking or functional degradation of the difficult-to-wet materials. Active filler metals containing active elements have been developed, which can successfully join the nonwetting materials at low temperatures (<250°C) in air. The active elements, such as titanium, magnesium, and rare earth elements, in active solders play an important role in wettability and reactivity between filler metals and difficult-to-wet materials. Solders with active element content have been shown to provide excellent wettability. Hence, direct active soldering has been developed to simplify the manufacturing of difficult-to-wet material joints. A practical understanding of the design and characterization of low melting point active solders and active soldering processes is elaborated in this chapter. The effects of active elements, active solder characteristics, mechanism of active soldering, active soldering techniques, and specific applications are introduced. The influence of the thermal and mechanical activation on the interfacial reactions between filler metals and difficult-to-wet materials during the active soldering process is also discussed.

Keywords: active soldering, difficult-to-wet materials, rare earth elements, titanium, magnesium, wetting, mechanical agitation, ultrasonic-assisted soldering

1. Introduction

Due to functional, structure, or property needs, joining of dissimilar materials is increasingly used to achieve components with improved or tailor-engineered properties. For example, ceramic-metal joints have found wide application in electrical engineering and electronics for their combination of ceramic insulating properties and metallic conductivity. Moreover, ceramic-metal seals are used extensively in applications such as engine ignitors, vacuum tubes, high-voltage feedthroughs, magnetic recorder heads, synthetic colorless sapphire-metal windows, and ceramic sputtering targets [1]. Most ceramics have very high melting temperatures, so the applicability of conventional fusion welding methods to the bonding of ceramic-metal is not feasible in cases of extremely high power requirements. During the fusion welding process, the high temperature can cause severe property degradation or fracture in surrounding heat-affected areas. Furthermore, the great thermal expansion coefficient mismatch between ceramics and metals can cause serious residual stresses at the interface of the ceramic and

metal [2]. In lightweight construction, the bonding of difficult-to-wet materials such as aluminum alloys, magnesium alloys, or titanium alloys, which easily forms an oxide passivation layer by natural oxidation, entails numerous difficulties. Brazing and soldering with fillers as interlayers are considered to be more feasible ways to bond dissimilar materials such as ceramics and difficult-to-wet metals. However, because ceramics provide mostly covalent or ionic bonding, have a very stable electron configuration, and are chemically inert, most brazing or soldering fillers cannot be wetted on their surfaces [3]. Thus, the filler metal is the most important key factor in determining wettability. Direct bonding has been developed to simplify wetting of difficult-to-wet materials by using active fillers containing active elements that improve the wettability of the filler on the difficult-to-wet material surface and eliminate the need for pre-metallization during the joining process [4].

2. Active solders

Both brazing and soldering are joining processes that use the principle of capillary action to distribute a molten filler metal between the surfaces of base materials [5]. In all cases, filler metal melting temperatures are below the melting temperatures of the base materials. Brazing filler metals melt completely at temperatures above 450°C, while soldering filler metals melt below that temperature [5]. A variety of alloys are used as filler metals for brazing, depending on the workpieces and the intended use or application method. In general, braze alloys are made up of Cu, Ag, Ni, or precious metals [6]. Low melting point metals such as Pb, Sn, Zn, Sb, and In are usually used for soldering filler [7]. Filler metals can be divided into three types according to their melting points, namely, high melting point, medium melting point, and low melting point fillers, as shown in **Figure 1** [8].

Chemical bonding at the interfaces of the filler metal and base materials is evaluated by wettability, defined as the ability of the molten filler metal to spread uniformly onto the surface of a base material. The molten filler metals must be able to be wetted on the surface of the base materials during the joining process, whether it is brazing or soldering. Ceramics and some materials, which easily form an oxide passivation layer by natural oxidation, such as aluminum alloys, magnesium alloys, titanium alloys and stainless steels, have surfaces of extreme physical and chemical stability that prevent filler metals from wetting the surface.

One critical parameter of wettability is the contact angle between the drop of molten filler and the wetting surface, as shown in **Figure 2a** and **2b** [2]. The contact angle can be calculated by Young's equation [9]:

$$\cos\theta = \frac{\gamma_{SV} - \gamma_{SL}}{\gamma_{LV}} \qquad (1)$$

where θ is the contact angle, γ_{SV} is the solid-vapor interfacial energy, γ_{LV} is the liquid-vapor interfacial energy, and γ_{SL} is the solid-liquid interfacial energy.

If the solid-vapor interfacial energy (γ_{SV}) is higher than the solid-liquid interfacial energy (γ_{SL}), the right side of Young's equation will be positive, so $\cos\theta$ must be positive and the contact angle will be less than 90° [9]. Small contact angles correspond to high wettability, as shown in **Figure 2a**. A contact angle of less than 90° indicates that wetting of the surface is favorable, and most strong chemical bonds can be formed at the interface. To improve the wettability of the filler, it is necessary to reduce the surface tension between the bonding material and the filler, usually by forming a chemical reaction between the filler and the bonded material surface, as shown in **Figure 3** [9].
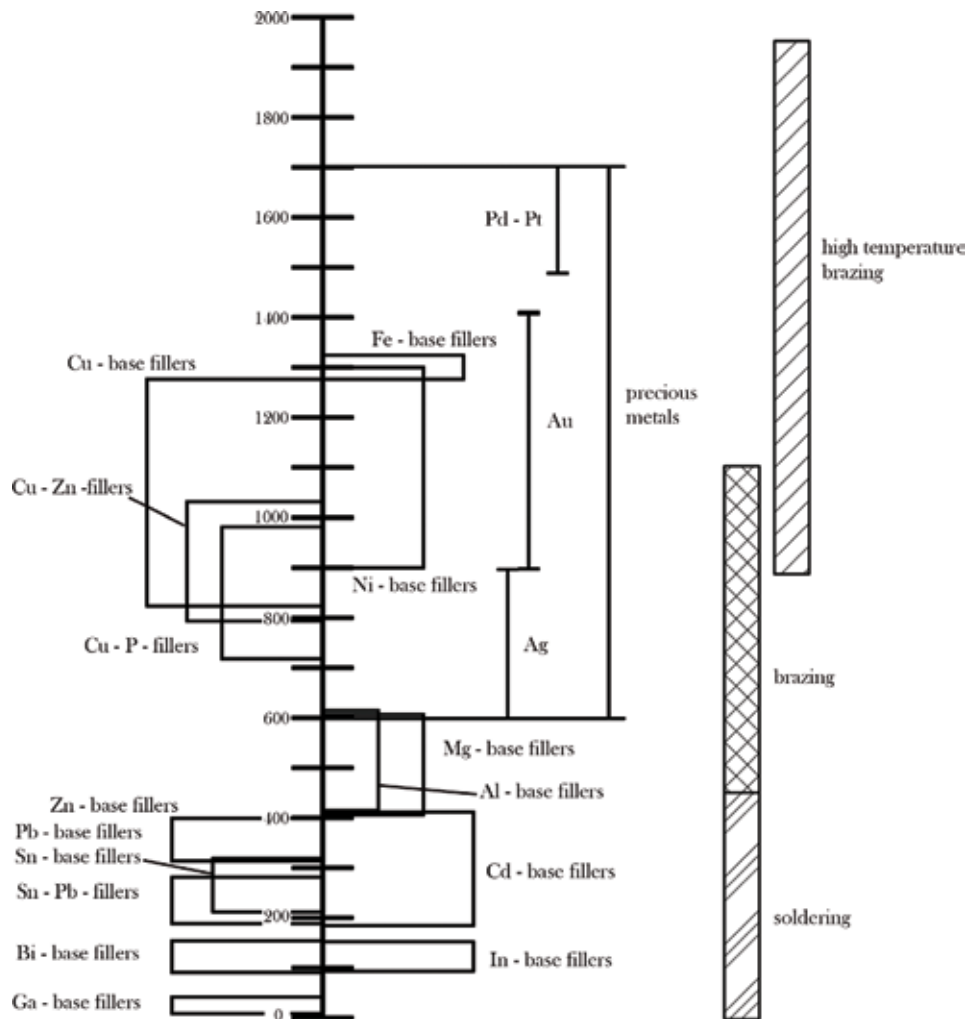
Figure 1.
The melting ranges of some typical solder and braze materials [8].

To obtain better bonding integrity, difficult-to-wet materials, especially ceramics, are usually metallized prior to brazing or soldering. To overcome the non-wetting of common filler metals on the surfaces of difficult-to-wet materials, pre-metallization by molybdenum-manganese method, electroless plating, physical vapor deposition (PVD), chemical vapor deposition (CVD), thermal spraying, or ion implantation can be used to increase the wettability [10]. The indirect joining process includes two steps and is costly; thus, it is difficult to implement. Recently, direct active brazing has been developed to join difficult-to-wet materials such as ceramic and graphite. The direct brazing process, without the need for pre-metallizing, is simpler than the indirect brazing. Active brazing fillers that include an active element, such as Ti, Zr, Ta, Nb, or Hf, are used to promote wetting [11–14]. It is believed that the addition of an active element to filler metals can effectively improve the wettability of difficult-to-wet materials by reducing the solid-liquid interfacial free energy and allowing chemical reactions in the interfaces between filler metals and substrates [15]. Due to its high chemical activity, titanium is often chosen as the active element in filler metals to improve the wetting on ceramic surfaces. For example, Ag–Cu–Ti active filler has been used widely to join ceramics because of its wettability and good bond strength [16–20]. However, the active filler metals for ceramic brazing have a high
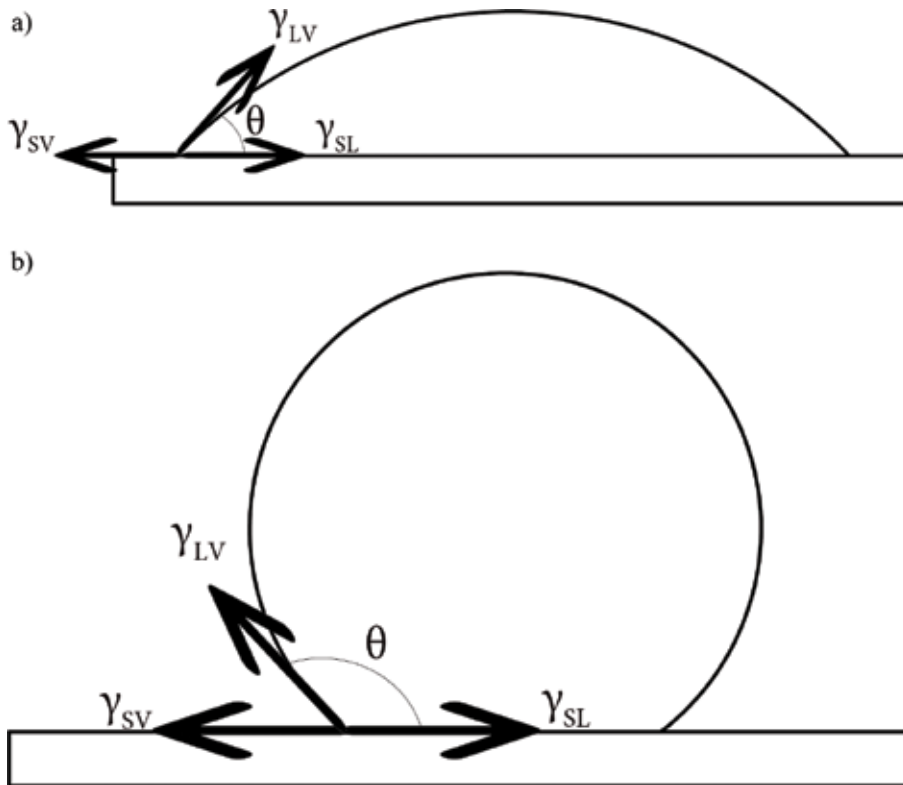
Figure 2.
Contact angle of sessile drop configurations (a) wetting and (b) nonwetting [2], where θ is the contact angle, γ$_{SV}$ is the solid-vapor interfacial energy, γ$_{LV}$ is the liquid-vapor interfacial energy, and γ$_{SL}$ is the solid-liquid interfacial energy.

melting point of about 750–850°C. Brazing is conducted at temperatures generally higher than 800°C. For some applications, the brazing temperature is so high that it causes hot cracking or functional degradation of the ceramics. Moreover, due to the difference in the thermal expansion coefficients of the metal and ceramic materials, high residual stress will develop upon cooling from the elevated temperature. Hence, the bonding temperature should be as low as possible to minimize the residual stresses. To solve this problem, low melting point filler metals containing titanium, such as $Sn_{10}Ag_4Ti$ and Pb_4In_4Ti, have been developed, and they exhibit excellent wettability on ceramic substrates at 850°C. Unlike the widely used Ag–Cu-based active filler metals, the low melting point filler metals possess a melting range below 300°C. However, brazing ceramics with low melting point active filler metals is always conducted above 850°C, such as the Ag–Cu–Ti brazing temperature, owing to the decent thermodynamic activation [21–23]. Although the act of brazing with low melting point filler metals must be conducted at elevated temperatures far above
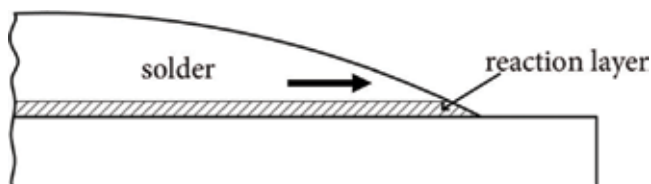
Figure 3.
Schematic of the spreading process of solder with the formation of reaction layer [9].

Solder	Sn	Zn	Ag	Al	Cu	Ti	In	Cr	Ni	Ce, Ga	Melting range, °C
Sn_4Ag_4Ti	Bal.	—	4	—	—	4	—	—	—	<0.5	220–232
$Sn_3Ag_3Cu_4Ti$	Bal.	—	3	—	1	4	—	—	—	<0.5	220–232
Sn_5In_4Ti	Bal.	—	—	—	—	4	5	—	—	<0.5	220–232
Zn_6Al_6Ag	—	Bal.	6	6	—	—	—	—	—	<0.5	140–220
$Zn_4Ag_4TiCr_{0.7}$	—	Bal.	4	—	—	4	—	0.7	—	<0.5	220–232
$Zn_4Ag_4TiNi_{0.3}$	—	Bal.	4	—	—	4	—	—	0.3	<0.5	180–220

Table 1.
Active solders developed by Hillen et al. [4].

their melting points, their lower solidification temperature can alleviate the thermal stresses in the ceramic-metal joint. Active soldering techniques, which provide for bonding of various ceramics and difficult-to-wet materials at low temperature, have also been developed [4]. The solders used for active soldering consist of a low melting point metal such as tin or zinc with active elements such as titanium and rare earth elements. There have been reports of active solders developed by adding rare earth elements (Ce, La) and a wetting promoter (Ga) into Sn–Ag–Ti, Zn–Ag–Ti, Sn–Bi–Ti, and In–Sn–Ti alloys [4, 24]. Hillen et al. initially developed active solders for soldering difficult-to-wet materials, as listed in **Table 1**. With these active solders, the joining process of ceramics can be performed at temperatures lower than 450°C without flux and without the need for premetallization or a protective atmosphere.

3. Effects of active elements

A number of active soldering filler metals for direct soldering of difficult-to-wet materials have been reported. S-Bond technologies LLC has developed a series of active solder metals and an active soldering process [25]. In a prior study, the active filler metallic alloy Sn–Ag–Ti(Ce, Ga) was successfully used to join indium tin oxide (ITO) targets with Cu backing plates at 250°C in air [26]. Moreover, a lower-melting-point-active-filler metal $Sn_{56}Bi_4Ti(Ce, Ga)$ with a low bonding temperature of 180°C was used to join ZnS–SiO$_2$ targets with Cu backing plates [27]. Due to the high chemical activity of Ti, it can easily form the required subsequent chemical reaction between filler metal and substrate. Fu et al. [28] studied the effect of Ti content on the wetting behavior of the $Sn_{0.3}Ag_{0.7}Cu/AlN$ system. They demonstrated that the addition of Ti to Sn–Ag–Cu filler resulted in a significant enhancement of wettability for Ti content of 4–10%. Chang et al. [24, 26, 29, 30] have shown that the affinity of rare earth elements to oxygen gives rise to the reaction of Ti with some difficult-to-wet materials at a low temperature. Moreover, rare earth elements have a very strong affinity for oxygen, nitrogen, carbon, or almost all metals and hence create chemical reactions at the interface [31]. Qu et al. [32] investigated the effect of Ti content and Y additions on the oxidation behavior of Sn–Ag–Ti solder. Their results indicated that the addition of Y significantly improved the oxidation resistance of Sn–Ag–Ti solder. Due to the higher affinity of Y for oxygen than Ti, the Y added to the solder efficiently inhibited the oxidation of Ti during the soldering process. Many researchers have demonstrated that rare earth element dopants can significantly enhance solder bonding with difficult-to-wet materials [33–36]. The addition of Ti and rare earth elements to Sn or In alloys improves the solderability by increasing the wettability on difficult-to-wet materials. Furthermore, the oxidation resistances of these soldering filler metals are somewhat limited. For example, the addition of the rare earth element Ce to $Sn_{3.5}Ag_4Ti$ solder protects Ti from oxidation and enhances the activity of Ti [26, 28, 32]. Magnesium is also very chemically active and has good electric and thermal conductivity. It is also a suitable additive active element for Sn or In alloys used to increase the wetting in some applications of electronic packaging [37, 38]. Chang et al. [39, 40] have also developed a series of magnesium-containing active solders, as listed in **Tables 2–4**. $Sn_{3.5}Ag_{0.5}Cu_1Mg$ filler metal was used for joining alumina with alumina at 250°C in air. The microstructure of the bonding interface of Al$_2$O$_3$/Al$_2$O$_3$ joint is shown in **Figure 4**, which demonstrates a good wettability of the filler metal on the alumina. Hence, a satisfactory joint can be obtained using the magnesium-containing active filler. A good bonding strength of 6.54 MPa can be achieved using the $Sn_{3.5}Ag_{0.5}Cu_1Mg$ filler metal.

Solder	Sn	In	Ag	Cu	Zn	Pb	Bi	Mg	Melting range, °C
M–S	Bal.	0	0	0	0	0	0	0.1–5	220–232
M–SA	Bal.	0	0.5–5	0	0	0	0	0.1–5	220–232
M–SAC	Bal.	0	0.5–5	0.1–2	0	0	0	0.1–5	220–232
M–SB	Bal.	0	0	0	0	0	10–60	0.1–5	140–220
M–SC	Bal.	0	0	0.1–2	0	0	0	0.1–5	220–232
M–SP	Bal.	0	0	0	0	10–50	0	0.1–5	180–220
M–SZ	Bal.	0	0	0	1–15	0	0	0.1–5	180–232

Table 2.
Magnesium-containing Sn-based active solders and melting ranges.

M–I	0	Bal.	0	0	0	0	0	0.1–5	150–160
M–IA	0	Bal.	0.5–5	0	0	0	0	0.1–5	144–160
M–IAC	0	Bal.	0.5–5	0.1–2	0	0	0	0.1–5	145–160
M–IC	0	Bal.	0	0.1–2	0	0	0	0.1–5	150–160
M–IS	30–60	Bal.	0	0	0	0	0	0.1–5	120–150
M–ISB	10–30	Bal.	0	0	0	0	10–40	0.1–5	60–100
M–IZ	0	Bal.	0	0	1–15	0	0	0.1–5	145–156

Table 3.
Magnesium-containing In-based active solders and melting ranges.

Solder	Sn	Zn	Bi	In	Ag	Cu	Mg
M–SZB	Bal.	5–15	0.1–10	0	0	0	0.1–5
M–SZI	Bal.	5–15	0	0.1–10	0	0	0.1–5
M–SZA	Bal.	5–15	0	0	0.1–10	0	0.1–5
M–SZBI	Bal.	5–15	0.1–10	0.1–10	0	0	0.1–5
M–SZBA	Bal.	5–15	0.1–10	0	0.1–10	0	0.1–5
M–SZBC	Bal.	5–15	0.1–10	0	0	0.1–5	0.1–5
M–SZIA	Bal.	5–15	0	0.1–10	0.1–10	0	0.1–5
M–SZIC	Bal.	5–15	0	0.1–10	0	0.1–5	0.1–5

Table 4.
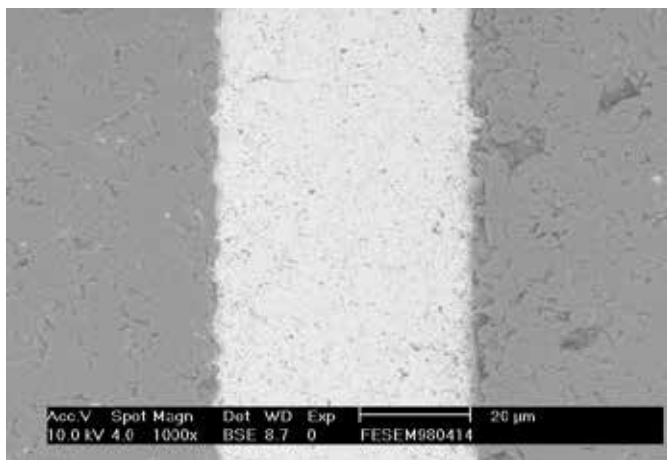*Magnesium-containing SnZn-based active solders.*

Figure 4.
Microstructure of the bonding interface of Al_2O_3/Al_2O_3 joint with $Sn_{3.5}Ag_{0.5}Cu_1Mg$ filler metal.

4. Active soldering

Active soldering is a flux-free soldering process. The active solders can be activated by exposure to high temperature or mechanical agitation [41, 42]. Joining with low melting point active solders such as $Sn_{10}Ag_4Ti$ and Pb_4In_4Ti is always conducted at elevated temperatures above 700°C, owing to the decent thermodynamic activation. Chai et al. [22] investigated the wettability of $Sn_{10}Ag_4Ti$ on SiC and Al_2O_3 substrates. They indicated that the contact angles decreased with increases in temperature and heating time. The contact angle of the $Sn_{10}Ag_4Ti$ filler metal on SiC decreased almost to 0° when the temperature was raised above 680°C. Ti aggregated strongly in the $Sn_{10}Ag_4Ti$/SiC and $Sn_{10}Ag_4Ti$/Al_2O_3 interfaces after brazing at 700°C. Koleňák et al. [43] indicated that the wettability of $Sn_{3.5}Ag_4Ti(Ce, Ga)$ solder depended on temperature and wetting time. Wettability of the $Sn_{3.5}Ag_4Ti(Ce, Ga)$ solder on Al_2O_3 was achieved with heating at 850°C for 43 min [42]. The schematic in **Figure 5** illustrates the wetting process of low melting point filler metal with high-temperature activation [43].

This soldering process, normally implemented under low temperature, requires mechanical activation to destruct the oxide layer forming on the liquid molten filler, after which the active elements Ti and rare earth elements can allow metallurgical
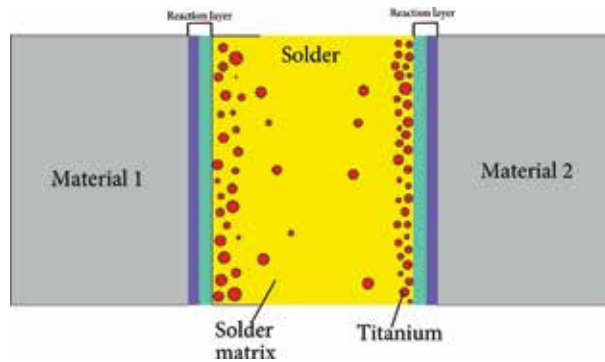
Figure 5.
Schematic of the wetting process of low melting point filler metal with high-temperature activation [44].

reaction with the substrate. Smith [41] has reported that mechanical agitation such as edge abrasion, brushing, vibration, and ultrasonic pressure can disrupt the molten active solder's surface oxide, thus permitting metallurgical interaction between the active elements, Ti and rare earth elements, and substrate. **Figure 6** illustrates mechanical agitation to disrupt the oxide layer to activate the molten active solder [41].
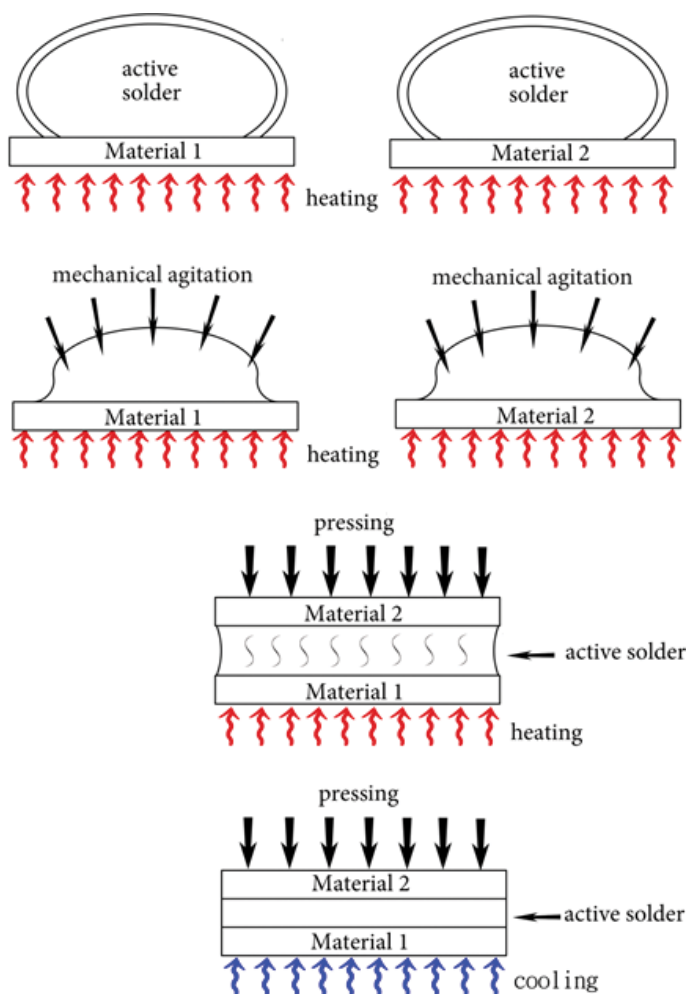

Figure 6.
Schematic of mechanical activation and soldering process [41].

Chang et al. [26, 29, 30] have investigated ITO/Cu, ZnS–SiO$_2$/Cu, and Al$_2$O$_3$/Cu joints using Sn$_{3.5}$Ag$_4$Ti(Ce, Ga) and mechanical agitation at 250°C. They have indicated that the affinity of rare earth elements to oxygen gives rise to the reaction of Ti with ITO, ZnS-SiO$_2$, and Al$_2$O$_3$ at a low temperature of 250°C. Their results have also shown a strong tendency of Ti to segregate at the ITO/solder, ZnS-SiO$_2$/solder, and Al$_2$O$_3$/solder interfaces. Cheng et al. [45, 46] investigated the influences of the active element Ti on interfacial reaction and soldering strength between Sn$_{3.5}$Ag$_4$Ti(Ce, Ga) alloy filler and Si substrate as well as SiO$_2$/SiO$_2$ joints. They also found that Ti played a critical role in obtaining reliable bonds for active soldering. The chemical adsorption of Ti on the substrate and the interfacial reaction between Ti and substrate were the active mechanisms. Similar to the cases in previous studies [24, 27], the joining process of ceramics can be performed using Sn$_{56}$Bi$_4$Ti(Ce, Ga) filler at temperatures lower than 180°C. The schematic in **Figure 7** illustrates the wetting process of low melting point filler metal with mechanical activation [47].
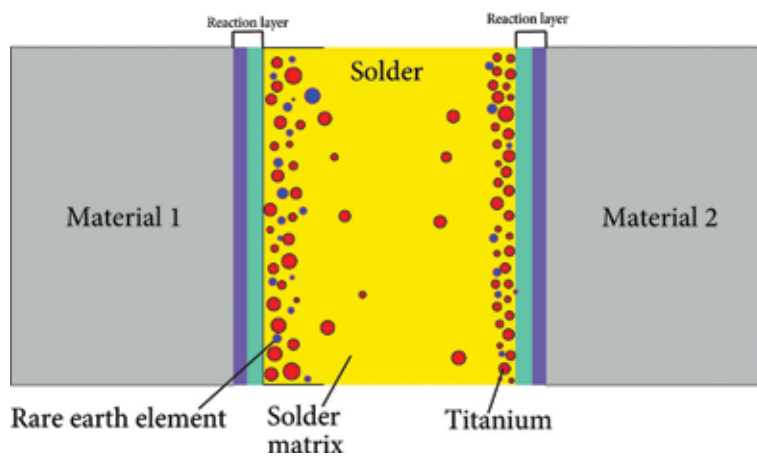

Figure 7.
Schematic of the wetting process of low melting point filler metal with mechanical activation [47].

Another promising option for solving the problems of oxidation and wetting of the filler metal on substrate is ultrasonic-assisted soldering technology. An ultrasonic vibration soldering system is illustrated in **Figure 8** [32]. The wettability study
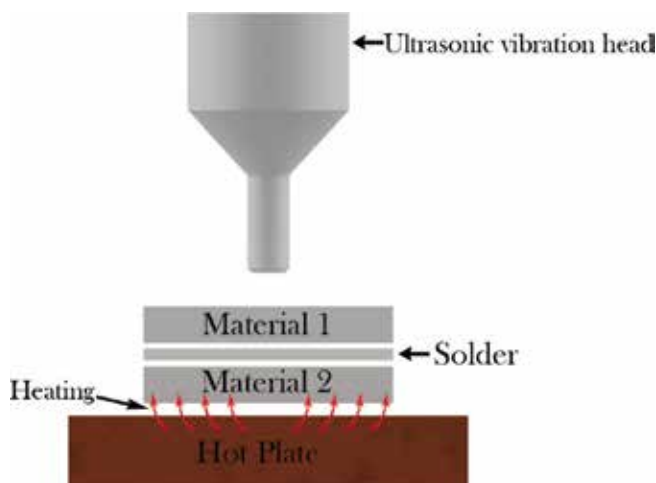

Figure 8.
Schematic of the ultrasonic vibration soldering system [32].

reported by Hillen et al. [4] presented an ultrasonic vibration method using an ultrasonic soldering iron, as shown in **Figure 9**. Ultrasonic vibration can effectively improve the wettability of active solder. Yu et al. [48] have reported that applying ultrasonic vibration during the soldering process causes the active solders Sn–Ag–Ti and Sn–Ag–Ti–Al to spread on the graphite surface at 450°C in air. Koleňák et al. [49] successfully used ultrasonic-assisted soldering to join SiC and copper with $In_{10}Ag_4Ti$ solder at 230°C.
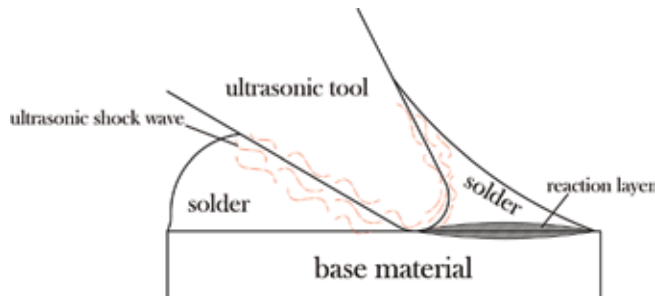

Figure 9.
Schematic of ultrasonic vibration soldering with an ultrasonic soldering iron [4].

5. Conclusion

With the rapid development of new materials and advanced technology in various industries, joining technologies play increasingly important roles. The poor wettability of ceramics for conventional filler metals and the large thermal residual stress make it extremely difficult to obtain sound ceramic/metal joints. Adding active elements such as titanium, rare earth elements, and magnesium to conventional solders provides improved wettability and bonding strength of most metals, glasses, and ceramics. The newly developed low melting point active solders and flux-free active soldering technology can effectively reduce the thermal stress between the ceramic and metal. Moreover, the active soldering process can be performed without the need for premetallization of difficult-to-wet materials and without flux or a protective atmosphere. In a number of cases, fluxless soldering is a necessary condition of optoelectrical devices, glass-to-metal, and ceramic-to-metal sealing. Additionally, active soldering can offer an economic metallization process for high-power ceramic substrates such as direct bonded copper (DBC), direct bonded aluminum (DBA), and active metal bonded (AMB). It has been shown that the active soldering has a great potential to improve the joining properties of difficult-to-wet materials. A gas-tight joint of ceramic/metal can be realized at low temperature (<250°C) in air without the need of premetallization for ceramic. Moreover, the active soldering process can also be applied to metallize the ceramics for electric and heat conduction and electroplating. Thus, this process provides low-cost, high-quality, environmental benefits and convenient joining technology.

Author details

Shih-Ying Chang[1*], Yan-Hua Huang[1] and Lung-Chuan Tsao[2]

1 Department of Mechanical Engineering, National Yunlin University of Science and Technology, Touliu, Yunlin, Taiwan

2 Graduate Institute of Materials Engineering, National Pingtung University of Science and Technology, Neipu, Pingtung, Taiwan

*Address all correspondence to: changsy@yuntech.edu.tw

IntechOpen

References

[1] Nicholase MG, editor. Joining of Ceramics. London: Chapman and Hall; 1990. ISBN: 0-412-36750-5

[2] do Nascimento RM, Martinelli AE, Buschinelli AJA. Review article: Recent advances in metal–ceramic brazing. Ceramics. 2003;**49**:178-198

[3] Mizuhara H, Mally K. Ceramic-to-metal joining with active brazing filler metals. Welding Journal. 1985;**10**:27-32

[4] Hillen F, Pickart–Castillo D, Rass IJ, Lugscheider E. Solder alloy and soldering processes for flux–free soldering of difficult–to. Wet Materials, Welding & Cutting. 2000;**52**:162-165

[5] Olson DL, Siewert TA, Liu S, Edwards GR. ASM Handbook. Volume 6: Welding, Brazing, and Soldering. American Society for Metals, ASM International; 1993. ISBN: 978-0-87170-382-8

[6] Nicholase MG, editor. Joining Process–Introduction to Brazing and Diffusion Bonding. Dordrecht: Kluwer Academic Publishers; 1998. ISBN: 0-412-7936-0

[7] Bath J, editor. Lead–Free Soldering. New York: Springer; 2007. ISBN: 978-0-687-32466-1

[8] Lugscheider E, Zhuang HS, editors. High Temperature Brazing. Beijing: National Defence Industry Press; 1989. ISBN: 7-118-00437-5

[9] Eustahopoulos N. Dynamics of wetting in reactive metal/ceramic systems. Acta Materialia. 1998;**46**(7):2319-2327

[10] Lugscheider E, Tillmann W. Methods for brazing ceramic and metal–ceramic joints. Materials and Manufacturing Processes. 1993;**8**(2):219-238

[11] Oyama T, Mizuhara H. Direct brazing of graphite using a copper-base active-brazing filler metal. Welding in the World. 1998;**41**:412-419

[12] Huh D, Kim DH. Joining of AlN to Cu using In-base active brazing fillers. Journal of Materials Research. 1997;**12**(4):1048-1055

[13] Akselsen OM. Review—Advances in brazing of ceramics. Journal of Materials Science. 1992;**27**:1989-2000

[14] Elssner G, Petzow G. Metal/ceramic joining. ISIJ International. 1990;**30**(12):1011-1032

[15] Suganuma K. Recent advances in joining technology of ceramics to metals. ISIJ International. 1990;**30**(12):1046-1058

[16] Paulasto M, Kivilahti J. Metallurgical reactions controlling the brazing of Al_2O_3 with Ag–Cu–Ti filler alloys. Journal of Materials Research. 1998;**13**(2):343-352

[17] Weng WP, Chai YH, Chuang TH. Interfacial characteristics for active brazing of alumina to superalloys. Journal of Advanced Materials. 1997;**28**(2):35-40

[18] Moret F, Eustathopoulos N. Ceramic to metal direct brazing. Journal de Physique. 1993;**3**:1043-1052

[19] Ali M, Knowles KM, Mallinson PM, Fernie JA. Interfacial reactions between sapphire and Ag–Cu–Ti-based active braze alloys. Acta Materialia. 2016;**103**:859-869

[20] Ning H, Lan L, Wang L, Peng J, Peng Z, Ma JS. Interface reaction thermodynamics of AgCuTi brazing filler metal and alumina ceramic. Advanced Materials Research. 2014;**936**:1239-1246

[21] Chang SY, Hung YT, Chuang TH. Joining alumina to Inconel 600 and UMCo–50 Superalloys using an $Sn_{10}Ag_4Ti$ active filler metal. Journal of Materials Engineering and Performance. 2003;**12**(2):123-127

[22] Chai YH, Weng WP, Chuang TH. Relationship between wettability and interfacial reaction for $Sn_{10}Ag_4Ti$ on Al_2O_3 and SiC substrates. Ceramics International. 1998;**24**:273-279

[23] Kapoor RR, Eagar TW. Tin–based reactive solders for ceramic/metal joints. Metallurgical Transactions B. 1989;**20B**:919-924

[24] Chang SY, Lu MH, Tsao LC, Chuang TH. Active soldering of ITO to copper. Welding Journal. 2006;**4**:81-83

[25] http://www.s–bond.com/

[26] Chang SY, Tsao LC, Chiang MJ, Tung CN, Pan GH, Chuang TH. Active soldering of indium tin oxide (ITO) with Cu in air using an $Sn_{3.5}Ag_4Ti(Ce,Ga)$ filler. Journal of Materials Engineering and Performance. 2003;**2**(4):383-389

[27] Chang SY. Active soldering of $ZnS–SiO_2$ sputtering targets to copper backing plates using an $Sn_{56}Bi_4Ti(Ce,Ga)$ filler. Materials and Manufacturing Processes. 2006;**21**:761-765

[28] Fu W, Song XG, Zhao YX, Cao J, Feng JC, Jin C, et al. Effect of Ti content on the wetting behavior of $Sn_{0.3}Ag_{0.7}Cu/AlN$ system. Materials and Design. 2017;**115**:1-7

[29] Chang SY, Chuang TH, Yang CL. Low temperature bonding of alumina/alumina and alumina/copper in air using $3.5Ag_4Ti(Ce,Ga)$ filler. Journal of Electronic Materials. 2007;**36**(9):1193-1198

[30] Chang SY, Chuang TH, Tsao LC, Yang CL, Yang ZS. Active soldering of $ZnS–SiO_2$ sputtering targets to copper backing plates using an $Sn_{3.5}Ag_4Ti(Ce,Ga)$ filler metal. Journal of Materials Processing Technology. 2008;**202**:22-26

[31] Liu CH, Kim YJ, Chun DW, Kim GW, Chen RK. Universal solder for direct bonding and packaging of optical devices. Materials Letters. 2015;**152**:232-236

[32] Qu WQ, Zhou SS, Zhuang HS. Effect of Ti content and Y additions on oxidation behavior of SnAgTi solder and its application on dissimilar metals soldering. Materials and Design. 2015;**88**:737-742

[33] Wu CML, Yu DQ, Law CMT, Wang L. Properties of lead-free solder alloys with rare earth element additions. Materials Science and Engineering. 2004;**44**:1-44

[34] Yu DQ, Zhao J, Wang L. Improvement on the microstructure stability, mechanical and wetting properties of Sn–Ag–Cu Lead-free solder with the addition of rare earth elements. Journal of Alloys and Compounds. 2004;**376**:170-175

[35] Tsao LC. Direct active soldering of micro-arc oxidized Ti/Ti joints in air using $Sn_{3.5}Ag_{0.5}Cu_4Ti(RE)$ filler. Materials Science and Engineering A. 2013;**565**:63-71

[36] Ramirez AG, Mavoori H, Jin S. Bonding nature of rare-earth-containing lead-free solders. Applied Physics Letters. 2002;**80**(3):398-400

[37] Lu S, Wang BH, Chen J. Evolutions in microstructure and property of Sn–Ag–Cu lead-free solders with trace addition of magnesium. In: 9th Electronics Packaging Technology Conference; December 10-12, 2007; Singapore

[38] Lu S, Wei CG. Effect of Mg on the microstructure and properties of

Sn–Ag–Cu lead-free solders. In: 6th International Conference on Electronic Packaging Technology; 30 August–2 September 2005; Shenzhen, China

[39] Chang SY, Liu LC. TW Patent No. I322737

[40] Chang SY, Liu LC. TW Patent No. I511827

[41] Smith RW. Active solder joining of metals, ceramics and composites. Welding Journal. 2001;**10**:30-35

[42] Koleňák R, Prach M. Research of joining brittle nonmetallic materials with an active solder. Advances in Materials Science and Engineering. 2014. pp. 1-9

[43] Koleňák R, Šebo P, Provazník M, Koleňáková M, Ulrich K. Shear strength and wettability of active $Sn_{3.5}Ag_4Ti(Ce,Ga)$ solder on Al_2O_3 ceramics. Materials and Design. 2011;**32**:3997-4003

[44] Koleňák R. Soldering of Ceramic Materials. Available from: https://www.mtf.stuba.sk/buxus/docs/internetovy_casopis/2009/kolenak.pdf

[45] Cheng LX, Li GY, Wang XQ, Li ZL, Wu ZZ. Influence of active element Ti on interfacial reaction and soldering strength between $Sn_{3.5}Ag_4Ti(Ce, Ga)$ alloy filler and Si substrate. Materials Science and Engineering A. 2016;**658**:42-49

[46] Cheng LX, Liu MR, Wang XQ, Yan BH, Li GY. Effect of active element Ti on interfacial microstructure and bonding strength of SiO_2/SiO_2 joins soldered using $Sn_{3.5}Ag_4Ti(Ce, Ga)$ alloy filler. Materials Science and Engineering A. 2017;**680**:317-323

[47] Smith RW, Salem A. Lead-Free Active Solder Joining in Electronic Packaging. Available from: www.materialsresources.com

[48] Yu WY, Liu Y, Liu XY. Spreading Sn–Ag–Ti and Sn–Ag–Ti–(Al) solder droplets on the surface of porous graphite through ultrasonic vibration. Materials and Design. 2018;**150**:9-16

[49] Koleňák R, Kostolný I, Drápala J, Sahul M, Urminský J. Characterizing the soldering alloy type In-Ag-Ti and the study of direct soldering of SiC ceramics and copper. Metals. 2018;**274**:1-17

Carbothermal Synthesis of Spherical AlN Fillers

Qi Wang, Kexin Chen and Wenbin Cao

Abstract

Micro-sized spherical AlN particles have presented great commercial potential as thermally conductive fillers for high-performance thermal interface materials, benefiting from their high thermal conductivity and good fluidity in the polymers. In this chapter, recent research progress in the carbothermal synthesis of spherical AlN fillers is highlighted. The influences of various synthetic parameters, including N_2 gas pressure, additive content, additive particle size, reaction temperature, reaction time, carbon content, and additive types, on the nitridation rate and the particle size and morphology of final AlN powders are summarized. More importantly, the growth mechanism of micro-sized spherical AlN granules is deeply discussed as well.

Keywords: carbothermal synthesis, spherical AlN particles, thermally conductive fillers, thermal interface materials, growth mechanism

1. Introduction

With the rapid progress of microelectronics technology, electronic products and devices are developing toward the direction of miniaturization and high integration. Although powerful functions are introduced, the heat dissipation has become an important bottleneck restricting the development of electronic technology. In the field of heat dissipation, thermal interface materials (TIMs) play an important role. TIMs are mainly used to fill the microvoids or uneven holes generated by the contact between heating devices and radiators, establishing an effective channel and improving the efficiency of heat dissipation [1]. Therefore, the TIMs are receiving more and more attention.

In order to achieve optimum heat dissipation, the TIMs should have good ductility to fill the air gap completely. Polymeric materials have attracted increasing interest owing to their excellent processability, high ductility, and low cost. However, most of the polymers have thermal conductivity lower than 0.5 W/m K [2], which is difficult to meet the demand for heat dissipation. To solve this problem, one effective approach is to introduce high–thermal-conductivity fillers into the polymers. Inorganic ceramic powders have been considered as ideal fillers benefiting from their high thermal conductivity, low dielectric constant, and good insulating properties. At present, oxides and nitrides are the most commonly considered fillers.

Silica (SiO_2) is widely used in the field of electronic heat dissipation because of its safety, reliability, and low cost [3, 4]. However, its intrinsic thermal conductivity is only 1.5–1.6 W/m K [5], so it is difficult to obtain composite materials with higher

thermal conductivity. Zinc oxide (ZnO) has a high thermal conductivity up to 60 W/m K, but the high dielectric constant greatly restricts its practical application as fillers [6]. Beryllia (BeO) has the highest thermal conductivity (~240 W/m K) in all the inorganic oxides. However, the high cost and high toxicity make it unattractive for commercial use [5]. Comparatively, alumina (Al_2O_3) has a much higher thermal conductivity than SiO_2 and also presents remarkable electrical and mechanical properties, as well as the cheap producing cost [7–9], so it is the most widely used commercial filler at present. Kozato et al. [7] successfully prepared epoxy composites filling with 60 vol% Al_2O_3, achieving a high thermal conductivity of 4.3 W/m K. However, due to the relatively low intrinsic thermal conductivity of 38~42 W/m K [5], it is still difficult for Al_2O_3 to prepare high-performance TIMs to satisfy the increasing heat-dissipation requirements in future.

Compared with oxides, nitride powders are more attractive owing to the relatively high thermal conductivity. For example, boron nitride (BN) has a thermal conductivity as high as 280 W/m K and also shows the stable chemical property [10]. Xu et al. [11] used modified BN particles as fillers and finally prepared the composites with a high thermal conductivity of 10.3 W/m K. Nevertheless, the high price still limits its wide application. Silicon nitride (Si_3N_4) has a low coefficient of thermal expansion and a low dielectric constant, but it has been seldom used as fillers for high-thermal conductivity TIMs owing to its moderate thermal conductivity of 86~120 W/m K [12].

In comparison, aluminum nitride (AlN) has attracted tremendous attention in the electronic industry thanks to its outstanding properties such as high intrinsic thermal conductivity (~320 W/m K), good electrical resistivity, low dielectric constant, and low thermal expansion coefficient close to that of silicon [13, 14]. Ohashi et al. [15] filled epoxy resin with 74 vol% approximately spherical AlN particles, obtaining a composite thermal conductivity as high as 8.2 W/m K. Zhou et al. [16] prepared TIMs using angular AlN powders to replace Al_2O_3, and the composite thermal conductivity was increased to 2.6 times with a filling fraction of 68.5 vol%. Therefore, AlN fillers have shown prosperous application prospects for preparing high-performance TIMs.

Besides the intrinsic thermal conductivity of fillers, the thermal properties of TIMs are also affected by the filling fraction, the shape and particle size of fillers. In order to prepare the composites with higher thermal conductivity, it is important to raise the filler loading as high as possible and meanwhile retain the good fluidity of the composites for facile processability [17]. Compared with angular and plate-like particles, spherical fillers offer greater advantages in this regard owing to their better fluidity in the polymers [2]. In addition, it is generally believed that the thermal conductivity of composites increases with increasing the particle size of fillers [18]. This can be explained by the following two reasons: on the one hand, larger particles tend to result in the smaller fillers/matrix interfaces, leading to less photon scattering and lower thermal resistance; on the other hand, the fillers with a larger particle size are more easy to achieve higher filling fraction owing to the better fluidity and lower viscosity of the fillers/matrices. In general, the micro-sized fillers can give higher composite thermal conductivity than nano-sized fillers. Therefore, with the above considerations in mind, it is great significant and imperative to synthesize micro-sized spherical AlN particles as thermally conductive fillers for the next generation TIMs.

Despite the potentially high commercial importance, the large-scale synthesis of micro-sized spherical AlN fillers remains a huge challenge to date since nitrides tend to decompose at high temperature and cannot be converted to a spherical morphology just by the traditional surface tension method [19]. Up to now, limited related literatures can be retrieved. Among the existing studies, Ohashi et al. [15]

successfully synthesized spherical AlN particles via solution-reprecipitation treatment of angular AlN powders in a low-melting Ca-Al-O flux. Nevertheless, the particle size of the products was limited by the raw AlN powders, and the necessary hydrochloric acid treatment for removing residual Ca-Al-O was harmful to the product purity and the environment as well. Chowdhury et al. [20] first prepared core-shell structured C@Al_2O_3 composited particles, following the nitridation process in the flowing nitrogen at high temperature to ultimately obtain spherical AlN particles. However, the sphericity of the final product is very low due to the limitation of the heterogeneous mixing process. Suehiro et al. [21] synthesized spherical AlN particles by gas nitridation of spherical Al_2O_3, using a NH_3-C_3H_8 gas mixture as the reduction-nitridation agent, but the undesired impurities were still presented owing to the incomplete conversion. In addition, an effective two-step method, involving the freezing granulation and subsequent sintering process, was also developed to prepare spherical AlN granules with the high sphericity and particle size more than tens of microns [22, 23]. Nevertheless, the AlN was used as raw materials, resulting in the relatively high production cost. Therefore, it is still highly desirable to explore suitable methods to directly synthesize spherical AlN fillers with high sphericity and enhanced properties.

In general, commercial AlN powders are mainly synthesized by two methods. One is the direct nitridation of aluminum powders with N_2 or NH_3 ($2Al + N_2 \rightarrow 2AlN$); the other one is carbothermal reduction nitridation (CRN) of alumina powders in the presence of N_2 ($Al_2O_3 + 3C + N_2 \rightarrow 2AlN + 3CO$) [24]. Comparatively, the CRN method is a better choice for industry production since the resultant AlN powders exhibit more attractive properties such as high purity, facile sinterability, and resistance against humidity.

To date, many efforts have been devoted to ameliorating the quality of AlN powders synthesized by the CRN method [25–28]. Unfortunately, most of them just aimed at fabricating fine or ultrafine AlN powders via low-temperature synthesis to improve the sintering ability and reduce the fabricating cost. The obtained nano or submicron particles are too small to meet the basic requirements as promising fillers. Until recently, increasing attention has been paid on the carbothermal synthesis of coarser AlN granules, especially micro-sized spherical AlN fillers. Based on a series of studies [29–33], the authors have successfully synthesized micro-sized spherical AlN fillers by using appropriate additives and high-pressure N_2 in the CRN process. The as-synthesized AlN granules presented high sphericity, uniform size distribution, and good dispersing behavior, which exhibited great potential as high-performance thermally conductive fillers. Based on this, this chapter will focus on the research progress in the carbothermal synthesis of spherical AlN fillers. The influence of various synthetic parameters on the morphology and particle size of final products will be summarized, and the growth mechanism of micro-sized spherical AlN particles will be discussed as well.

2. Influence of carbothermal synthetic parameters

The typical carbothermal process for synthesizing spherical AlN fillers consists of three steps: first, the raw materials (Al_2O_3, carbon black, and additives) were homogenized by ball milling; second, the CRN process was conducted in a graphite furnace with a high temperature and an elevated N_2 gas pressure; finally, the obtained powders were transferred to a muffle oven and heated in air to remove the residual carbon. It was found that various synthetic parameters, such as N_2 pressure, additives, reaction temperature, reaction time, and carbon content had an important impact on the nitridation rate, the morphology, and the particle size of the final products.

2.1 Effects of N_2 gas pressure

In order to evaluate the effects of N_2 gas pressure on the nitridation rate and the morphology of AlN particles, the raw mixtures containing 5 wt.% CaF_2 additive were heated at a temperature ranging from 1400 to 1800°C and under various N_2 pressure (0.1, 0.1, and 1 MPa), respectively. The AlN conversion fraction was determined based on XRD peak intensities of the plane (100) of AlN and (104) of Al_2O_3. **Figure 1** shows the relationship between AlN conversion fraction and N_2 pressure at various reaction temperatures.

As observed, AlN conversion fraction was significantly decreased with increasing the N_2 pressure, indicating an elevated N_2 pressure hampered the reduction-nitridation process. Based on the studies of Forslund et al. [34, 35], under a high N_2 pressure, the removal of produced CO vapor became more difficult. Thus, a barrier was set up on the surface of solid raw materials by the increased CO level, which limited the contact between Al_2O_3 and N_2, and eventually decreased the reduction-nitridation rate. In addition, it can also be observed in **Figure 1** that the nitridation rate increased with the reaction temperature. When the reaction temperature was higher than 1600°C, the nitridation rate was significantly improved due to the high reaction activity. As a result, Al_2O_3 was completely converted into AlN irrespective of the tested N_2 pressure values.

Figure 2 further presents the SEM images of the AlN powders synthesized at 1800°C but under various N_2 pressures. Under the N_2 pressure of 0.1 Mpa, as shown in **Figure 2a**, irregular AlN particles were obtained. When the N_2 pressure was increased to 0.5 Mpa, approximately spherical AlN particles could be observed in **Figure 2b**. With the N_2 pressure further increasing to 1 Mpa, micro-sized spherical AlN fillers were successfully prepared, as shown in **Figure 2c**. It should be noted that the both particle size and the sphericity of the as-synthesized AlN particles were improved with increasing the N_2 pressure. As established, the elevated N_2 pressure tended to improve the CO level in the system. The AlN nucleation rate was slowed down, resulting in the large particle size. Additionally, CaF_2 additive was expected to react with Al_2O_3 to form low-melting Ca-aluminates, providing the liquid catalyst for AlN nucleation [36]. The slow reaction rate under the elevated N_2 pressure was also beneficial for the migration and uniform distribution of Ca-aluminate liquid phases in the system. Therefore, the uniform liquid-assisted
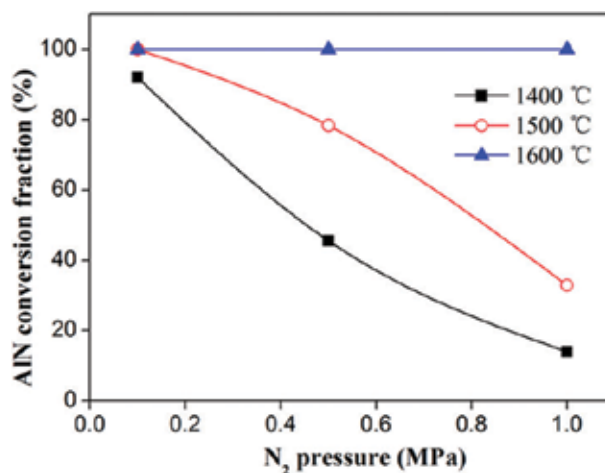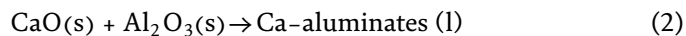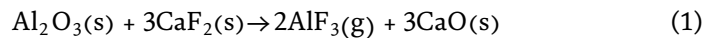

Figure 1.
Relationship between AlN conversion fraction and N_2 gas pressure at various reaction temperatures [31].

nucleation further promoted the formation of AlN particles with the larger particle size, uniform distribution, and spherical morphology.

2.2 Effects of additive content

As mentioned above, the aluminates formed from the reaction between additives and Al_2O_3 played an important role to determine the CRN reaction rate and the morphology of AlN particles. Therefore, the investigation of the additive was helpful to verify the previous inference and better understand the formation mechanism of spherical AlN particles. In this section, the raw materials with various CaF_2 contents (0, 3, 5, and 10 wt.%) were used to proceed the CRN reaction under the high N_2 pressure of 1 MPa and at different temperatures of 1500 and 1800°C. The XRD patterns of the as-synthesized products were shown in **Figure 3**.

As observed from **Figure 3a**, Al_2O_3 was identified in all samples, indicating the incomplete nitridation at 1500°C. In the absence of CaF_2, the peaks of Al_2O_3 were detected strongly. When 3 wt.% CaF_2 was introduced, the relative intensity of the Al_2O_3 diffraction peaks decreased obviously, which indicated that a small amount of CaF_2 could effectively accelerate the nitridation rate. However, with the CaF_2 content further increased to 5 and 10 wt.%, the peaks of Al_2O_3 increased instead, suggesting the conversion fraction of AlN was decreased. This is mainly because the reaction between CaF_2 and Al_2O_3 was relatively slow at the low temperature of 1500°C; excessive and unreacted CaF_2 existed in the system, hindering the contact between reactants and further retarding the nitridation process [37]. In addition, the secondary phase of $CaAl_{12}O_{19}$ was detected in all samples with CaF_2. The Ca-aluminates were mainly formed from the reaction between Al_2O_3 and CaF_2. The process can be described by the following equations [38]:

$$Al_2O_3(s) + 3CaF_2(s) \rightarrow 2AlF_3(g) + 3CaO(s) \qquad (1)$$

$$CaO(s) + Al_2O_3(s) \rightarrow Ca\text{–}aluminates \, (l) \qquad (2)$$

As the reaction proceeds, the low-melting Ca-aluminates tended to be reduced and further transformed into AlN, providing some Ca-compounds [39]:

$$Ca\text{–}aluminates \, (l) + C(s) + N_2(g) \rightarrow AlN(s) + CO(g) + Ca\text{–}compounds \qquad (3)$$

The reduction and nitridation of intermediate Ca-aluminate liquid undergo an easier nitridation process, promoting the conversion rate from Al_2O_3 to AlN.
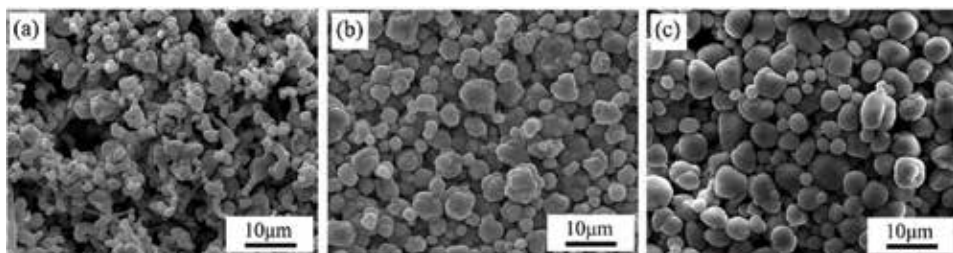

Figure 2.
SEM images of the AlN powders synthesized at 1800°C but under various N_2 pressures: (a) 0.1 Mpa, (b) 0.5 Mpa, and (c) 1 Mpa [31].
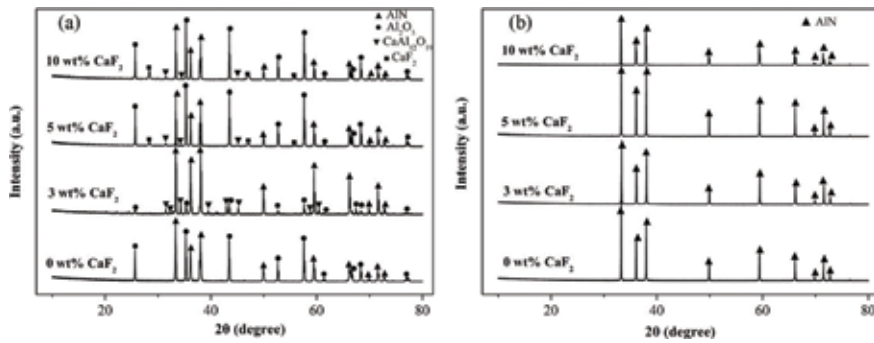
Figure 3.
XRD patterns of the products synthesized with various CaF_2 contents at (a) 1500°C and (b) 1800°C.

When the reaction temperature was increased to 1800°C, only the peaks of AlN were observed in **Figure 3b**, suggesting the full conversion of Al_2O_3 to AlN. Moreover, it is necessary to note that no diffraction peaks ascribed to the CaF_2 or Ca-compounds were detected, inferring that Ca-compounds were just formed at relatively low temperature; afterwards, they were reduced and further vaporized in the atmosphere with the increase of synthesis temperature. The process was established as follows [39, 40]:
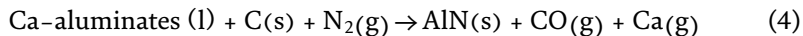
$$Ca-aluminates\ (l) + C(s) + N_2(g) \rightarrow AlN(s) + CO(g) + Ca(g) \qquad (4)$$

Figure 4 further shows the SEM images of the AlN products synthesized at 1800°C. As observed in **Figure 4a**, small particles accompanied with some irregular grains were obtained in the absence of the CaF_2 additive. When a different amount of CaF_2 ranging from 1 to 10 wt.% was added, both the sphericity and particle size of AlN granules significantly increased with the CaF_2 content, as shown in **Figure 4b–d**. Clearly, the higher CaF_2 content meant more Ca-aluminate liquids were generated, providing the liquid environment for AlN nucleation and material transport. A large amount of Ca-aluminate liquid explicitly favored for the complete wrap of AlN particles, promoting the formation of a smooth spherical morphology. In addition, the small AlN particles were more easy to dissolve in the excessive liquid phase and reprecipitate on the surface of large particles, which finally promoted the growth of AlN particles via the dissolution-precipitation mechanism.

2.3 Effects of the additive particle size

In this section, CaF_2 granulations with different particle sizes (<75 μm, 75~150 μm, and >150 μm) were used to evaluate the effects of the additive particle size on the nitridation rate and morphology of the final products. The nitridation pressure in the CRN process was maintained at 1 MPa. According to the particle size of CaF_2 granulations changing from small to large, the obtained powders were briefly named as ACF-S, ACF-M, and ACF-L. **Table 1** summarized the AlN conversion fraction of the products synthesized at 1500 and 1800°C.

It could be clearly inferred that the AlN conversion fraction decreased with the increase of the CaF_2 particle size at the low temperature of 1500°C. This is mainly because the large CaF_2 particle size tended to reduce the reaction rate between CaF_2 and Al_2O_3, leading to the slow formation rate of Ca-aluminates. This observation further demonstrated that the Ca-aluminates played a central role in the nitridation process. When the temperature increased to 1800°C, full nitridation
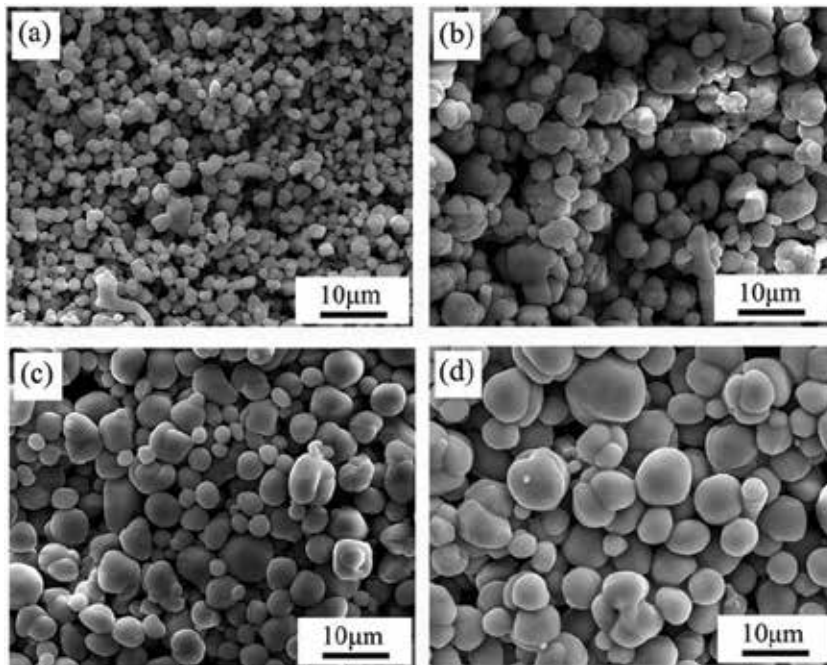
Figure 4.
SEM images of the AlN products synthesized at 1800°C with various CaF$_2$ contents: (a) 0, (b) 3, (c) 5, and (d) 10 wt.% [31].

Samples	CaF$_2$ particle size (μm)	AlN conversion fraction (%)	
		1500°C	1800°C
ACF-S	<75	88.03	100
ACF-M	75~150	73.01	100
ACF-L	>150	57.36	100

Table 1.
The AlN conversion fraction of the products synthesized with different CaF$_2$ particle sizes at 1500 and 1800°C [29].

was achieved for all samples, and the corresponding SEM images are shown in
Figure 5.

As observed, the particle size of AlN products significantly decreased with
increasing the particle size of the CaF$_2$ additive. As mentioned, the large CaF$_2$
particle size could lead to a low formation rate of liquid aluminates. Therefore,
insufficient liquid aluminates existed in the system. As a result, small AlN particles
were difficult to precipitate on the surface of large particles through the dissolution-
precipitation mechanism. The rearrangement and growth of AlN particles were
limited, leading to the AlN products with a small particle size.

2.4 Effects of reaction temperature

Figure 6 shows the typical SEM images of the AlN granules synthesized from
a typical mixture of Al$_2$O$_3$/C with 5 wt.% CaF$_2$ at various reaction temperatures
(1600–1900°C) under the N$_2$ pressure of 1 MPa for 2 h. As can be seen, the tempera-
ture has a great influence on the morphology and particle size of the as-synthesized
AlN granules. At 1600°C, angular AlN granules along with several tadpole-like
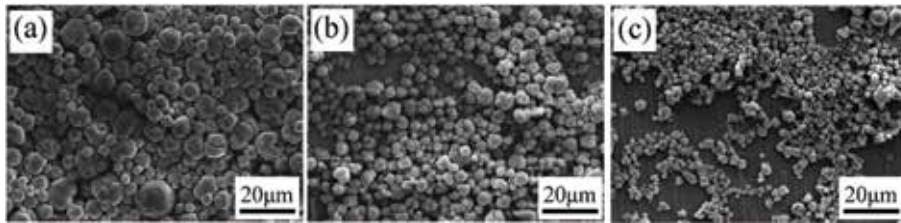
Figure 5.
SEM images of the products synthesized with different CaF$_2$ particle sizes at 1800°C: (a) ACF-S, (b) ACF-M, and (c) ACF-L [29].
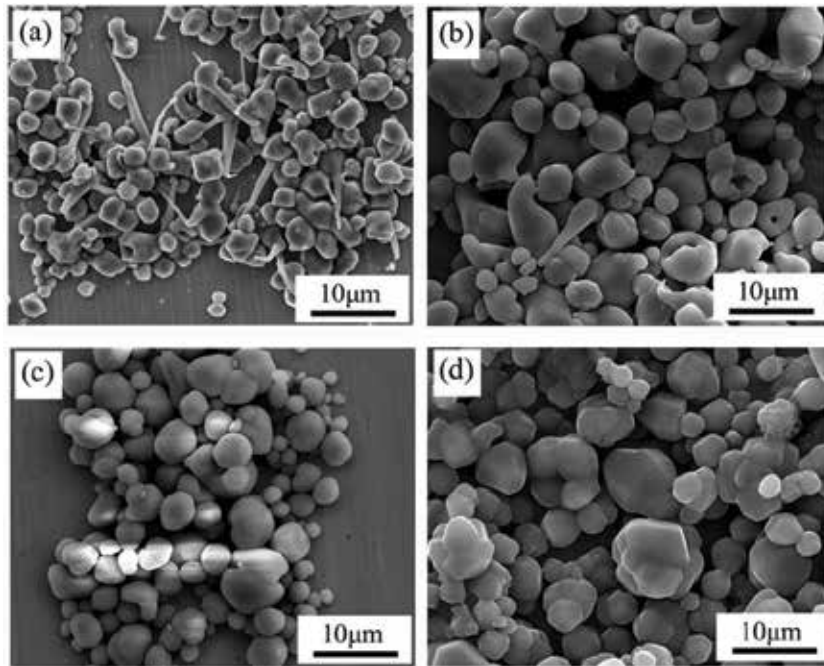

Figure 6.
SEM images of the AlN products synthesized at various temperatures: (a) 1600 [31], (b) 1700 [31], (c) 1800, and (d) 1900°C.

particles were obtained. As the temperature increased to 1700 and 1800°C, the tadpole-like morphology gradually disappeared, while the shape of AlN particles was changed from angular to spherical. However, when the temperature was further raised to 1900°C, the morphology was abnormal again, changing from spherical to angular.

This interesting observation can be understood from the formation and distribution of liquid aluminates. In general, two main reaction processes existed in the system: one is the formation process of Ca-aluminates through the reaction between Al$_2$O$_3$ and CaF$_2$, and the other one is the nitridation process of Ca-aluminates, promoting the formation of AlN. The low formation rate and the high nitridation rate of Ca-aluminates could both result in the reduced content of liquid phases in the system, which would obviously affect the morphology of AlN particles. At a low temperature of 1600°C, the Ca-aluminates appeared in a small amount and tended to distribute unevenly in the system due to the slow reaction rate between CaF$_2$ and Al$_2$O$_3$. As a consequence, AlN had a higher growth rate in the liquid concentration area, leading to the appearance of "tadpole tail." In addition, the small amount of liquid phases also resulted in a relatively slow material migration rate, thus the

AlN granules preferred growing into the angular morphology according to the crystal structure [41]. When the temperature was increased to 1700 and 1800°C, the amount of liquid Ca-aluminates remarkably increased. The rapid material migration aiding with the liquid phases eventually promoted the formation of the spherical morphology with the lowest surface free energy. However, when the temperature was further increased to 1900°C, the nitridation rate of liquid Ca-aluminates increased significantly, even larger than that of the formation rate. In other words, the Ca-aluminates were nitrided immediately as soon as they were formed. There were not enough liquid phases in the system to modify the morphology of AlN. As a result, AlN presented the angular morphology again in accordance with its own structure.

2.5 Effects of reaction time

To investigate the effects of reaction time on the morphology of AlN products, the raw materials with 5 wt.% CaF_2 were heated at 1800°C and under the N_2 pressure of 1 MPa for various reaction times (0.5, 1, 2, and 4 h). **Figure 7** shows the SEM images of the as-synthesized powders.

As the reaction time prolonging from 0.5 to 1 h and further to 2 h, the size and uniformity of AlN particles significantly increased. It was expected that the dissolution and reprecipitation of AlN aiding with liquid phases contributed greatly to the particle growth. In addition, as the prolongation of reaction time, the residual liquid phases in the system could also adjust themselves under the action of the interfacial energy to uniformly wrap the AlN particles, further improving the uniformity of the particle size. However, when the reaction time further increased to 4 h, the growth of AlN particles was no longer obvious. Instead, most of the AlN particles were sintered each other to form large aggregates, and the individual particles tended to change from the spherical to angular morphology, as demonstrated by the
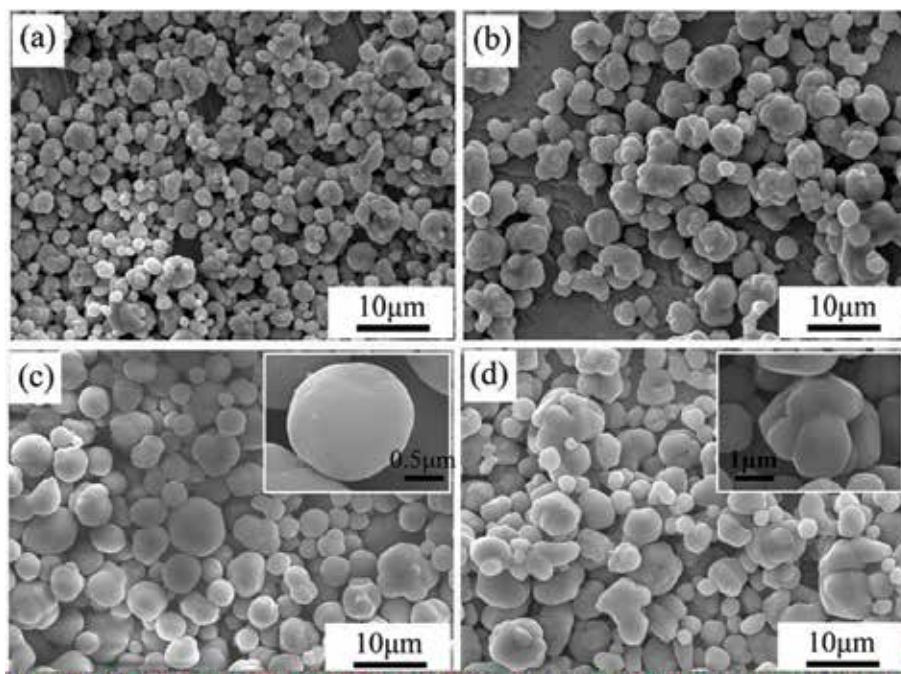

Figure 7.
SEM images of the AlN products synthesized for various reaction times: (a) 0.5, (b) 1, (c) 2, and (d) 4 h [29].

inserted images in **Figure 7c** and **d**. As the reaction proceeding, Ca-aluminates were continuously consumed until they were completely reduced to Ca vapor following Eq. (4). The residual liquid phase was too less to completely encapsulate the AlN particles. The driving force of small AlN particles migrating to large particles decreased, and the energy required for the growth of individual particles increased. Therefore, the AlN particle growth gradually stopped and was replaced by the neck sintering between particles.

2.6 Effects of the carbon content

It is generally believed that the ratio of carbon and Al_2O_3 has a great effect on the CRN process. Traditionally, excessive carbon was used to guarantee the full conversion of Al_2O_3 to AlN [42]. In order to evaluate the effects of carbon content on the synthesis of spherical AlN particles, the raw powder mixtures with 5 wt.% CaF_2 and various C/Al_2O_3 mole ratios (2.5, 3.0, 4.0, and 5.0) were used, and the CRN process was conducted under the N_2 pressure of 1 MPa and at different temperatures for 2 h.

Figure 8 shows the relationship between the AlN conversion fraction and the C/Al_2O_3 mole ratio at 1500 and 1800°C, respectively. At 1500°C, no samples achieved full nitridation. When the mole ratio of C to Al_2O_3 was 3.0, namely, the theoretical value of the CRN reaction, a highest AlN conversion fraction of ~79% was obtained, while a lower or higher C/Al_2O_3 mole ratio tended to reduce the AlN conversion fraction. As discussed, the formation and nitridation process of liquid Ca-aluminates played a crucial role in the CRN process. When the carbon content was insufficient, the contact interface between carbon and Ca-aluminates decreased. As a consequence, the nitridation rate of Ca-aluminates was reduced, leading to the decrease of the AlN conversion fraction. On the other hand, when the ratio of C to Al_2O_3 exceeded the theoretical value, the excessive carbon tended to hinder the contact between CaF_2 and Al_2O_3. The formation rate of Ca-aluminates was decreased correspondingly, resulting in the low AlN conversion fraction as well.

In addition, it can also be observed from **Figure 8** that the full AlN conversion occurred for the samples with the C/Al_2O_3 mole ratios of 3.0, 4.0, and 5.0 at 1800°C. As for the sample with the C/Al_2O_3 mole ratio of 2.5, a small amount of
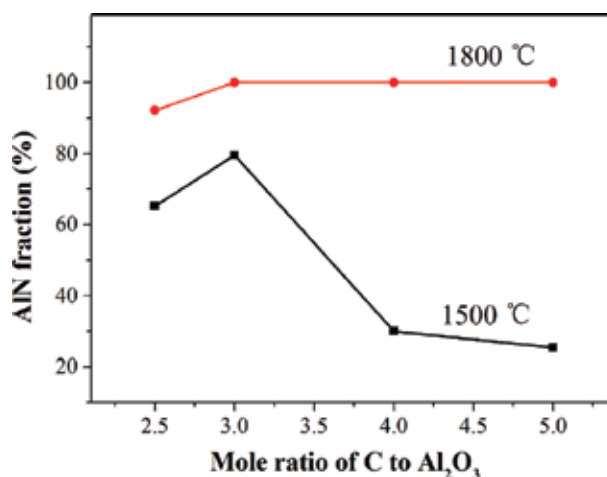

Figure 8.
Relationship between the AlN conversion fraction and the mole ratio of the C/Al_2O_3 mole ratio at 1500 and 1800°C [29].

Al_2O_3 still existed in the system due to the lack of carbon black. The SEM images of all samples synthesized at 1800°C were shown in **Figure 9**.

When the carbon content was less than the theoretical value, many large sintering aggregates could be observed (**Figure 9a**). As increasing the carbon content, the large aggregates gradually disappeared, while the particle size significantly decreased. As known, the growth of particles was not only affected by their growth rate but also restricted by external growth space. When insufficient carbon black was used, the residual carbon black in the late stage was scare. Thus, the AlN particles were likely to contact each other, promoting the formation of large particles and hard aggregates. When the carbon content was excessive, a large amount of unreacted carbon dispersed between AlN particles, which enlarged the migration distance of small particles to AlN nucleus, and limited the growth space of AlN. As a result, AlN powders with smaller particle size were obtained.

2.7 Effects of additive types

In Sections 2.1–2.6, CaF_2 was selected as the typical additive to synthesize spherical AlN fillers by the CRN method. Actually, many single or composite compounds can be used as additives to promote the enhancement of the nitridation rate and the formation of the spherical morphology of AlN particles [37, 43–46]. These compounds have the same characteristic that they can react with Al_2O_3 to produce low-melting liquid aluminates at a relatively low temperature. However, different kinds of additives showed a slight different effect on the nitridation process and the product morphology. **Table 2** shows the powder mixtures with different additive types that the authors previously investigated. The CRN process was carried out at 1400–1800°C and under the N_2 pressure of 1 MPa for 2 h. The influence of additive types on the AlN conversion fraction was summarized in **Table 3**.
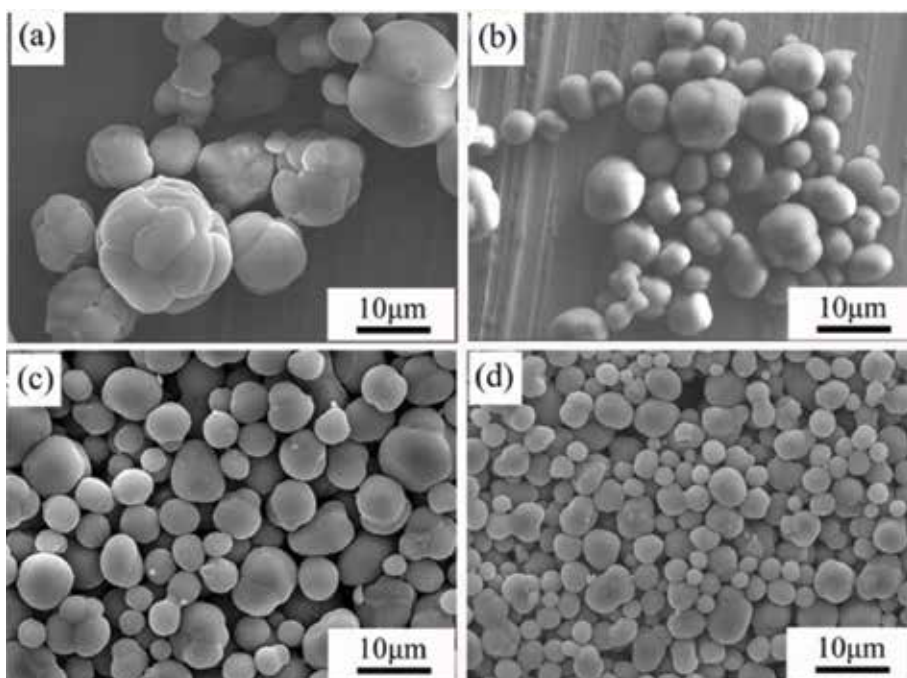

Figure 9.
SEM images of the AlN particles synthesized at 1800°C from samples with various C/Al_2O_3 mole ratios: (a) 2.5, (b) 3.0, (c) 4.0, and (d) 5.0 [29].

Samples	Formulation (in wt.%)				
	Al_2O_3	C	CaF_2	Y_2O_3	YF_3
AP	66.7	33.3	—	—	—
ACF	63.3	31.7	5.0	—	—
AYO	63.3	31.7	—	5.0	—
ACFYO	63.3	31.7	3.0	2.0	—
ACFYF	63.3	31.7	3.0	—	2.0

Table 2.
Compositions of the investigated powder mixtures [32].

Samples	AlN conversion fraction (%)				
	1400°C	1500°C	1600°C	1700°C	1800°C
AP	1.78	42.94	96.02	100.00	100.00
ACF	13.96	32.85	100.00	100.00	100.00
AYO	11.21	67.48	100.00	100.00	100.00
ACFYO	10.70	50.45	100.00	100.00	100.00
ACFYF	35.60	75.62	100.00	100.00	100.00

Table 3.
The AlN conversion fraction at different temperatures for the investigated samples [32].

At 1400°C, all samples with additives showed a higher AlN conversion fraction than that of without additives, further indicating additives favored for the nitridation process. However, it should be noted that the sample ACF showed a lower AlN fraction than AP at 1500°C. This was mainly because most of CaF_2 melts to the liquid phase due to the general melting point of 1418°C. As a result, excessive CaF_2 liquid wrapped on the surface of raw materials, hindering the nitridation process. The rest of samples all present higher AlN conversion fraction than that of AP and ACF, in accordance with the order of ACFYF > AYO > ACFYO. The sample ACFYF presented the highest AlN conversion fraction among all samples. According to the studies of Qiao et al. [38], the formation of $(Ca,Y)F_2$ intermediate and the further appearance of liquid Ca-Y-aluminates at a relatively low temperature of 1350°C were the main reasons for achieving the highest nitridation rate for the Al_2O_3-CaF_2-YF_3 system.

Figure 10 further shows the SEM images of the AlN particles synthesized at 1800°C from various samples. As observed, micro-sized spherical AlN fillers were successfully synthesized from all samples, but their morphology and particle size were slightly different, which might be related to the different formation rate and viscosity of liquid aluminates in the process. From the whole, the sample ACF presented the highest individual sphericity and the best uniformity. Although the near-spherical morphology can also be observed in the remaining samples of AYO, ACFYO, and ACFYF, several hard agglomerates cannot be overlooked. **Figure 11** shows the typical morphology of these hard agglomerates. It can be seen that many compounds precipitated on the particle surface and the neck of sinter particles, which were identified as Y-aluminates by EDS analysis. This indicated that Y-containing compounds could not volatilize as Ca-containing compounds after the CRN reaction, but deposited in the system in the form of precipitates.
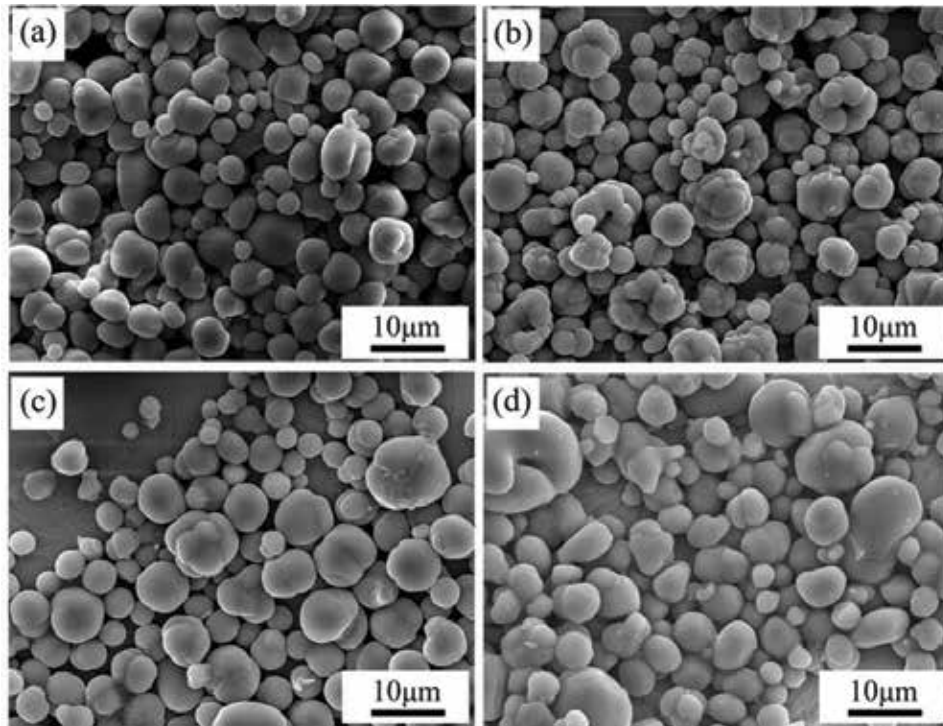
Figure 10.
SEM images of the AlN particles synthesized at 1800°C from samples with various kinds of additives: (a) ACF, (b) AYO, (c) ACFYO, and (d) ACFYF [32].
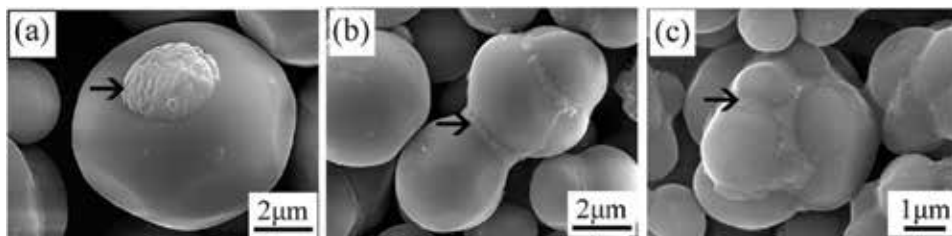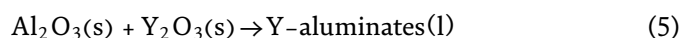

Figure 11.
SEM images of typical microstructures showing Y-aluminate compounds in the sample ACY5 after treatment at 1800°C for 2 h [32].

The appearance of these agglomerates was mainly related to the addition of Y_2O_3. According to other studies [47], in the CRN process, the additive Y_2O_3 firstly reacted with Al_2O_3 to form Y-aluminates, which were further reacted with carbon and N_2 to form AlN based on the following equations:

$$Al_2O_3(s) + Y_2O_3(s) \rightarrow Y-aluminates(l) \tag{5}$$

$$Y-aluminates(l) + C(s) + N_2(g) \rightarrow AlN(s) + CO(g) + Y-compounds \tag{6}$$

When the reaction temperature was high enough or the time was long enough, the Y-aluminates could be reduced completely to Y_2O_3:

$$\text{Y–aluminates (l)} + C(s) + N_2(g) \rightarrow AlN(s) + CO(g) + Y_2O_3(s) \qquad (7)$$
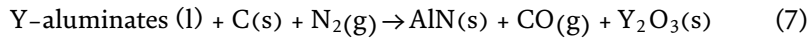
According to the studies of sintering AlN ceramics, the existence of these Y-aluminates tended to hinder the connection between AlN grains, leading to the decrease of thermal conductivity of AlN products [48]. However, direct experimental evidence was still necessary for the spherical AlN fillers.

3. Formation mechanism of micro-size spherical AlN fillers

In the above section, we summarized the influence of synthetic parameters on the morphology of final AlN products. It can be concluded that high N_2 pressure, suitable additives, and appropriate reaction temperature were essential to synthesize the micro-sized spherical AlN fillers. Compared with the traditional CRN method, the as-synthesized AlN fillers exhibited two main obvious morphological changes: the growth of the particle size and the sphericity of the particle shape. In this section, we will discuss the formation mechanism of the two morphological changes based on the experimental results.

3.1 Growth mechanism of the AlN particle size

In the process of carbothermal synthesis of spherical AlN fillers, two typical processes occurred: the reaction between Al_2O_3 and additives to form the liquid aluminates and the further reduction and nitridation of aluminates to produce AlN. After formation, the process of AlN particles enlargement could be divided into three stages: nucleation, growth, and coarsening [49]. First, AlN was nucleated in the liquid aluminates, and the number of AlN grains was continuously increased. After that, the newly generated AlN grew on the basis of crystal nucleus, and the AlN particle size was continuously improved. Finally, as the reaction entered the later stage, the small AlN particles were constantly swallowed by the large particles, leading to the rearrangement and coarsening of AlN particles. Therefore, the AlN particle size was determined jointly by the three stages. The low nucleation rate, high growth rate, and high coarsening rate were all advantageous to obtain the AlN fillers with a large particle size.

As demonstrated, the elevated N_2 pressure favored the formation of AlN granules with a large particle size. Under a high N_2 pressure, the release of CO vapor was inhibited, becoming a barrier to limit the contact between Al_2O_3 and N_2. As a result, the AlN nucleation rate was significantly decreased, resulting in a large particle size.

The AlN growth rate was mainly influenced by the formation and nitridation rate of liquid aluminates. In general, when the nucleation rate and holding time were constant, the fast growth rate meant that AlN particles stayed longer in the coarsening stage, which was conducive to the particle size growth. For example, both the small CaF_2 particle size and high reaction temperature could accelerate the formation rate of aluminates, enhancing the AlN growth rate and further promoting the appearance of large AlN particles.

In the later stage of the reaction, the coarsening rate played a decisive role in the final particle size. Since small particles had higher interface energy, they were more easy to be swallowed by the large particles in order to reduce the overall energy of the system, leading to the growth of the AlN particle size. Therefore, the coarsening stage could be considered as the process of interface migration, and the coarsening rate was affected by the reaction time, temperature, and the difficulty of interface migration.

It could be easily understood that longer reaction time meant longer coarsening stage, hence larger particles were more easy to be obtained. However, it should be noticed that too long reaction time could lead to the complete disappearance of small particles, and the interface migration required much more energy than the system could provide. Thus, the growth of the particle size was not that obvious, as demonstrated in Section 2.5.

High reaction time tended to accelerate the rate of interface migration, promoting the growth of the particle size as well. In addition, when more liquid aluminates existed in the system, it got much easier for small particles to migrate to large particles, so the coarsening rate was significantly increased. This can well explain why more CaF_2 content resulted in a larger particle size in Section 2.2.

Moreover, the final particle size was also influenced by the dispersion of second-phase particles. As demonstrated in Section 2.6, excessive carbon black could become the barriers for small particles to large particles. The external growth space of AlN particles were limited, leading to the small AlN particle size.

In summary, the particle size of the as-synthesized AlN fillers was influenced by a variety of synthetic parameters. In the preparation process of the raw materials, decreasing the additive particle size, increasing the additive content, and decreasing the amount of the carbon black all could lead to the increase of the AlN particle size. Additionally, using a high N_2 gas pressure, increasing the reaction temperature and prolonging the holding time in the CRN reaction process could result in larger AlN particles as well.

3.2 Sphericity mechanism of the AlN particle shape

According to the comprehensive investigations in Section 2, it can be concluded that the amount and distribution of liquid aluminates were important for the formation of the spherical AlN morphology. Based on the crystal growth theory [41], crystals preferred to grow into the lowest energy state. When there were no liquids in the system, the AlN morphology was mainly determined by the internal intrinsic structure. Thus, AlN particles tended to grow in the angular morphology to achieve the most stable state of energy. However, when additives were used in the CRN process, AlN was nucleated in the liquid aluminates, and thus its morphology was consequentially influenced by the external liquid phase environment. The solid AlN and liquid phase constituted a common system, and hence the lowest solid-liquid interface energy became the main driving force for the growth of AlN. Compared with the angular morphology, spherical particles showed the least specific surface area and the corresponding lowest solid-liquid interface energy. Therefore, AlN tended to grow into the spherical morphology with the aid of liquid Ca-aluminates.

Based on the above inference, only when the AlN particles were completely wrapped in the liquids during the growth stage, the spherical morphology could be obtained. Thus, both the low liquid content and the fast AlN growth rate could lead to the disappearance of the solid-liquid interface and the difficulty to form the spherical shape. For example, when a low N_2 pressure was used, the AlN growth rate was significantly increased so that the AlN particles could not be completely wrapped by the liquids, resulting in the poor sphericity. In addition, the low reaction temperature and the little additive content both led to the small liquid content, thus the spherical AlN particles could not be obtained as well. It can be concluded that the elevated N_2 pressure, suitable additives, and relatively high reaction temperature greatly favored for carbothermally synthesizing AlN particles with a smooth spherical morphology.

4. Conclusion and perspective

In conclusion, this chapter presents the recent advances on the carbothermal synthesis of spherical AlN fillers. The influence of various synthetic parameters on the morphology and particle size of final products is summarized. During the CRN process, the elevated N_2 gas pressure favored the growth of the particle size and the formation of the uniform spherical morphology, but hampered the nitridation rate. The relatively high reaction temperature could result in the increasing nitridation rate, the growth of the particle size, and the sphericity of AlN particles, but a too high temperature above 1900°C was not beneficial for the spherical morphology due to the decreasing liquid content. Prolonging the reaction time properly was also conducive to the formation of large spherical AlN particles. As for the raw materials, increasing the additive content tended to enhance the sphericity and particle size of AlN particles; excessive carbon black reduced the nitridation rate and particle size, but increased the sphericity of AlN particles; the use of the additive with a large particle size could slow down the nitridation rate and reduce the AlN particle size.

In summary, the liquid aluminates forming from the reaction between Al_2O_3 and additives played an important role in the carbothermal synthesis of spherical AlN fillers by improving the nitridation rate, increasing the particle size, and promoting the formation of smooth spherical appearance. The condition that AlN particles were completely wrapped with liquid aluminates during the growth stage was necessary for the spherical morphology.

Although the micron-sized spherical AlN particles, which showed great potentiality to be used as fillers, were successfully synthesized by the CRN method, further research is still necessary aiming at evaluating the actual thermal conductivity of the AlN fillers and the performance of the as-prepared thermal interface materials.

Acknowledgements

Conflict of interest

The authors declare no conflict of interest.

Author details

Qi Wang[1*], Kexin Chen[2] and Wenbin Cao[1]

1 Department of Inorganic Nonmetallic Materials, School of Materials Science and Engineering, University of Science and Technology Beijing, Beijing, China

2 State Key Laboratory of New Ceramics and Fine Processing, School of Materials Science and Engineering, Tsinghua University, Beijing, China

*Address all correspondence to: wangqi15@ustb.edu.cn

IntechOpen

References

[1] Chung DDL. Thermal interface materials. Journal of Materials Engineering and Performance. 2001;**10**:56-59. DOI: 10.1361/105994901770345358

[2] Chen H, Ginzburg VV, Yang J, Yang Y, Liu W, Huang Y, et al. Thermal conductivity of polymer-based composites: Fundamentals and applications. Progress in Polymer Science. 2016;**59**:41-85. DOI: 10.1016/j.progpolymsci. 2016.03.001

[3] Afzal A, Siddiqi HM, Iqbal N, Ahmad Z. The effect of SiO_2 filler content and its organic compatibility on thermal stability of epoxy resin. Journal of Thermal Analysis and Calorimetry. 2013;**111**:247-252. DOI: 10.1007/s10973-012-2267-9

[4] Procter P, Solc J. Improved thermal conductivity in microelectronic encapsulants. In: Proceedings of the 41st Electronic Components & Technology Conference; 11-16 May 1991; Atlanta. New York: IEEE; 1991. pp. 835-842

[5] Huang X, Jiang P, Tanaka T. A review of dielectric polymer composites with high thermal conductivity. IEEE Electrical Insulation Magazine. 2011;**27**:8-16. DOI: 10.1109/MEI.2011.5954064

[6] Varlow BR, Robertson J, Donnelly KP. Nonlinear fillers in electrical insulating materials. IET Science, Measurement and Technology. 2007;**1**:96-102. DOI: 10.1049/iet-smt:20060007

[7] Kozako M, Okazaki Y, Hikita M, Tanaka T. Preparation and evaluation of epoxy composite insulating materials toward high thermal conductivity. In: Proceedings of the 10th IEEE International Conference on Solid Dielectrics; 4-9 July 2010; Potsdam. New York: IEEE; 2010. pp. 1-4

[8] Sim LC, Ramanan SR, Ismail H, Seetharamu KN, Goh TJ. Thermal characterization of Al_2O_3 and ZnO reinforced silicone rubber as thermal pads for heat dissipation purposes. Thermochimica Acta. 2005;**430**:155-165. DOI: 10.1016/j.tca.2004.12.024

[9] Zhou W, Qi S, Tu C, Zhao H, Wang C, Kou J. Effect of the particle size of Al_2O_3 on the properties of filled heat-conductive silicone rubber. Journal of Applied Polymer Science. 2007;**104**:1312-1318. DOI: 10.1002/app.25789

[10] Donnay M, Tzavalas S, Logakis E. Boron nitride filled epoxy with improved thermal conductivity and dielectric breakdown strength. Composites Science and Technology. 2015;**110**:152-158. DOI: 10.1016/j.compscitech.2015.02.006

[11] Xu Y, Chung DDL. Increasing the thermal conductivity of boron nitride and aluminum nitride particle epoxy-matrix composites by particle surface treatments. Composite Interfaces. 2000;**7**:243-256. DOI: 10.1163/156855400750244969

[12] Furuya K, Munakata F, Matsuo K, Akimune Y, Ye J, Okada A. Microstructural control of b-silicon nitride ceramics to improve thermal conductivity. Journal of Thermal Analysis and Calorimetry. 2002;**69**:873-879. DOI: 10.1023/A:1020660006988

[13] Slack GA. Nonmetallic crystals with high thermal conductivity. Journal of Physics and Chemistry of Solids. 1973;**34**:321-335. DOI: 10.1016/0022-3697(73)90092-9

[14] Slack GA, Tanzilli RA, Pohl RO, Vandersande JW. The intrinsic thermal conductivity of AIN. Journal of Physics and Chemistry of

Solids. 1987;**48**:641-647. DOI:
10.1016/0022-3697(87)90153-3

[15] Ohashi M, Kawakami S, Yokogawa
Y, Lai G-C. Spherical aluminum nitride
fillers for heat-conducting plastic
packages. Journal of the American
Ceramic Society. 2005;**88**:2615-2618.
DOI: 10.1111/j.1551-2916.2005.00456.x

[16] Zhou Y, Wang H, Wang L, Yu K,
Lin Z, He L. Fabrication and
characterization of aluminum nitride
polymer matrix composites with high
thermal conductivity and low dielectric
constant for electronic packaging.
Materials Science and Engineering
B. 2012;**177**:892-896. DOI: 10.1016/j.
mseb.2012.03.056

[17] Burger N, Laachachi A, Ferriol M,
Lutz M, Toniazzo V, Ruch D. Review
of thermal conductivity in composites:
Mechanisms, parameters and
theory. Progress in Polymer Science.
2016;**61**:1-28. DOI: 10.1016/j.
progpolymsci.2016.05.001

[18] Chon CH, Kihm KD, Lee SP, Choi
SUS. Empirical correlation finding the
role of temperature and particle size for
nanofluid (Al_2O_3) thermal conductivity
enhancement. Applied Physics Letters.
2005;**87**:153107. DOI: 10.1063/1.2093936

[19] Fan ZY, Newman N. Experimental
determination of the rates of
decomposition and cation desorption
from AlN surfaces. Materials Science
and Engineering B. 2001;**87**:244-248.
DOI: 10.1016/S0921-5107(01)00720-6

[20] Chowdhury SA, Maiti HS, Biswas S.
Synthesis of spherical Al_2O_3 and AlN
powder from C@Al_2O_3 composite
powder. Journal of Materials Science.
2006;**41**:4699-4705. DOI: 10.1007/
s10853-006-0039-2

[21] Suehiro T, Tatami J, Meguro T,
Matsuo S, Komeya K. Morphology-
retaining synthesis of AlN particles by
gas reduction–nitridation. Materials

Letters. 2002;**57**:910-913. DOI: 10.1016/
S0167-577X(02)00894-7

[22] Wang Q, Ge Y, Sun S, Kuang J,
Ferreira JMF, Cao W. Preparation of
dense spherical AlN fillers by aqueous
granulation and post-sintering
process. Ceramics International.
2017;**43**:2027-2032. DOI: 10.1016/j.
ceramint.2016.10.171

[23] Wang Q, Olhero SM, Ferreira JMF,
Cui W, Chen K, Xie Z. Hydrolysis
control of AlN powders for the aqueous
processing of spherical AlN granules.
Journal of the American Ceramic
Society. 2013;**96**:1383-1389. DOI:
10.1111/jace.12288

[24] Selvaduray G, Sheet L. Aluminium
nitride: Review of synthesis methods.
Materials Science and Technology.
1993;**9**:463-473. DOI: 10.1179/
mst.1993.9.6.463

[25] Wu H, Qin M, Chu A, Wan Q, Cao
Z, Liu Y, et al. AlN powder synthesis by
sodium fluoride-assisted carbothermal
combustion. Ceramics International.
2014;**40**:14447-14452. DOI: 10.1016/j.
ceramint.2014.07.014

[26] Qin M, Du X, Wang J, Humail IS,
Qu X. Influence of carbon on the
synthesis of AlN powder from
combustion synthesis precursors.
Journal of the European Ceramic
Society. 2009;**29**:795-799. DOI:
10.1016/j.jeurceramsoc.2008.07.019

[27] Wang H, Yang Q, Jia G, Lei R,
Wang S, Xu S. Influence of yttrium
dopant on the synthesis of ultrafine AlN
powders by CRN route from a sol–gel
low temperature combustion precursor.
Advanced Powder Technology.
2014;**25**:450-456. DOI: 10.1016/j.
apt.2013.07.008

[28] Yamakawa T, Tatami J,
Wakihara T, Komeya K, Meguro T,
MacKenzie KJD, et al. Synthesis of
AlN nanopowder from γ-Al_2O_3 by

reduction–nitridation in a mixture of NH_3–C_3H_8. Journal of the American Ceramic Society. 2006;**89**:171-175. DOI: 10.1111/j.1551-2916.2005.00693.x

[29] Wang Q, Cao W, Kuang J, Jiang P. Spherical AlN particles synthesized by the carbothermal method: Effects of reaction parameters and growth mechanism. Ceramics International. 2018;**44**:4829-4834. DOI: 10.1016/j.ceramint.2017.12.071

[30] Wang Q, Cui W, Ge Y, Chen K, Xie Z. Preparation of spherical AlN granules directly by carbothermal reduction-nitridation method. Journal of the American Ceramic Society. 2015;**98**:392-397. DOI: 10.1111/jace.13324

[31] Wang Q, Ge Y, Cui W, Chen K, Ferreira JMF, Xie Z. Carbothermal synthesis of micro-scale spherical AlN granules with CaF2 additive. Journal of Alloys and Compounds. 2016;**663**:823-828. DOI: 10.1016/j.jallcom.2015.12.178

[32] Wang Q, Ge Y, Kuang J, Jiang P, Liu W, Cao W. Effects of additives on the synthesis of spherical aluminum nitride granules by carbothermal reduction-nitridation process. Journal of Alloys and Compounds. 2017;**696**:220-225. DOI: 10.1016/j.jallcom.2016.11.252

[33] Wang Q, Kuang J, Jiang P, Cao W. Carbothermal synthesis of spherical AIN particles using sucrose as carbon source. Ceramics International. 2018;**44**:3480-3483. DOI: 10.1016/j.ceramint.2017.11.056

[34] Forslund B, Zheng J. Carbothermal synthesis of aluminium nitride at elevated nitrogen pressures, part I: Effect of process parameters on conversion rate. Journal of Materials Science. 1993;**28**:3125-3131. DOI: 10.1007/BF00354225

[35] Forslund B, Zheng J. Carbothermal synthesis of aluminium nitride at elevated nitrogen pressures, part II: Effect of process parameters on particle size and porphology. Journal of Materials Science. 1993;**28**:3132-3136. DOI: 10.1007/BF00354226

[36] Ide T, Komeya K, Meguro T, Tatami J. Synthesis of AlN powder by Carbothermal reduction-Nitridation of various Al_2O_3 powders with CaF_2. Journal of the American Ceramic Society. 1999;**82**:2993-2998. DOI: 10.1111/j.1151-2916.1999.tb02193.x

[37] Molisani AL, Yoshimura HN. Low-temperature synthesis of AlN powder with multicomponent additive systems by carbothermal reduction–nitridation method. Materials Research Bulletin. 2010;**45**:733-738. DOI: 10.1016/j.materresbull.2010.02.012

[38] Qiao L, Zhou H, Fu R. Thermal conductivity of AlN ceramics sintered with CaF_2 and YF_3. Ceramics International. 2003;**29**:893-896. DOI: 10.1016/S0272-8842(03)00033-6

[39] Komeya K, Kitagawa I, Meguro T. Effect of Ca-compound addition on synthesis of AlN powder by carbothermal reduction-nitridation method. Journal of the Ceramic Society of Japan. 1994;**102**:670-674. DOI: 10.2109/jcersj.102.670

[40] Xiong Y, Wang H, Fu Z. Transient liquid-phase sintering of AlN ceramics with CaF_2 additive. Journal of the European Ceramic Society. 2013;**33**:2199-2205. DOI: 10.1016/j.jeurceramsoc.2013.03.024

[41] Cahn JW. Theory of crystal growth and interface motion in crystalline materials. Acta Metallurgica. 1960;**8**:554-562. DOI: 10.1016/0001-6160(60)90110-3

[42] Cho YW, Charles JA. Synthesis of nitrogen ceramic povvders by carbothermal reduction and nitridation, part 3 aluminium nitride. Materials

Science and Technology. 1991;**7**:495-504. DOI: 10.1179/mst.1991.7.6.495

[43] Kume S, Yasuoka M, Lee S-K, Kan A, Ogawa H, Watari K. Dielectric and thermal properties of AlN ceramics. Journal of the European Ceramic Society. 2007;**27**:2967-2971. DOI: 10.1016/j.jeurceramsoc.2006.11.023

[44] Nakano H, Watari K, Hayashi H, Urabe K. Microstructural characterization of high-thermal-conductivity aluminum nitride ceramic. Journal of the American Ceramic Society. 2002;**85**:3093-3095. DOI: 10.1111/j.1151-2916.2002.tb00587.x

[45] Hundere AM, Einarsrud M-A. Microstructural development in AlN (YF$_3$) ceramics. Journal of the European Ceramic Society. 1997;**17**:873-878. DOI: 10.1016/S0955-2219(96)00199-9

[46] Liu Y, Zhou H, Qiao L, Wu Y. Low-temperature sintering of aluminum nitride with YF$_3$–CaF$_2$ binary additive. Journal of Materials Science Letters. 1999;**18**:703-704. DOI: 10.1023/A:1006692111736

[47] Ide T, Komeya K, Tatami J, Meguro T, Naito M, Hotta T. Effect of Y$_2$O$_3$ addition on synthesis of AlN powder by carbothermal reduction-nitridation of Al$_2$O$_3$. Journal of the Ceramic Society of Japan. 2001;**109**:372-375. DOI: 10.2109/jcersj.109.1268_372

[48] Virkar AV, Jackson TB, Cutler RA. Thermodynamic and kinetic effects of oxygen removal on the thermal conductivity of aluminum nitride. Journal of the American Ceramic Society. 1989;**72**:2031-2042. DOI: 10.1111/j.1151-2916.1989.tb06027.x

[49] Chen IW, Davenport A, Wang L. Accelerated precipitate coarsening due to a concomitant secondary phase transformation. Acta Materialia. 2003;**51**:1691-1703. DOI: 10.1016/S1359-6454(02)00570-0

Edited by Amar Patnaik

Fillers - Synthesis, Characterization and Industrial Application comprises a set of chapters that brings an interdisciplinary perspective to accomplish a more detailed understanding of filler materials for the synthesis and characterization of different industrial applications. This book embraces all the chapters that are concerned with the effect of incorporating different fillers or particulates in fabricated composites. Significant research efforts all around the world are continuing to explore the properties of composite materials. Researchers are collectively focusing their efforts on the use of particulate fillers in composites for miscellaneous applications. This book delivers a comprehensive study associated with the sections of material science, polymer technology, anisotropic elasticity phenomena, fracture mechanics, applied mechanics, material synthesis, mechanical and thermo-mechanical characteristics, tribological behavior, etc.

IntechOpen